10. Electroweak Model and Constraints on New Physics

Revised November 2025 by J. de Blas (Granada U.), S. Dittmaier (Freiburg U.) and R. Kogler (DESY, Hamburg).

10.1	Intro	oduction	1
10.2	Rene	ormalization and radiative corrections	3
	10.2.1	Ultraviolet and infrared divergences and regularization	3
	10.2.2	Renormalization procedure and renormalization schemes	4
	10.2.3	Electroweak input parameter schemes	7
	10.2.4	Particle masses	9
	10.2.5	Radiative corrections to electroweak processes	11
10.3	Low	-energy observables	14
	10.3.1	The electromagnetic coupling	14
	10.3.2	The Fermi constant	17
	10.3.3	The muon anomalous magnetic moment	18
10.4	Elec	troweak precision physics	18
	10.4.1	Z- and W -boson masses and widths	18
	10.4.2	Higgs-boson mass and width	20
	10.4.3	Quark masses	20
	10.4.4	The strong coupling constant	22
	10.4.5	The weak mixing angle	22
	10.4.6	Z-pole physics	24
	10.4.7	W and Z decays	31
10.5	Glob	pal fit results	32
10.6	Cons	straints on new physics	39

10.1 Introduction

The Standard Model of the electroweak interactions (SM) [1–4] is a renormalizable gauge quantum field theory based on the group SU(2) × U(1), with gauge bosons W^i_μ , i=1,2,3, and B_μ for the SU(2) and U(1) factors, respectively, and the corresponding gauge coupling constants g and g'. The quantum numbers of the two subgroups are known as weak isospin and weak hypercharge, respectively. The left-handed lepton and quark fields of the $i^{\rm th}$ fermion family transform as doublets $\Psi_i = \begin{pmatrix} \nu_i \\ \ell_i^- \end{pmatrix}$ and $\begin{pmatrix} u_i \\ d_i' \end{pmatrix}$ under SU(2), respectively. Here we assume a flavor basis where the lepton and up-quark fields are aligned with the physical basis, whereas for the down-type quarks the interaction and mass bases are related by the Cabibbo–Kobayashi–Maskawa mixing [5,6] matrix $V^{\rm CKM}$: $d_i' \equiv \sum_j V_{ij}^{\rm CKM} d_j$. The right-handed fermion fields transform as SU(2) singlets. From Higgs and electroweak (EW) precision data it is known that there are precisely three sequential fermion families. Constraints on $V^{\rm CKM}$ and tests of universality are discussed in Ref. [7] and in Section 12 on the "CKM Quark-Mixing Matrix" in this Review. The extension of the formalism to allow for an analogous leptonic mixing matrix is discussed in Section 14 on "Neutrino Masses, Mixing, and Oscillations" in this Review.

A complex scalar Higgs doublet, ϕ , is added to the model for mass generation through spontaneous symmetry breaking with potential given by

$$V(\phi) = \mu^2 \phi^{\dagger} \phi + \frac{\lambda^2}{2} (\phi^{\dagger} \phi)^2 , \qquad \phi \equiv \begin{pmatrix} \phi^+ \\ \phi^0 \end{pmatrix} . \tag{10.1}$$

For μ^2 negative, ϕ develops a vacuum expectation value, $\langle \phi \rangle = (0, v/\sqrt{2})^{\rm T}$, where $v = \sqrt{2}|\mu|/\lambda \approx 246$ GeV, breaking the EW symmetry down to the remaining $U(1)_{\rm em}$ symmetry of Quantum Electrodynamics (QED). After this, only one neutral Higgs scalar, H, remains in the physical particle spectrum. The three remaining degrees of freedom in the doublet ϕ correspond to would-be Goldstone fields, which open up longitudinal polarizations of the W/Z bosons, but do not correspond to additional particles. In the following we assume the use of the unitary gauge, in which the would-be Goldstone fields formally vanish and the vector fields for the W/Z bosons directly describe three physical polarizations. In non-minimal models there are additional charged and neutral scalar Higgs particles. Higgs-boson physics is reviewed in Section 11 on the "Status of Higgs Boson Physics" in this Review.

After symmetry breaking the Lagrangian for the fermion fields, ψ_i , is

$$\mathcal{L}_{F} = \sum_{i} \bar{\psi}_{i} \left(i \not \partial - m_{i} - \frac{m_{i} H}{v} \right) \psi_{i} - \frac{g}{2\sqrt{2}} \sum_{i} \overline{\Psi}_{i} \gamma^{\mu} (1 - \gamma^{5}) (T^{+} W_{\mu}^{+} + T^{-} W_{\mu}^{-}) \Psi_{i}$$

$$- e \sum_{i} Q_{i} \bar{\psi}_{i} \gamma^{\mu} \psi_{i} A_{\mu} - \frac{g}{2 \cos \theta_{W}} \sum_{i} \bar{\psi}_{i} \gamma^{\mu} (g_{V}^{i} - g_{A}^{i} \gamma^{5}) \psi_{i} Z_{\mu} .$$

$$(10.2)$$

Here $\theta_W \equiv \tan^{-1}(g'/g)$ is the weak mixing angle and $e = g \sin \theta_W$ is the positron electric charge. Furthermore,

$$A_{\mu} \equiv B_{\mu} \cos \theta_W + W_{\mu}^3 \sin \theta_W , \qquad (10.3a)$$

$$Z_{\mu} \equiv -B_{\mu} \sin \theta_W + W_{\mu}^3 \cos \theta_W , \qquad (10.3b)$$

$$W_{\mu}^{\pm} \equiv \frac{W_{\mu}^{1} \mp iW_{\mu}^{2}}{\sqrt{2}} \tag{10.3c}$$

are the photon field (A) and the neutral (Z) and charged (W^{\pm}) weak boson fields, respectively.

The Yukawa coupling of H to ψ_i in the first term in \mathcal{L}_F , which is flavor diagonal in the minimal model, is $gm_i/2M_W$. From the bosonic interaction Lagrangian,

$$\mathcal{L}_{HV} = \frac{1}{2}(v+H)^2 \left[\frac{g^2}{2} W_{\mu}^+ W^{\mu-} + \frac{g^2 + g'^2}{4} Z_{\mu} Z^{\mu} \right] - \frac{\mu^2}{2} (v+H)^2 - \frac{\lambda^2}{8} (v+H)^4 , \qquad (10.4)$$

one obtains the EW boson masses (at tree level, i.e., to lowest order in perturbation theory)

$$M_H = \sqrt{2}|\mu| = \lambda v , \qquad (10.5a)$$

$$M_W = \frac{gv}{2} = \frac{ev}{2\sin\theta_W} \,, \tag{10.5b}$$

$$M_Z = \sqrt{g^2 + g'^2} \frac{v}{2} = \frac{ev}{2\sin\theta_W \cos\theta_W},$$
 (10.5c)

$$M_{\gamma} = 0. \tag{10.5d}$$

The second term in \mathcal{L}_F represents the charged-current weak interaction [8–10], where $T^{\pm} = (\sigma_1 \pm i\sigma_2)/2$ are the weak isospin raising and lowering operators, with σ_a denoting the Pauli matrices. For example, the coupling of a W to an electron and a neutrino is

$$-\frac{e}{2\sqrt{2}\sin\theta_W} \left[W_{\mu}^- \bar{e} \gamma^{\mu} (1 - \gamma^5) \nu + W_{\mu}^+ \bar{\nu} \gamma^{\mu} (1 - \gamma^5) e \right] . \tag{10.6}$$

For momenta small compared to M_W , this term gives rise to the effective four-fermion interaction with the Fermi constant given by $G_F/\sqrt{2} = 1/(2v^2) = g^2/(8M_W^2)$. CP violation is incorporated into the EW model by a single observable phase in V_{ij}^{CKM} .

The third term in \mathcal{L}_F describes electromagnetic interactions [11,12], and the last is the weak neutral-current interaction [9,10,13]. The vector and axial-vector couplings are

$$g_V^i \equiv T_i^3 - 2Q_i \sin^2 \theta_W , \qquad (10.7a)$$

$$g_A^i \equiv T_i^3 \,\,, \tag{10.7b}$$

where $T_i^3 = \sigma_3/2$ is the third component of the weak isospin of fermion i (+1/2 for left-handed u_i and ν_i ; -1/2 for left-handed d_i and e_i ; zero for right-handed fields), and Q_i is the charge of ψ_i in units of e. The weak hypercharge Y_i is related to weak isospin and electric charge according to the Gellman-Nishijima relation, $Q_i = T_i^3 + Y_i/2$.

The first term in Eq. (10.2) also gives rise to Dirac fermion masses. In the SM, for the case of the neutrinos, the absence of the corresponding right-handed fields prevents the existence of such terms. Furthermore, the requirements of gauge invariance and renormalizability prevents writing Lagrangian terms with the SM fields that can give rise to Majorana neutrino masses after EW symmetry breaking. We refer to Section 14 on "Neutrino Mass, Mixing, and Oscillations" in this Review for a discussion on the possible origin of neutrino masses.

This review is organized as follows: In Section 10.2 we cover several theoretical aspects that are fundamental for the understanding of the SM at the quantum level and the calculation of the phenomenology of the EW sector. Section 10.3 describes several low-energy observables that are key inputs for the SM description of EW interactions, such as the electromagnetic and Fermi constants. We also comment on the latest updates in the experimental status of the determination of the muon anomalous magnetic moment; however, this section has been substantitally simplified with respect to previous editions of the *Review*. Section 10.4 focuses mostly on the description of the so-called EW precision observables that are used in the global EW fit, whose results are presented and discussed in Section 10.5. Finally, in Section 10.6 we move our focus to scenarios of physics beyond the SM and discuss the implications of the global EW fit from the point of view of constraining new physics.

10.2 Renormalization and radiative corrections

Before going into detail in the confrontation of the EW theory with experimental results, we clarify some notions and concepts that are essential in the perturbative evaluation of quantum field theories.

10.2.1 Ultraviolet and infrared divergences and regularization

Perturbative calculations in quantum field theories are typically plagued with different types of divergences. Ultraviolet (UV) divergences originate from the high-momentum regions in loop diagrams, while singularities resulting from finite momentum transfer are known as infrared (IR) divergences. Before eliminating the various divergences from predictions, it is necessary to map them to finite quantities in a mathematically consistent way, a step called regularization. This step embeds the whole theory into a wider class of theories parametrized by some new parameter δ ,

and the original theory corresponds to a specific value δ_0 . Quantities that diverge in the original theory are finite for $\delta \neq \delta_0$, but diverge for $\delta \to \delta_0$, typically like $\ln(\delta - \delta_0)$ or some power of $1/(\delta - \delta_0)$. The most common regularization scheme is dimensional regularization, where the whole theory is formulated in D-dimensional flat space—time and both UV and IR divergences take the form of poles in the parameter $\epsilon = (4-D)/2$, which is consistently treated as a complex parameter. Other regularization schemes are possible as well, such as the use of small mass parameters for regularizing IR singularities, but dimensional regularization has the advantage of maximal simplicity and preserving gauge and Lorentz invariance.

While the IR divergences are eliminated from physical predictions upon properly designing observables in such a way that IR singularities cancel by virtue of the Kinoshita–Lee–Nauenberg (KLN) theorem [14, 15], UV singularities are dealt in the context of the *renormalization* of the quantum field theory, as described in the next section.

Since symmetries are central in the construction of successful quantum field theories, regularization schemes should respect symmetries as much as possible. However, it might happen that a specific symmetry is necessarily broken by any regularization scheme. In this case the symmetry is anomalous, and the underlying theory is in danger of developing an anomaly in the sense that the quantized theory is less symmetric than the corresponding classical theory. Anomalies seriously jeopardize the cancellation of UV divergences, even if the cancellation existed in the presence of the considered symmetry. In this context, one of the most important symmetries is the *chiral symmetry*, which rules the relation between right- and left-handed fermions, because there is no regularization scheme that fully respects all algebraic properties of the Dirac matrix γ_5 as well as Lorentz and gauge symmetry simultaneously—a fact known as the γ_5 problem (see, e.g., Ref. [16] for general facts and Refs. [17–20] for more recent developments and further literature). In spite of the existence of chiral couplings in the standard EW theory, the model does not develop a corresponding anomaly owing to special relations among the quantum numbers within the fermion spectrum. In practice, this means that chiral symmetry might be broken in intermediate steps of calculations, a fact that can seriously complicate higher-order calculations, but complete predictions do respect the symmetry.

10.2.2 Renormalization procedure and renormalization schemes

In the SM briefly outlined above, the mass parameters m_i have been identified such that the squared masses correspond to the locations of the poles of the lowest-order propagators of the corresponding fields. In the full theory, however, m_i does not have this property owing to higher-order corrections. Similarly, coupling parameters c_i appearing in the Lagrangian determine certain processes, such as decay rates, in lowest-order, but the relation between c_i and observables are modified by perturbative corrections as well. Finally, the fields encoding particle creation and annihilation are typically canonically normalized (to produce normalized states) in lowest order, but lose this property owing to corrections. The intended physical meaning of model parameters (e.g. masses and couplings) and the normalization of quantum fields of an underlying theory, generically denoted p and p in the following, can be restored by proper redefinitions, a step known as renormalization.

Marking the initial bare parameters and fields with subscript "0", p_0 and F_0 , the renormalized parameters and fields p and F can be introduced by the renormalization transformation

$$p_0 \equiv Z_p p \equiv p + \delta p, \quad F_0 \equiv Z_F F,$$
 (10.8)

¹The KLN theorem states that singularities cancel in predictions for observables that are "sufficiently inclusive" with respect to the selected initial and final states, a property called *IR safety*. If IR safety cannot be achieved, IR singularities often exhibit *universal factorization properties* allowing for their absorption into non-perturbative quantities, such as *parton distribution* or *fragmentation functions* in the theory of strong interactions (see Section 9 on "Quantum Chromodynamics" in this *Review*).

where Z_p , δp and Z_F are parameter and field renormalization constants, which have to be determined by imposing appropriate renormalization conditions on field-theoretical quantities or physical observables. Assuming that the leading-order quantities p_0 and F_0 already fulfill the conditions, the deviations $\delta Z_i \equiv Z_i - 1$ are due to higher-order corrections. Substituting the bare quantities in favor of the renormalized quantities in the original Lagrangian $\mathcal{L}(p_0, F_0)$ according to (10.8), the leading-order parts of Z_i reproduce the original Lagrangian, $\mathcal{L}(p, F)$, but now parametrized in terms of renormalized quantities p and F, and the parts containing all δZ_i dependence form the counterterm Lagrangian

$$\delta \mathcal{L}(p, F, \delta Z_p, \delta Z_F) = \mathcal{L}(p_0, F_0) - \mathcal{L}(p, F) = \mathcal{L}(Z_p p, Z_F F) - \mathcal{L}(p, F), \tag{10.9}$$

which implies Feynman rules for *counterterm* contributions to Green functions. In other words, the step of renormalization just represents a reparametrization of the original theory.

The choice of renormalization conditions defines the renormalization scheme, which, thus, gives the model parameters their physical meaning. The details of the field renormalization, on the other hand, are merely a matter of convenience without any influence on predictions for observables. In order to avoid mixing between asymptotic states used in the calculation of scattering amplitudes, matrix-valued field renormalization constants Z_F are necessary in general. The form of the renormalization transformation (10.8) corresponds to the multiplicative renormalization of a theory, which might not be general enough in the presence of anomalies, which appear if symmetries observed for a classical Lagrangian do not survive the step of quantization. On the other hand, the use of multiplicative (Z_p) or additive (δp) renormalization constants for parameters is a mere question of taste.

Theories that allow for the complete elimination of UV divergences from predictions are called renormalizable, otherwise they are non-renormalizable. Note that even UV-finite theories require the step of renormalization to define the precise meaning of input parameters, i.e. renormalization is more than eliminating UV divergences. In spite of the fact that predictions of non-renormalizable theories are not free of UV divergences, such theories can often still be exploited in the framework of effective field theories which involve a cutoff scale Λ that sets the order of the maximal energy up to which predictions can be made; for energies above Λ , effects of a more comprehensive UV-complete theory are expected to restore renormalizability.

Giving the model parameters their physical meaning, the renormalization scheme determines the parametrization of predictions for physical observables in terms of the renormalized input parameters p. The actual scheme choice might depend on various factors, such as the accessibility or precision to which a parameter can be determined by experiment, the perturbative stability of predictions, i.e. whether the size of higher-order corrections show the necessary decrease with increasing orders, or the transportability of the input parameters to predictions of observables that are connected to very different energy scales. In practice, a confrontation of a very comprehensive theory, such as the EW SM, with experimental results requires the use of different schemes adapted to different observables, so that a conversion of parameters and fields between different renormalization schemes is necessary. To this end, the renormalized parameters and fields in one scheme have to be expressed in terms of the ones in another scheme. For EW physics two different types of schemes are in use: (i) on-shell (OS) renormalization and (ii) renormalization based on modified minimal subtraction (\overline{MS}) . Some schemes also mix these types of conditions, i.e. different parameters might employ different types of schemes. However, it is crucial that independent renormalization conditions are posed only for truly independent parameters, and that one and the same condition is consistently used for each independent input parameter within a given scheme.

In OS schemes, the renormalization conditions are entailed on S-matrix elements, i.e. on (at least in principle) measurable quantities. Typical examples are OS conditions for masses that tie

mass parameters to the locations of the poles in full propagators, which might be experimentally reconstructed from event kinematics. On-shell conditions for coupling parameters can, e.g., be tied to specific decay widths of particles or specific scattering cross sections in certain kinematic regimes. The advantage of OS schemes often lies in the accessibility of input parameters by experiment and the fact that predictions are rather safe against the introduction of artificial gauge dependences in predictions. On the other hand, MS renormalization has the advantage of maximal simplicity, because MS conditions reduce all renormalization constants to the UV-divergent contributions that are necessary to render all Green functions of the underlying theory UV finite in the framework of dimensional regularization. Moreover, the necessity of keeping all input parameters and fields at their canonical mass dimension introduces an arbitrary renormalization scale $\mu_{\rm ren}$ in the $\overline{\rm MS}$ scheme, so that Green functions obey renormalization group equations (RGEs) which rule the behaviour of input parameters, fields, and Green functions under the change of $\mu_{\rm ren}$ while keeping (all-order) predictions for physical observables fixed. The RGEs can, thus, be used to transport the input quantities from one scale to another, and the residual $\mu_{\rm ren}$ -dependence of predictions, which occurs because the perturbative series is necessarily truncated somewhere, offers a convenient device for estimating (at least part of) the theoretical uncertainty due to missing higher-order corrections.

The concept for renormalization and explicit schemes have been worked out in the 1970s to 1990s for the EW SM in different variants. The idea of EW OS renormalization dates back to Ref. [21] and has, e.g., been worked out in Refs. [22–25]. Electroweak renormalization in the $\overline{\rm MS}$ scheme is, for instance, described in Ref. [26]. A detailed review and more original references can be found in Ref. [27]. Most formulations are restricted to the one-loop level, a complete renormalization framework for the EW SM at the two-loop level is laid out in Refs. [28–30]. The renormalization of the EW SM is considerably more involved than for Quantum Electrodynamics and Quantum Chromodynamics; major issues are:

- Any solution to the γ_5 problem actually goes beyond pure multiplicative renormalization. For instance, in dimensional regularization one of the defining algebraic properties of γ_5 valid in four dimensions has to be abandoned, and counterterms involving *evanescent operators* have to be fixed to restore symmetries. For more details and possible solutions, see, Ref. [16].
- Most particles of the EW SM are unstable, and experimental analyses of W/Z bosons, the Higgs boson, and the top-quark have to be based on event signatures of their decay products. Predictions for resonance processes necessarily go beyond any fixed perturbative order, since lowest-order propagators involve a pole, which diverges, instead of a proper resonance structure, which remains finite. Perturbation theory solves this problem by an infinite power series, known as $Dyson\ series$, of propagator corrections that shifts the pole into the complex k^2 plane for four-momentum transfer k, leading to a Breit-Wigner-like resonance structure with the total decay width of the unstable particle delivering the finite width of the resonance. Identifying the mass square of an unstable particle with the location of the propagator pole, renders the mass of an unstable particle a complex quantity, posing a challenge for the renormalization of the input mass parameter, which is a real quantity. Moreover, the Dyson summation of propagator corrections has to be done with great care, since it necessarily leads to perturbative orders that are only partially included. This jeopardizes the mathematical consistency in predictions, as further discussed at the end of Sec. 10.2.4.
- Non-vanishing vacuum expectation values (vevs) in quantum field theories lead to the appearance of tadpole graphs, which are subdiagrams with exactly one external field leg. It is very convenient to eliminate such diagrams by generating a corresponding tadpole counterterm in the renormalization transformation. It is a matter of choice, defining the tadpole scheme, to generate the tadpole counterterm in the context of parameter renormalization [24, 25, 31]

or field renormalization [28, 32], or both [33]. While predictions within pure OS renormalization schemes do not depend on this choice, predictions employing $\overline{\text{MS}}$ -renormalized mass parameters in general do depend on the tadpole scheme. Since some tadpole schemes are prone to lead to very large higher-order corrections and others introduce gauge dependences in predictions, care is needed in applications, especially in the context of $\overline{\text{MS}}$ -renormalized masses, see, e.g., Ref. [33].

10.2.3 Electroweak input parameter schemes

Starting from its original form, the Lagrangian of the EW SM contains the following free parameters: the couplings g and g' from the gauge interactions, the parameters μ^2, λ from the Higgs potential, and three complex 3×3 matrices y^ℓ, y^u, y^d from the Yukawa interactions of charged leptons and quarks to the Higgs field—there is no such interactions for neutrinos, which are massless in the SM. Owing to possible reparametrizations of the fermion fields that have no effect on observables, not all coefficients of the matrices y^f ($f = \ell, u, d$) are "physical": Only the nine fermion masses $m_{f,i}$, with i = 1, 2, 3 labelling the fermion generations, and four independent variables (three angles and one phase) parametrizing the unitary CKM matrix V^{CKM} describing quark mixing are "physical" and have to be taken from experiment. In total, this makes a set of 17 free parameters of the EW model, which are completed to the full SM input by the strong coupling constant α_s and possibly a non-zero parameter θ quantifying strong CP-violation.

The choice of the input parameters for the fermionic sector is widely independent from the input in the bosonic sector. The use of OS-renormalized lepton masses is uncontroversial and common practice. If perturbative predictions sensitively depend on the masses of light quarks, this is a sign of significant non-perturbative effects and mostly connected to strong interactions. In such cases, an input scheme for the perturbative part of a prediction should be chosen to avoid mass-singular contributions from light quarks; if non-perturbative contributions are unavoidable (such as in the running of the electromagnetic coupling at low energies, in parton distribution, or fragmentation functions) these require dedicated additional input from experiment or non-perturbative calculations. Concerning input and renormalization schemes for heavy quarks (top, bottom, etc., in detail depending on the considered observables), the aspects relevant for EW physics are discussed in Sec. 10.4.3; more details can be found in the "Quantum chromodynamics" and "Heavy-quark and soft-collinear effective theory" sections of this *Review*. The determination and use of the CKM parameters is discussed in the section "CKM Quark-Mixing Matrix".

The original set g, g', μ^2, λ of free parameters of the bosonic sector, in practice, is replaced by an equivalent set of four parameters that are more directly accessible by experiment. Candidates for such parameters are the electromagnetic coupling $\alpha = e^2/(4\pi)$, the weak mixing angle θ_W , the weak-boson masses M_W, M_Z, M_H , and the Fermi constant G_F . The ideal choice of four input parameters, which aims at minimal uncertainty in predictions, depends on actual applications. However, it is crucial to consistently stick to one choice for the set of four parameters within a prediction for an observable, in order to guarantee the self-consistency of the result (finiteness, gauge invariance). Apart from the selection of the set of input parameters, the choice of renormalization scheme for each input parameter matters as well. Below we describe the most important choices of input sets and renormalization schemes, also known as EW input schemes that are used in calculations of EW precision observables and EW corrections to particle processes. All of these schemes take the (OS-renormalized) Higgs-boson mass M_H as direct input, but differ in the choice or scheme of the other three EW parameters (see, e.g., Refs. [27, 34, 35] for more details):

• LEP scheme with input parameters $\alpha(0)$, G_F , M_Z . The W-boson mass M_W can be calculated to high precision in this scheme, exploiting the prediction for muon lifetime τ_{μ} including radiative corrections, which are encoded in the quantity Δr [22]. In most applications the

masses M_Z and M_W are renormalized on-shell, but $\overline{\rm MS}$ masses can be used as well, proper scheme conversion assumed. The evaluation of Δr requires non-perturbative input in terms of the running effect of $\alpha(Q^2)$ from $Q^2=0$ to the EW scale, which is quantified in terms of the quantity $\Delta\alpha(Q^2)$, which in turn is obtained from the R-ratio in e^+e^- annihilation via dispersion relations or from lattice calculations. Since M_W , $c_W \equiv \cos\theta_W^{\rm OS} = M_W/M_Z$, and $s_W \equiv \sin\theta_W^{\rm OS}$ enter the prediction for τ_μ in a rather complicated way, technically M_W is obtained by solving the experimental τ_μ constraint numerically. Calculations for observables other than the W-boson mass, then best proceed in one of the following schemes employing the calculated value for M_W and dropping $\alpha(0)$ or G_F from the input set.

- $\alpha(0)$ -scheme with input parameters $\alpha(0), M_W, M_Z$. The electromagnetic coupling is directly fixed by the fine-structure constant $\alpha(0)^{-1} = 137.035999084(21)$ (see below), and the weak mixing angle by the on-shell relation $c_W \equiv \cos \theta_W^{OS} = M_W/M_Z$. Radiative corrections to most processes at and above the GeV energy range involve the running effect $\Delta \alpha(M_Z^2)$, which then has to be taken as additional non-perturbative input.
- $\alpha(M_Z^2)$ -scheme with input parameters $\alpha(M_Z^2)$, M_W , M_Z . This scheme takes the running coupling constant $\alpha(M_Z^2) \equiv \alpha(0)/[1 \Delta\alpha(M_Z^2)]$ as input instead of $\alpha(0)$ as in the $\alpha(0)$ -scheme. For many processes at and above the EW energy scale, this absorbs the non-perturbative running effects of α into the coupling constant and, thus, into lowest-order predictions, so that no additional non-perturbative input beyond the value of $\alpha(M_Z^2)$ is required in the radiative corrections.
- G_F -scheme with input parameters G_F , M_W , M_Z . In this scheme the electromagnetic coupling α , called α_{G_F} in the following, is derived from the lowest-order prediction for τ_{μ} (i.e. G_F) in the $\alpha(0)$ scheme. This procedure effectively absorbs the correction Δr [22] to muon decay into the electromagnetic coupling, which can be expressed by

$$\alpha_{G_F} \equiv \frac{\sqrt{2}G_F M_W^2 (1 - M_W^2 / M_Z^2)}{\pi} = \alpha(0)[1 + \Delta r]. \tag{10.10}$$

Since muon decay is a charged-current process, the G_F -scheme effectively absorbs the universal corrections related to the transition from the electromagnetic to the weak charged-current interaction into the lowest-order coupling. These universal corrections are intrinsically connected to the ρ -parameter [36, 37], which relates the ratio of neutral- to charged current-current interactions to the corresponding gauge-boson mass ratio and is discussed in more detail in Sec. 10.2.5 below. Similarly, and although not completely, the G_F -scheme also absorbs into the lowest-order weak neutral-current couplings a large part of corrections to the ρ -parameter.

• EW input parameter schemes with the leptonic effective weak mixing angle $\sin^2 \theta_{\text{eff}}^{\ell}$ as free parameter [38] (for the precise definition of $\sin^2 \theta_{\text{eff}}^{\ell}$, see Sec. 10.4.5). Such schemes are motivated by an analysis of neutral-current processes, such as Drell-Yan production, to fit $\sin^2 \theta_{\text{eff}}^{\ell}$ to experimental data and can be obtained from the $\alpha(0)$ -, $\alpha(M_Z^2)$ -, or G_F -schemes upon replacing M_W by $\sin^2 \theta_{\text{eff}}^{\ell}$ in the list of input parameters. Using $\sin^2 \theta_{\text{eff}}^{\ell}$ as input, the renormalized mass M_W is derived from $\sin^2 \theta_{\text{eff}}^{\ell}$ and M_Z via their LO relation, and the renormalization constant δM_W^2 contains the EW corrections contained in the difference $\sin^2 \theta_{\text{eff}}^{\ell} - (1 - M_W^2/M_Z^2)$ from the renormalization scheme change. The schemes should not be used to predict processes where M_W enters already at LO apart from its indirect appearance via gauge couplings, since the derived LO value for M_W is not in line with precision data. Although this mismatch is cured in higher orders, the scheme would be prone to large corrections, e.g., in predictions for charged-current processes.

From the above, it is clear that a judicious choice of the EW input scheme can be used to absorb the universal effects from the running of α and the ρ -parameter into lowest-order predictions, which systematically helps to minimize EW corrections and, thus, to stabilize predictions. Processes dominated by charged- or neutral-current weak interactions at the EW scale or somewhat above are best described in the G_F -scheme, while processes dominated by the electromagnetic interaction are best described by the $\alpha(0)$ or $\alpha(M_Z^2)$ schemes. Which of the two is more appropriate depends on the number of external photons involved that are truly identified as photons, *i.e.* that are distinguishable from low-virtuality photons splitting in $f\bar{f}$ pairs. True on-shell photons effectively couple with strength $\alpha(0)$, while photons that include splittings $\gamma^* \to f\bar{f}$ up to some scale Q effectively couple with strength $\alpha(Q^2)$.

Note that there are many particle processes for which none of the EW input schemes directly absorbs all universal corrections from $\Delta\alpha$ and $\Delta\rho$ (where $\rho=1/(1-\Delta\rho)$) because neither weak nor electromagnetic interactions are dominating all involved couplings. In many cases, however, uniformly² rescaling cross-section contributions that are proportinal to some power α^N according to $\alpha(0)^k\alpha(M_Z^2)^l\alpha_{G_F}^m$ with N=k+l+m can help to absorb these universal corrections into lowest-order predictions. Finally, note that any change in the input value of α comes along with some additive contribution from $\Delta\alpha$ and/or Δr to the EW corrections. More details on optimal scheme choices and the necessary modifications in the renormalization procedure can be found in Ref. [27].

10.2.4 Particle masses

The masses of the SM particles are a cornerstone in the phenomenological input of the EW SM and its extensions. The masses of the leptons are most uncontroversial in this context: The masses of the charged leptons are measured to very high precision, and the instability of the μ and the τ leptons does not entail any problems owing to their long lifetimes (with ratios of width over mass $\sim 10^{-18}$ and $\sim 10^{-12}$, respectively). We note that, despite the knowledge from neutrino oscillations, which imply that said particles posses non-vanishing masses, neutrinos are treated to be massless in the SM. However, because of the smallness of neutrino masses compared to the energy scales in collider experiments, this approximation is valid to high precision in collider physics.

The situation with quarks is rather different and more complicated: Because of quark confinement, the masses of the quarks u, d, s, c, and b are not directly experimentally accessible; their role in EW physics is described in Sec. 10.4.3 below and more generally in Section 60 on "Quark Masses" in this *Review*. The top-quark is special, since it decays before hadronization. Its mass is directly accessible via kinematical reconstruction in collider experiments or through cross section measurements of processes involving top-quarks; see the above-mentioned sections as well.

The masses of the EW gauge bosons Z and W play a key role in EW precision physics. Due to the large ratio of total decay width over mass, $\Gamma_V/M_V \sim 3\%$ with V=Z,W, and the experimental accessibility of their decay signatures, the masses M_Z and M_W can be extracted from the analysis of differential cross sections featuring resonance structures, i.e. via kinematical reconstruction. On the other hand, the significant ratio Γ_V/M_V implies theoretical subtleties in the calculation of predictions for EW observables, as discussed in the subsequent section.

Since the total decay width Γ_H is rather small ($\sim 4\,\mathrm{MeV}$ in the SM), the resonance lineshape of the Higgs boson cannot be resolved at the LHC, and Γ_H is accessible only indirectly with the caveat of model-dependent assumptions. On the other hand, the smallness of $\Gamma_H/M_H \sim 3 \times 10^{-5}$ implies that there are no subtleties in theory predictions for a SM-like Higgs boson originating from its instability.

Up to higher-order corrections, resonances of an unstable particle P are of Breit-Wigner type,

²Uniformly, in this context means that contributions of a given perturbative order are not taken apart, in order to avoid any disturbance in the cancellation of divergences or gauge dependences.

i.e. the scattering matrix elements involve contributions enhanced by propagator factors of the form

$$P_P(p^2) = \frac{1}{p^2 - M_P^2 + iM_P\Gamma_P(p^2)},$$
(10.11)

where p is the momentum transferred by the propagator. If the experimental resolution is of the order of the decay width Γ_P , cross-section predictions featuring this resonance, such as invariant-mass distributions of decay products of P, can be fitted to experimental data with fit values for the mass M_P and $\Gamma_P(M_P^2)$. In detail, the fit result depends on the assumed or predicted momentum dependence of $\Gamma_P(p^2)$. Fitting the resonance structure for a constant width, $\Gamma_P(M_P^2) \equiv \overline{\Gamma}_P$, produces the location

$$\mu_P^2 = \overline{M}_P^2 - i\overline{M}_P \overline{\Gamma}_P \tag{10.12}$$

of the propagator pole in the complex p^2 -plane, and the resulting masses μ_P and \overline{M}_P are called complex and real pole masses of P, respectively. Note, however, that most of the existing results on the Z- and W-boson masses M_V (V=Z,W) have been based on the parametrization $\Gamma_V(p^2)=p^2/M_P^2\times \Gamma_V$ with constant Γ_V , which parametrizes the momentum dependence of propagator corrections near the resonance ($p^2\sim M_V^2$) for the decay of V=Z,W into massless particles. The corresponding mass and width values, M_V and Γ_V , are known as LEP masses and LEP widths, owing to their first use in the analysis of LEP precision data. The two sets of mass and width are related by [39]

$$\overline{M}_V = \frac{M_V}{\sqrt{1 + \Gamma_V^2 / M_V^2}}, \qquad \overline{\Gamma}_V = \frac{\Gamma_V}{\sqrt{1 + \Gamma_V^2 / M_V^2}}, \tag{10.13}$$

in particular implying

$$M_W - \overline{M}_W \approx 27 \,\text{MeV}, \qquad M_Z - \overline{M}_Z \approx 34 \,\text{MeV}, \qquad (10.14)$$

i.e. the scheme differences are much larger than the corresponding experimental uncertainties on the W and Z masses (see next section).

To make use of the masses obtained via fitting resonances, it is necessary to identify renormalization schemes that lead to the parametrizations of the resonances employed in the fit:

- In OS renormalization schemes that identify the renormalized (squared) mass with the real part of the location μ_P^2 of the complex pole of the propagator $G^{PP^{\dagger}}$, the renormalized mass directly corresponds to \overline{M}_P . The location of the propagator pole is identical to the complex position of the zero in the (physical part) of the corresponding inverse propagator, also known as two-point vertex function $\Gamma^{P^{\dagger}P} = -i(G^{PP^{\dagger}})^{-1}$. Since the location of the propagator pole is an intrisine (and measurable) property of the S-matrix, adopting \overline{M}_P as independent input quantity of the theory does not induce any gauge dependences in predictions [40,41]. The OS renormalization for \overline{M}_Z and \overline{M}_W is worked out in Ref. [30, 42] at the two-loop level. The complex-mass scheme [43] (see also [27,44]), which is employed in most EW NLO calculations for resonance processes at the LHC, is an OS renormalization scheme with the complex renormalized mass μ_P based on \overline{M}_P and the (measured or calculated) value of $\overline{\Gamma}_P$.
- Tying the OS renormalized mass to the real zero in Re $\{\Gamma^{P^{\dagger}P}\}$ (which is the prescription in the real OS scheme, see e.g. Refs. [22,24,25]), instead of taking the real part of the complex zero of $\Gamma^{P^{\dagger}P}$, is equivalent at NLO, but not beyond. For the Z and W masses, these differences have, e.g., been worked out in Refs. [27,30,42,45,46], revealing that the Z and W masses in the real OS scheme (based on the zeroes of Re $\{\Gamma^{V^{\dagger}V}\}$, V=Z,W) correspond to the LEP

masses M_Z and M_W introduced above that result from the fit to Breit-Wigner distributions with running widths (at least in the 't Hooft-Feynman gauge). As already pointed out in Ref. [45], using renormalized masses of this real OS scheme to parametrize predictions leads to gauge dependences starting at the two-loop level.³ For predictions beyond NLO precision, the use of \overline{M}_P is, thus, preferable over the use of M_P .

- $\overline{\text{MS}}$ -renormalized masses are not directly related to parameters appearing in any form of Breit–Wigner-like resonances. To extract them from data, one either has to make use of precision calculations for measured observables (such as cross sections or decay widths) with complicated mass dependences, or to convert measured OS masses into the $\overline{\text{MS}}$ scheme. For the Z and W bosons this scheme conversion is carried out in Refs. [47–50].
- Extracting the top-quark mass from kinematical distributions is impeded by strong-interaction effects, limiting the concept of long-distance top-quark masses such as OS-renormalized masses. Perturbative predictions are more stable if a short-distance top-quark mass is employed, such as provided by the $\overline{\rm MS}$ scheme. More details on this subject can be found section "Top Quark" of this Review.

We finally emphasize that the issue of calculating higher-order corrections to processes with unstable particles goes far beyond a proper definition of mass and width of the unstable particle, and beyond parametrizing resonance patterns and identifying resonance parameters with renormalized parameters of the underlying field theory. Issues with gauge invariance, unitarity, UV and IR divergences, and the embedding of resonances into full off-shell processes concern the complete underlying matrix elements. These issues are due to the fact that the identities ruling gauge invariance (Ward and Slavnov-Taylor identities) and finiteness are typically working order by order in perturbation theory, but the inclusion of finite-width effects in resonance propagators originates from a Dyson summation of propagator corrections, necessarily resulting in perturbative orders that are taken into account only partially in predictions. Different solutions to these problems have been described in the literature, targeting at different kinematical situations and different levels of sophistication: If resonances need not be resolved, variants of narrow-width approximations based on production and decay subprocesses might be sufficient (depending on the experimental precision). The neighborhood of resonances can be described via dedicated pole expansions [51,52] of matrix elements leading to pole approximations, as described for single resonances in Refs. [35, 53–58]. The concept of leading pole approximations has also been successfully applied to processes with multiple resonances, see, e.g., Refs. [59–63]. Many modern analyses of many-particle processes even require precision in resonant and non-resonant regions of phase space, as, e.g., provided by the complex-mass scheme [43,44] at NLO. Descriptions of these concepts as well as further references can be found in Ref. [27].

10.2.5 Radiative corrections to electroweak processes

Radiative corrections, in particular the ones induced by the EW interactions, play an integral role in the simulation of EW processes and predictions for corresponding observables analyzed at particle colliders. For instance, for a proper analysis of data collected at the LHC [64–67], most precision calculations have reached the standard that QCD and EW corrections are known at NLO for virtually all EW key processes and even at next-to-next-to-leading order (NNLO) QCD for the $2 \rightarrow 2$ processes [68–70]. The underlying modern methods for calculating radiative corrections are very well advanced and implemented in public tools that make (semi-)automatic calculations possible, depending on their complexity (see, e.g., Refs. [27,71] and references therein). Predictions for specific kinematic configurations, such as low- $p_{\rm T}$ production of W/Z production, might

³This means that all higher-order calculations beyond NLO (including the ones used to extract M_Z and M_W from data) would have to be carried out in the same gauge, or proper parameter conversions would have to be made when changing the gauge.

call for improvements beyond fixed perturbative orders; details and references on the corresponding QCD resummation and parton-shower techniques can be found in Section 9 on "Quantum Chromodynamics" in this *Review*. Event simulations typically require additional improvements on particle emission effects in QCD and QED via matching fixed-order predictions, as provided by dedicated precision Monte Carlo programs or MADGRAPH/MADEVENT [72,73], with *parton showers* and merging them with corrections for higher jet multiplicities based on matrix elements. This matching and merging is provided in different variants within the multi-purpose Monte Carlo event generators HERWIG [74,75], PYTHIA [76], and SHERPA [77–79]. For the analysis of high-precision EW observables (see, *e.g.*, Ref. [80]) even NNLO EW corrections and the dominant effects beyond the two-loop level are relevant.

Different types of radiative corrections to particle processes have to be combined with care in order to avoid double-counting of effects, to respect gauge invariance, and to guarantee a proper cancellations of IR singularities.

- Complicated processes, such as vector-boson scattering, often receive LO contributions from different perturbative orders $\propto \alpha_s^m \alpha^n$, so that already NLO corrections lead to a tower of mixed orders formed by contributions $\propto \alpha_s^{m+1} \alpha^n$ or $\propto \alpha_s^m \alpha^{n+1}$. In such cases, a strict classification of corrections into QCD and EW contributions is not generally possible, but separating the various orders is possible and often instructive.
- Single perturbative orders $\propto \alpha_s^m \alpha^n$ can be further split into gauge-invariant subcontributions by considering contributions featuring closed fermion loops or the emission of fermion—antifermion pairs.⁴ These fermionic corrections can be further classified according to their multiplicity factor N_f^k , where N_f is the number of light fermion flavors. Isolating such subcontributions often helps to locate dominant corrections that warrant the inclusion of higher-order corrections with similar enhancements.
- Since photonic corrections can be potentially large, their separation from the remaining EW corrections is desirable, but this is not always possible in a gauge-invariant way. For processes that feature only neutral-current interactions at LO, this separation can be achieved, however. Arguments for this gauge-invariant separation of QED effects, which can be further decomposed into photonic and fermionic parts as described in the previous item, can be based on the observation that the charged-current sector can be removed from the SM in such a way that a fully consistent "neutral-current theory" with gauge group U(1)_Z×U(1)_{em} results [27]. The separation of photonic corrections was extremely useful in precision calculations for Z production via e⁺e⁻ annihilation at LEP and SLC, e⁺e⁻ → Z/γ* → ff̄, so that the inclusion of higher-order photonic corrections to the Z lineshape was possible without knowing the full EW corrections beyond NLO [34, 35, 54].

The analysis of the Z resonance in $e^+e^- \to Z/\gamma^* \to f\bar{f}$ is a cornerstone of EW precision physics. The separation of the large photonic corrections from the remaining weak corrections to the Z lineshape, in combination with the smallness of the irreducible (box) weak corrections near the Z resonance, is the basis of the parametrization of the cross section and its asymmetries in terms of pseudo-observables, such as the Z peak cross section, the total and partial Z decay widths, forward–backward (FB) as well as polarization asymmetry variables, effective Z couplings, and the effective weak mixing angle for each fermion f quantified by $\bar{s}_f^2 \equiv \sin^2\theta_{\rm eff}^f$, etc. (see Section 10.4 for a precise definition of these quantities). The Z-pole pseudo-observables can be predicted to high precision, independent of the full prediction of the Z-boson lineshape, and play a key role in the global SM fit to data:

⁴This is due to the fact that adding or removing fermion generations to or from the SM respects gauge invariance. (Working in a field basis corresponding to mass eigenstates, the added/removed generations should not mix with the other generations.)

 \bullet EW corrections to the Z-pole pseudo-observables comprise (flavor-dependent) Zff vertex

a closed fermion loop).

- corrections (see, e.g., Refs. [24, 81]) as well as (flavor-independent) contributions to the $\gamma\gamma$, γZ , ZZ, and WW gauge-boson self-energies (i.e.vacuum polarization diagrams), the latter entering via EW renormalization constants (see, e.g., Refs. [24,25]). While being gauge dependent in general, there are several distinct and important contributions from gauge-boson self-energies that lead to gauge-invariant corrections to EW precision observables, in particular contributions from closed fermion loops and the corresponding QCD corrections. For instance, the mixed QCD–EW contributions to gauge-boson self-energies of orders $\alpha\alpha_s m_t^2$ [82, 83], $\alpha\alpha_s^2 m_t^2$ [84, 85], and $\alpha\alpha_s^3 m_t^2$ [86–88] increase the predicted value of m_t by 6%.⁵ The sub-leading $\alpha\alpha_s$ corrections [89–93] are also included in the predictions for the Z-pole pseudo-observables. Further three-loop corrections of order $\alpha\alpha_s^2$ [94, 95], $\alpha^3 m_t^6$, $\alpha^2\alpha_s m_t^4$ [96, 97], α_f^3 and $\alpha_f^2\alpha_s$ [98, 99] are rather small (here α_f denotes EW corrections with
- Z-pole pseudo-observables are among the still very few examples for which complete NNLO EW corrections are known. The EW two-loop corrections for the relation between \bar{s}_{ℓ}^2 and s_W^2 are given in Refs. [100–105], the ones to \bar{s}_f^2 ($f \neq \text{top}$), the effective couplings of fermions f to the Z boson, and the partial and total Z decay widths in Refs. [58, 106–110].
- All EW observables that depend on the weak mixing angle θ_W in LO receive contributions from its renormalization, in particular significant corrections from the ρ parameter [36, 37], $\rho = 1/(1 \Delta \rho)$, as defined from the neutral-to-charged-current cross-section ratio at low energies, *i.e.*

$$\Delta \rho = \frac{\Sigma_{\rm T}^{ZZ}(0)}{M_Z^2} - \frac{\Sigma_{\rm T}^{WW}(0)}{M_W^2},\tag{10.15}$$

where $\Sigma_{\mathrm{T}}^{VV}(0)$ is the (transverse part of the) Z/W boson self-energy at zero momentum transfer, following the notation of Refs. [24, 25, 27]. The largest contribution $\Delta \rho_t$ to $\Delta \rho$,

$$\Delta \rho_t = \frac{3G_F m_t^2}{8\sqrt{2}\pi^2} = 0.00934 \times \frac{m_t^2}{(172.61 \text{ GeV})^2} , \qquad (10.16)$$

results from one-loop diagrams with closed fermion loops involving the top-quark. Two-loop corrections involving the top-quark modify $\Delta \rho_t$ by

$$\Delta \rho_t \to \Delta \rho_t \left[1 + R(M_H, m_t) \frac{\Delta \rho_t}{3} \right]$$
 (10.17)

The function $R(M_H, m_t)$ can be described as an expansion in M_Z^2/m_t^2 , for which the leading m_t^4/M_Z^4 [111,112] and next-to-leading m_t^2/M_Z^2 [113,114] terms are known. Beyond the two-loop level, leading top-mass-enhanced contributions to $\Delta \rho$ have been calculated to the orders $\alpha_s^2 \alpha m_t^2$ [84,85,95], $\alpha_s \alpha^2 m_t^4$ and $\alpha^3 m_t^6$ [96,97], and $\alpha_s^3 \alpha m_t^2$ [86–88].

The extraction of the W-boson mass M_W from the measured muon decay lifetime (or Fermi constant) is another cornerstone in the fit of the SM to precision observables. In detail, M_W is obtained by solving the implicit equation (10.10) for M_W , where the Fermi constant G_F is extracted from the measured muon lifetime (see Section 10.3.2) and the quantity Δr [22] represents the radiative corrections to muon decay. At NLO, the correction Δr receives sizeable contributions from $\Delta \alpha$ and $\Delta \rho$ of $\sim +6\%$ and $\sim -3\%$, respectively, leaving only a small remainder $\Delta r_{\rm rem}$ of $\sim 1\%$,

$$\Delta r^{(1)} = \Delta \alpha - \frac{c_W^2}{s_W^2} \Delta \rho + \Delta r_{\text{rem}} . \qquad (10.18)$$

⁵This is, however, almost entirely an artifact of using the pole mass definition for m_t . The equivalent corrections when using the $\overline{\text{MS}}$ definition $\widehat{m}_t(\widehat{m}_t)$ increase m_t by less than 0.5%.

The complete two-loop calculation of Δr in the OS renormalization scheme has been performed in Refs. [42,115–118]. The two-loop QCD correction of order $\alpha \alpha_s$ and the fermionic⁶ electroweak two-loop correction of order α^2 amount to about 10% of the one-loop correction to Δr , both with the same sign, $\sim +0.4\%$ and $\sim 0.3\%$, respectively. The three-loop QCD correction, $\alpha \alpha_s^2$, amounts to $\sim 0.07\%$ while the bosonic two-loop electroweak correction is very small ($\sim 0.006\%$). Taking into account leading higher-order effects from $\Delta \rho$, the theoretical uncertainty from unknown higher-order corrections is estimated to 4 MeV for the prediction of M_W [119]. In an alternative approach, Ref. [120] obtained the $\overline{\rm MS}$ quantities $\Delta \hat{r}$ and $\hat{\rho}$ to two-loop accuracy, confirming the prediction of M_W in the OS scheme from Refs. [42, 119] within about 4 MeV. More recently, Δr has been calculated within an alternative ("tadpole-free") version of EW $\overline{\rm MS}$ renormalization at the two- and three-loop levels in Refs. [121, 122], respectively, the latter in the approximation of the "gauge-less limit"; the calculations within this scheme, however, have not yet been applied to predictions for the OS-renormalized W-boson mass.

Throughout this Review we utilize predictions for EW precision observables including the relevant EW radiative corrections from the programs Gfitter [123–126] and HEPfit [127–131]. Both Gfitter and HEPfit follow the OS renormalization scheme in their implementations of the radiative corrections for EW precision observables, in contrast to the GAPP package [132], used in the fits presented in previous editions of this Review, which works entirely in the $\overline{\rm MS}$ scheme. Observables including corrections beyond NLO, such as the W-boson mass, the effective weak mixing angle(s), and the pseudo-observables at the Z resonance are implemented via the semi-analytical approximations provided in Refs. [105, 106, 110, 119]. The uncertainties from missing higher-order corrections on the different (pseudo-)observables are also taken into account, using the estimates given in those references, in the computation of the SM predictions. The W-boson decay width is computed at the one-loop level, using the expressions in Refs. [55, 133, 134] (in agreement with the independent results of Ref. [135]). This observable is currently known with comparatively lower precision than those at the Z pole, but the corresponding theory uncertainty is still smaller than the experimental precision.

Several other tools are available in the literature for the calculation of EW corrections to the considered (pseudo-)observables and to perform the EW fit. The package GRIFFIN [58] provides a framework for the calculation of $2 \to 2$ fermion processes which, in its current version provides the full NNLO and the leading higher-order corrections for processes at the Z pole. Among the different codes for calculating EW precision observables available in the literature, ZFITTER has a prominent place [136, 137], due to its key role in the original studies of the LEP Electroweak Working Group [138, 139].

After this overview of the practical aspects relevant to SM calculations in the EW sector, we next discuss some of the most important observables that validate the SM description of EW interactions.

10.3 Low-energy observables

10.3.1 The electromagnetic coupling

As in pure QED, the coupling constant e is identified with the electromagnetic coupling strength of physical (on-shell) electrons in the limit of low-energy transfer (Thomson limit), i.e., e is the electric unit charge of classical electrodynamics.⁷ This OS renormalization of e in the Thomson

 $^{^6}$ Fermionic contributions at NNLO denote contributions from diagrams with closed fermion loops, whereas bosonic contributions are all remaining two-loop diagrams.

⁷ Thirring's QED theorem [140], which is valid in the EW theory as well [141], makes this link between quantum field theory and classical electrodynamics very explicit, as it states that the Compton scattering cross section turns into the classical Thomson cross section in the low-energy limit, *i.e.*, the radiative corrections to Compton scattering vanish in the Thomson limit to all perturbative orders.

limit ensures the property of *charge universality*, *i.e.* it guarantees that, in this limit, one can renormalize e via the electromagnetic interaction of any fermion (actually any charged particle), obtaining the same result as for electrons.

The fine structure constant $\alpha(0) \equiv e^2/(4\pi)$ can be extracted from the anomalous magnetic moment of the electron, $a_e = (1\,159\,652\,180.59 \pm 0.13) \times 10^{-12}$ [142]. Application of QED corrections up to five-loop order [143–145] produces the value $\alpha(0)^{-1} = 137.035\,999\,166(15)$. Here, the number in parentheses denotes the uncertainty in the last digits shown. This determination of $\alpha(0)^{-1}$ from a_e has recently been re-evaluated [146], updating the tenth-order QED term of a_e and the evaluation of the hadronic vacuum polarization (HVP) contribution, finding a slightly smaller value $\alpha(0)^{-1} = 137.035\,999\,163(15)$. Another approach combines measurements of the Rydberg constant and atomic masses with interferometry of atomic recoil kinematics. Applied to 87 Rb [147] and 133 Cs [148], this method implies the results $\alpha(0)^{-1} = 137.035\,999\,206(11)$ and $\alpha(0)^{-1} = 137.035\,999\,046(27)$, respectively. These two measurements differ by 5.5 σ , where the origin of this discrepancy is currently not understood. While it is not advisable to combine measurements with such a tension, it is worth pointing out that the absolute magnitude of this discrepancy is at a level where it has no significant impact on the EW fit. We use the value quoted in Section 1 ("Physical Constants") in this Review,

$$\alpha(0)^{-1} = 137.035999084(21), \tag{10.19}$$

which is a combination of the results from a_e and atomic interferometry.

As explained in Section 10.2.3, in EW higher-order calculations it can be convenient to define a running α dependent on the energy scale of the process, with $\alpha(0)^{-1} \approx 137.036$ appropriate at very low energy, *i.e.* close to the Thomson limit. The L3 [149] and OPAL [150] collaborations at LEP could also observe the running directly in small and large angle Bhabha scattering, respectively. For scales above a few hundred MeV the low-energy hadronic contribution to the electromagnetic vacuum polarization introduces a theoretical uncertainty in α , so that it is often convenient to use the value

$$\alpha(M_Z^2) = \frac{\alpha(0)}{1 - \Delta\alpha(M_Z^2)} \tag{10.20}$$

as phenomenological input, where $\Delta\alpha(M_Z^2)$ contains the running effects of $\alpha(Q^2)$ from $Q^2=0$ to $Q^2=M_Z^2$. In particular, the hadronic contribution $\Delta\alpha_{\rm had}^{(5)}(M_Z^2)$, corresponding to five active quark flavors (i.e. without top-quark contribution) driving the running, is a non-perturbative input obtained from measurements of the R ratio in e^+e^- annihilation at low energies, and perturbative QCD predictions of R at medium and large energies. Various evaluations of $\Delta\alpha_{\rm had}^{(5)}(M_Z^2)$ are summarized in Table 10.1.

The quantity $\alpha(Q^2)$ is closely related to the running electromagnetic coupling $\widehat{\alpha}(Q^2)$ in the $\overline{\rm MS}$ scheme⁸ [26] used in previous editions of this *Review*. With $\alpha_s(M_Z^2)=0.1187\pm0.0017$ we have $\widehat{\alpha}^{(4)}(m_\tau^2)^{-1}=133.450\pm0.006$ and $\widehat{\alpha}^{(5)}(M_Z^2)^{-1}=127.930\pm0.008$ for four and five active quark flavors, respectively. The precise relation between $\alpha(M_Z^2)$ and $\widehat{\alpha}(M_Z^2)$ is determined by the

⁸In this Section we denote quantities defined in the $\overline{\rm MS}$ scheme by a caret; the exception is the strong coupling constant, α_s , which will always correspond to the $\overline{\rm MS}$ definition and where the caret will be dropped. Furthermore, $\alpha^{(n)}$ and $\alpha_s^{(n)}$ denote the running couplings with n active quark flavors.

Table 10.1: Evaluations of the on-shell $\Delta \alpha_{\rm had}^{(5)}(M_Z^2)$ by different groups. For better comparison we adjusted central values and errors to correspond to a common and fixed value of $\alpha_s(M_Z^2) = 0.120$, except for Ref. [155], for which α_s is not an explicit input. References quoting results without the top-quark decoupled are converted to the five flavor definition. Ref. [156] uses $\Lambda_{\rm QCD} = 380 \pm 60$ MeV; for the conversion we assumed $\alpha_s(M_Z^2) = 0.118 \pm 0.003$.

Reference	Result	Comment
Krasnikov, Rodenberg (1997) [157]	0.02737 ± 0.00039	pQCD for $\sqrt{s} > 2.3 \text{ GeV}$
Kühn & Steinhauser (1998) [158]	0.02778 ± 0.00016	full $\mathcal{O}(\alpha_s^2)$ for $\sqrt{s} > 1.8$ GeV
Groote et al. (1998) [156]	0.02787 ± 0.00032	use of QCD sum rules
Martin et al. (2000) [159]	0.02741 ± 0.00019	incl. new BES data
de Troconiz, Yndurain (2001) [160]	0.02754 ± 0.00010	pQCD for $s > 2 \text{ GeV}^2$
Burkhardt, Pietrzyk (2011) [161]	0.02750 ± 0.00033	pQCD for $\sqrt{s} > 12 \text{ GeV}$
Erler, Ferro-Hernández (2017) [162]	0.02761 ± 0.00010	conv. from $\overline{\rm MS}$ scheme
Jegerlehner (2019) [163]	0.02755 ± 0.00013	Euclidean split technique
Davier et al. (2019) [164]	0.02761 ± 0.00010	pQCD for $\sqrt{s} = 1.8-3.7 \& > 5 \text{ GeV}$
Keshavarzi $et \ al. \ (2019) \ [165]$	0.02761 ± 0.00011	pQCD for $\sqrt{s} > 11.2 \text{ GeV}$
Cè et al. (2022) [155]	0.02773 ± 0.00015	LQCD for Euclidian $Q^2 < 5 \text{ GeV}^2$

difference in $\Delta\alpha(M_Z^2)$ (obtained using Refs. [151,152]),

$$\Delta \widehat{\alpha}(M_Z^2) - \Delta \alpha(M_Z^2) = \frac{\alpha}{\pi} \left[\frac{100}{27} - \frac{1}{6} - \frac{7}{4} \ln \frac{M_Z^2}{M_W^2} + \frac{\alpha_s(M_Z^2)}{\pi} \left(\frac{605}{108} - \frac{44}{9} \zeta(3) \right) \right. \\
+ \frac{\alpha_s^2}{\pi^2} \left(\frac{976481}{23328} - \frac{253}{36} \zeta(2) - \frac{781}{18} \zeta(3) + \frac{275}{27} \zeta(5) \right) \\
+ \frac{\alpha_s^3}{\pi^3} \left(\frac{1483517111}{3359232} - \frac{22781}{144} \zeta(2) - \frac{3972649}{7776} \zeta(3) - \frac{31}{81} \zeta(2)^2 + \frac{521255}{7776} \zeta(5) \right. \\
- \frac{7315}{324} \zeta(7) + \frac{5819}{54} \zeta(2)\zeta(3) + \frac{14675}{162} \zeta(3)^2 \right] = 0.007122(2)(5) , \tag{10.21}$$

where the first part of the lowest-order term is from fermions and the other two are from W^{\pm} loops, which are usually excluded from the OS definition. Fermion mass effects and corrections of $\mathcal{O}(\alpha^2)$ contributing to Eq. (10.21) are small, partly cancel each other and are not included here. The first error in Eq. (10.21) is parametric from α_s and the second is from the truncation of the perturbative expansion.

The most recent results of $\Delta\alpha_{\rm had}^{(5)}(M_Z^2)$ [162–165] typically assume the validity of perturbative QCD (pQCD) at scales of about 2 GeV and above for the continuum contribution and are in good agreement with each other. In regions where pQCD cannot be trusted, one can use $e^+e^- \to {\rm hadrons}$ cross-section data (for a list of references see, e.g., Ref. [164]) and isospin rotated information derived from τ decay spectral functions [166], where the latter derive from ALEPH [167], Belle [168], CLEO [169], and OPAL [170]. More recently, new results at low energy $(\pi^+\pi^-)$ have been published from the CMD-3 experiment [171] at the e^+e^- collider VEPP-2000. There is noticeable spread

 $^{^{9}\}alpha(M_Z^2)$ is directly evaluated in the $\overline{\rm MS}$ scheme using the FORTRAN package GAPP [132], including the QED contributions of both leptons and quarks. The leptonic three-loop [153] and four-loop [154] contributions in the OS scheme are known as well.

in the existing results, with lattice QCD [155] and CMD-3 suggesting a stronger running than KLOE data. While VEPP-2000 and VEPP-4M scanned center-of-mass (CM) energies up to 2 GeV and between about 3 and 4 GeV, respectively, the BABAR collaboration studied multi-hadron events radiatively returned from the $\Upsilon(4S)$, reconstructing the radiated photon and normalizing to $\mu^+\mu^-\gamma$ final states. A discrepancy in the $e^+e^-\to\pi^+\pi^-$ data from BABAR and KLOE has been taken into account in Ref. [164] as an additional uncertainty. The new results from CMD-3 cannot be included in determinations of $\Delta\alpha_{\rm had}^{(5)}(M_Z^2)$ without introducing additional uncertainties to accommodate for the discrepancy with KLOE data or taking into account small p-values. We use the value $\Delta\alpha_{\rm had}^{(5)}(M_Z^2)=0.02760\pm0.00010$ from Ref. [164] in our fit, which has been obtained for $\alpha_s(M_Z^2)=0.1193\pm0.0028$. The dependence on $\alpha_s(M_Z^2)$ is taken into account in the fit. The uncertainty on $\Delta\alpha_{\rm had}^{(5)}(M_Z^2)$ is dominated by systematic effects in the cross-section data and the uncertainty in the pQCD prediction.

10.3.2 The Fermi constant

Owing to its extraordinarily high experimental precision, the Fermi constant G_F is often taken as input in the EW model, e.g., replacing the electromagnetic coupling α or the W-boson mass M_W in the list of input parameters. The parameter G_F is derived from the muon lifetime $\tau_{\mu} = 2196981.1 \pm 2.2$ ps, obtained in the Particle Listings in this Review. The average is dominated by the result of the MuLan Collaboration [172, 173] at the PSI that reduced the uncertainty by an order of magnitude compared to previous results. The Fermi constant is derived from τ_{μ} according to τ_{μ}

$$\frac{\hbar}{\tau_{\mu}} = \frac{G_F^2 m_{\mu}^5}{192\pi^3} F(\rho) \left[1 + H_1(\rho) \frac{\widehat{\alpha}(m_{\mu}^2)}{\pi} + H_2(\rho) \frac{\widehat{\alpha}^2(m_{\mu}^2)}{\pi^2} + H_3 \frac{\widehat{\alpha}^3(m_{\mu}^2)}{\pi^3} \right] , \qquad (10.22)$$

where $\rho = m_e^2/m_\mu^2$, $\hat{\alpha}(Q^2)$ is the electromagnetic coupling in the $\overline{\rm MS}$ scheme, and

$$F(\rho) = 1 - 8\rho + 8\rho^3 - \rho^4 - 12\rho^2 \ln \rho = 0.99981295 , \qquad (10.23a)$$

$$H_1(\rho) = \frac{25}{8} - \frac{\pi^2}{2} - \left(9 + 4\pi^2 + 12\ln\rho\right)\rho + 16\pi^2\rho^{3/2} + \mathcal{O}(\rho^2) = -1.80793 , \qquad (10.23b)$$

$$H_2(\rho) = \frac{156815}{5184} - \frac{518}{81}\pi^2 - \frac{895}{36}\zeta(3) + \frac{67}{720}\pi^4 + \frac{53}{6}\pi^2 \ln 2 - (0.042 \pm 0.002)_{\text{had}} - \frac{5}{4}\pi^2\sqrt{\rho} + \mathcal{O}(\rho) = 6.64 , \qquad (10.23c)$$

$$\widehat{\alpha}(m_{\mu}^2)^{-1} = \alpha^{-1} + \frac{1}{3\pi} \ln \rho + \mathcal{O}(\alpha) = 135.901 \ . \tag{10.23d}$$

 H_1 , H_2 , and H_3 capture the QED corrections within the Fermi model. The results for $\rho = 0$ have been obtained in Refs. [174] and [175,176] for H_1 and H_2 , respectively, where the term in parentheses is from the hadronic vacuum polarization [175]. The mass corrections to H_1 and H_2 have been calculated in [177] and [178], respectively. Notice the term linear in m_e in H_2 whose appearance was unforeseen and can be traced to the use of the muon pole mass in the prefactor [178]. The coefficient $H_3 = -15.3 \pm 2.3$ has been estimated in Refs. [179–181].

The estimation of H_3 reduces the uncertainty from missing higher orders significantly, resulting in

$$G_F = 1.1663785(6) \times 10^{-5} \text{ GeV}^{-2},$$
 (10.24)

where the remaining uncertainty in G_F is mostly from experimental sources in the measurement of τ_{μ} .

¹⁰In the spirit of the Fermi theory, the small propagator correction, $3/5 m_{\mu}^2/M_W^2$, is included into the correction Δr (see below). This is also the convention adopted by the MuLan collaboration [172]. While this breaks with historical consistency, the numerical difference was negligible in the past.

10.3.3 The muon anomalous magnetic moment

In 2025 the Muon g-2 Collaboration at Fermilab has released a new measurement [182] of the muon anomalous magnetic moment $a_{\mu} \equiv (g_{\mu} - 2)/2$, based on theirs Runs 4–6, which combines with their previous result from Runs 1–3 [183, 184] to

$$a_{\mu}^{\text{FNAL}} = (116592070.5 \pm 14.8) \times 10^{-11} \ . \tag{10.25}$$

Combining the FNAL result with the result from the BNL E821 collaboration [185], which is compatible with all FNAL results on a_{μ} , leads to the world average

$$a_{\mu}^{\text{exp}} = (116592071.5 \pm 14.5) \times 10^{-11} \ .$$
 (10.26)

This experimental result is in good agreement with the SM prediction released in the 2025 White Paper (WP25) [146],

$$a_{\mu}^{\text{SM}} = (116592033 \pm 62) \times 10^{-11} ,$$
 (10.27)

which contains a significant upward shift with respect to the previous SM prediction reported in the 2020 White Paper (WP20) [186], resolving a long-standing tension of $\sim 2-4\,\sigma$ between experiment and theory.

The by far dominating contribution to $a_{\mu}^{\rm SM}$ is due to QED corrections, which have been calculated to five loops [143, 145, 187–189] (fully analytic to three loops [190–194]). The SM EW contribution [195–200], reported in [146] to $a_u^{\text{EW}} = (154.4 \pm 4.0) \times 10^{-11}$, includes two-loop [201–205] and leading three-loop [206, 207] corrections and is roughly an order of magnitude larger than the current experimental uncertainty. The major part of the theory uncertainties result from HVP effects, which were entirely taken from lattice-QCD calculations in WP25 (see references therein). The small, but non-negligible NLO and NNLO HVP contributions are taken from mixing data from $e^+e^- \to \text{hadrons}$ with perturbative QCD predictions, with the corresponding uncertainties. The switch from the previously used experimental HVP results from $e^+e^- \to \text{hadrons}$ cross sections to lattice results accounts for the significant change in $a_{\mu}^{\rm SM}$ from WP20 to WP25. This paradigm shift was justified in WP25 in part by the great consolidation of lattice HVP results in recent years and in part by the increasing tension among the relevant experimental $e^+e^- \to \pi^+\pi^-$ cross-section data after including recent measurements by CMD-3 [171, 208]. The second largest uncertainty in a_u^{SM} is due to effects from hadronic light-by-light (HLbL) scattering. In the step from WP20 to WP25, the predictions for HLbL effects, both on the lattice and data-driven side (see WP25 for references) have increased in precision and show good mutual agreement. Further reducing the theory uncertainty in a_{μ}^{SM} and resolving the tension between lattice and data-driven HVP determinations will be an important goal for future work. For more details and references, see Section 56 on the "Muon Anomalous Magnetic Moment" in this Review.

The results on a_{μ} have not been taken into account in the SM fit to data below, because they do not influence the fit significantly. The sensitivity of $a_{\mu}^{\rm SM}$ to the EW parameters is way below the remaining theory uncertainty. On the other hand, predictions for a_{μ} are sensitive to new physics effects, such as in supersymmetric models with large $\tan \beta$ and moderately light superparticle masses [209], or a dark Z boson [210].

10.4 Electroweak precision physics

10.4.1 Z- and W-boson masses and widths

The most precise measurement of the mass of the Z boson has been obtained by a combination of the ALEPH, DELPHI, L3, and OPAL data from LEP 1 [138],

$$M_Z = 91.1876 \pm 0.0021 \,\text{GeV}$$
 (10.28)

The uncertainty in this result is dominated by the knowledge of the LEP beam energy. Recently, new results from hadron colliders have been obtained. The CDF Collaboration determined M_Z from fits to the dimuon and dielectron mass distributions [211], resulting in $M_Z = 91.1920 \pm 0.0075$ GeV and 91.1943 ± 0.0158 GeV, respectively. The CMS Collaboration used $Z \to \mu^+\mu^-$ decays and obtained $M_Z = 91.1858 \pm 0.0048$ GeV [212], with an uncertainty only about two times larger than the LEP 1 combination. We note that this result is not independent of the previous M_Z determinations, as these were included to define the systematic uncertainty in the muon momentum scale calibration. The LHCb Collaboration used $Z \to \mu^+\mu^-$ decays only and obtained a value of 91.1842 ± 0.0093 GeV [213], which will be included in future combinations of M_Z . We use the current world average

$$M_Z = 91.1880 \pm 0.0020 \,\text{GeV},$$
 (10.29)

in the fit, obtained from the LEP I average and the CDF result.

The values above correspond to a definition based on a Breit–Wigner shape with an energy-dependent width, which differs from \overline{M}_Z derived from the complex location of the propagator pole as given in Eq. (10.14).

The LEP 1 results also include a determination of the total Z-boson decay width with a precision of one per-mil [138,214],

$$\Gamma_Z = 2.4955 \pm 0.0023 \,\text{GeV}.$$
 (10.30)

Among the most important LEP 2 results were the measurements [215] of the W-boson mass, M_W , which were dominated by kinematic reconstruction, but included the complementary albeit statistics limited and thus much less precise determination from a WW threshold cross-section measurement.¹¹ The kinematic method was also employed at the Tevatron [216] and by ATLAS [217] and LHCb [218] at the LHC. A combination [219] of all M_W measurements available until 2023, using a careful calibration of simulation tools and PDFs, obtained the world average,

$$M_W = 80.395 \pm 0.012 \text{ GeV}$$
 (10.31)

However, the χ^2 probability of this combination is 0.5% or less, depending on the chosen PDF set, which is mostly due to the W-mass measurement by CDF from Run II at the Tevatron [211], $M_W = 80.432 \pm 0.016$ GeV (adjusted to the common PDF set CT18 [220] in Ref. [219]). It differs by almost 4σ from the other measurements of M_W , while the latter agree well among each other, with the average [219]

$$M_W = 80.369 \pm 0.013 \text{ GeV}$$
, (10.32)

without CDF II. In 2024, the ATLAS result has been updated [221], resulting in a significant downward shift of M_W . Most recently, the CMS collaboration has presented their first determination of M_W in Ref. [212]. Adjusted for the same CT18 PDF set used in Eq. (10.32) they find $M_W = 80.3618 \pm 0.010$ GeV. This value is in agreement with both the SM and previous determinations from LEP 2, DØ, ATLAS, and LHCb, and increases the tension of the latest CDF value of Ref. [211] with other existing measurements. For the global fits presented later in this review, in absence of an official combination of the different values of M_W , we will use the value in Eq. (10.32), i.e. without the CDF result, as recommended by the authors of Ref. [219] and consistent with what is reported in Section 54 on the "Mass and Width of the W Boson" in this Review. Again, these

¹¹LEP 2 [215] ran at several energies above the Z pole up to \sim 209 GeV. Measurements were made of a number of observables, including the total production cross sections of $f\bar{f}$ pairs for $f=\mu,\tau$, and q (hadrons), of four-fermion final states, of $\gamma\gamma$, ZZ, WW and $WW\gamma$. The differential cross sections for all three lepton flavors, and the leptonic and hadronic W branching ratios were also extracted, as discussed in Section 10.4.7. The measurements of single-and di-boson production were also used to set constraints on anomalous triple and quartic gauge couplings. These anomalous interactions have also been studied in hadron collisions at the Tevatron and the LHC. We refer the reader to the "Extraction of Triple Gauge Couplings (TGCs)", "Anomalous W/Z Quartic Couplings (QGCs)" notes in the W particle listing and the "Anomalous $ZZ\gamma$, $Z\gamma\gamma$, and ZZV Couplings" note in the Z particle listing for details.

values on M_W correspond to an energy-dependent W width in the resonance propagator and differ from \overline{M}_W from the complex location of the propagator pole as given in eq. (10.14).

The ATLAS update in [221] also included the first LHC measurement of the W-boson width, $\Gamma_W = 2.202 \pm 0.047$ GeV, the most precise single measurement of this quantity. When derived simultaneously with M_W , the two measurements show a 30% anticorrelation. Although consistent with the LEP 2 determination [215], the new and more precise ATLAS Γ_W value differs by about 2σ from the Tevatron result [222] and the SM prediction.

For more details and references, see Section 54 on the "Mass and Width of the W Boson" in this Review.

10.4.2 Higgs-boson mass and width

After their discovery of the Higgs boson [223, 224], the LHC experiments ATLAS and CMS have performed high precision measurements of its mass, M_H . We average the results, $M_H = 125.11 \pm 0.09_{\rm stat.} \pm 0.06_{\rm syst.}$ GeV from ATLAS [225] and $M_H = 125.04 \pm 0.11_{\rm stat.} \pm 0.05_{\rm syst.}$ GeV from CMS [226], by treating the smaller systematic error as common among the two determinations, and arrive at,

$$M_H = 125.08 \pm 0.07_{\text{stat.}} \pm 0.05_{\text{syst.}} \text{ GeV (LHC)}$$
 (10.33)

Measurements of the Higgs-boson width Γ_H at the LHC are based on the comparison between offshell and on-shell Higgs boson production rates assuming the validity of the SM. The most precise results are $\Gamma_H = 3.0^{+2.0}_{-1.5}$ MeV from CMS [226] and $\Gamma_H = 4.3^{+2.7}_{-1.9}$ MeV from ATLAS [227]. Both measurements are compatible with the SM prediction $\Gamma_H = 4.10 \pm 0.06$ MeV [228]. Owing to the smallness of $\Gamma_H/M_H \sim 3 \times 10^{-5}$, there is no significant difference between the two variants of OS masses and widths $(M_H, \Gamma_H \text{ versus } \overline{M}_H, \overline{\Gamma}_H)$ at the current (and most likely also future) level of precision.

For further references and more details on Higgs-boson properties, see Section 11 on the "Status of Higgs Boson Physics" in this *Review*.

10.4.3 Quark masses

The top-quark mass m_t , being the largest mass in the SM, plays a prominent role in the description of the EW sector, inducing some of the largest fermionic radiative corrections to EW precision observables. As in the case of the other SM parameters that can be obtained indirectly from the EW precision fit, it is important to have direct determinations of m_t to perform consistency tests of the SM. The top-quark mass has been measured in top quark decays by directly reconstructing the decay products, also known as "direct measurements", by the Tevatron collaborations, CDF and DØ, in leptonic, hadronic, and mixed channels with the result [229],

$$m_t = 174.30 \pm 0.35_{\text{stat.}} \pm 0.54_{\text{syst.}} \text{ GeV (Tevatron)}$$
 (10.34)

Likewise, using data from CM energies $\sqrt{s} = 7$ and 8 TeV (Run 1), ATLAS and CMS (including alternative technique measurements) at the LHC obtained [230],

$$m_t = 172.52 \pm 0.14_{\text{stat.}} \pm 0.30_{\text{syst.}} \text{ GeV (LHC Run 1)}.$$
 (10.35)

In addition, there are results derived from $\sqrt{s}=13$ TeV data (Run 2). The CMS collaboration obtained $m_t=171.77\pm0.37_{\rm tot.}$ GeV [231] in the lepton+jets channel with a kinematic fit of the decay products combined with a profile likelihood method. Using the same channel, CMS measured $m_t=173.06\pm0.24_{\rm stat.}\pm0.80_{\rm syst.}$ GeV [232] using a template fit to the jet mass in hadronic decays of highly boosted top quarks. In addition, CMS reports $m_t=172.33\pm0.14_{\rm stat.}\pm0.69_{\rm syst.}$ GeV [233] in the dilepton channel, $m_t=172.34\pm0.20_{\rm stat+JSE}\pm0.70_{\rm syst.}$ GeV [234] in the all-jets channel, and $m_t=172.13\pm0.32_{\rm stat.}\pm0.70_{\rm syst.}$ GeV [235] in t-channel single top

events (leptonic decays), where the uncertainty named stat+JSE denotes the combination of the statistical uncertainty and the uncertainty in the jet energy scale. A comprehensive summary of the CMS measurements of the top-quark mass is given in Ref. [236]. ATLAS measured $m_t = 174.41 \pm 0.39_{\rm stat.} \pm 0.71_{\rm syst.}$ GeV [237] in the lepton+jets channel by identifying soft leptons from the semileptonic decays of b-hadrons assigned to the leptonically decaying top quark, $m_t = 172.95 \pm 0.53$ GeV [238] in the lepton+jets channel with boosted hadronically decaying top quarks, and $m_t = 172.21 \pm 0.20_{\rm stat.} \pm 0.78_{\rm syst.}$ GeV [239] in the dilepton channel. There is some ambiguity in relating these measurements to the top-quark pole mass [240], which we discuss below. Alternatively, the experimental collaborations have determined the top-quark mass from inclusive cross-section measurements [241–247]. While these determinations represent unambiguous measurements of the top-quark pole mass, they have larger uncertainties than the direct measurements presently. For the fits discussed later we will use the average value of direct measurements reported in the Top Quark Listings in this Review, which is based exclusively on fully published results. It must be noted that this combination assumes vanishing correlations between the different measurements and across experiments. We take

$$m_t = 172.56 \pm 0.31 \,\text{GeV} + \Delta m_{\text{MC}} \,,$$
 (10.36)

where the term $\Delta m_{\rm MC}$ has been added to account for any difference between the top-quark pole mass, m_t , and the mass parameter implemented in the Monte Carlo event generators employed by the experimental groups. $\Delta m_{\rm MC}$ is expected to be of order $\alpha_s(Q_0)Q_0$ with a low scale $Q_0 \sim \mathcal{O}(1~{\rm GeV})$ [248], but its value is unknown in hadron collider environments so that we will treat it as an uncertainty instead,¹³ and choose for definiteness $Q_0 = \Gamma_t = 1.42~{\rm GeV}$ to arrive at $\Delta m_{\rm MC} = 0 \pm 0.52~{\rm GeV}$. We further assume that an uncertainty [251] of $\pm 0.32~{\rm GeV}$ in the relation [252] between m_t and the $\overline{\rm MS}$ definition, $\widehat{m}_t(\widehat{m}_t^2)$, entering EW radiative correction libraries, including the renormalon ambiguity [253], is already included in $\Delta m_{\rm MC}$, as m_t merely serves as an intermediate bookkeeping device in Ref. [248]. A complementary direction to arrive at a competitive independent constraint on m_t is to analyze differential top-quark pair production cross sections at NNLO QCD [254,255]. Extractions of m_t using fixed-order perturbative calculations can remove the $\Delta m_{\rm MC}$ uncertainty and benefit from the recently increased experimental precision of differential measurements [256–259]. We note that m_t determinations from cross sections assume the validity of the SM within the energy range accessible to the LHC. For more details and references, see Section 61 on the "Top Quark" and the Quarks Listings in this Review.

The charm and bottom quark masses play a minor but non-negligible role in the EW fit. We consider the running $\overline{\text{MS}}$ masses for these quarks, evaluated at a scale equal to the quark mass itself, $\widehat{m}_q(\widehat{m}_q^2)$:

$$\hat{m}_c(\hat{m}_c) = 1273.0 \pm 2.8 \text{ MeV}, \quad \hat{m}_b(\hat{m}_b) = 4183 \pm 4 \text{ MeV}.$$
 (10.37)

To improve the precisions in $\widehat{m}_c(\widehat{m}_c^2)$ and $\widehat{m}_b(\widehat{m}_b^2)$ in the future it would help to remeasure the threshold regions of the heavy quarks, as well as the electronic decay widths of the narrow $c\bar{c}$ and $b\bar{b}$ resonances. It would also be important to obtain data on the R-ratio in e^+e^- annihilation for center-of-mass energies $\gtrsim 11.2$ GeV, as in this region QCD perturbation theory cannot be sufficiently relied upon for b quarks [260].

The masses of the light quarks play a subordinate role in the calculation of EW observables. Indeed, in order to minimize non-perturbative effects in the predictions of high-energy observables, these observables are typically defined to be *infrared safe*, *i.e.* insensitive to energy scales near the QCD parameter $\Lambda_{\rm QCD}$, allowing to neglect the light-quark masses. In cases where these masses

¹²As pointed out in previous versions of this *Review*, we note that there exists some tension at the 2σ level between the Tevatron and LHC measurements of m_t .

 $^{^{13}}$ However, see Refs. [249, 250] for proposed procedures to calibrate the Monte Carlo mass parameter at hadron colliders.

are relevant, they are typically defined in the $\overline{\text{MS}}$ scheme. As further explained in Section 60 on "Quark Masses" in this *Review*, a fit for the u, d, and s masses gives

$$\hat{m}_u = 2.16 \pm 0.04 \text{ MeV}, \quad \hat{m}_d = 4.70 \pm 0.04 \text{ MeV}, \quad \hat{m}_s = 93.5 \pm 0.5 \text{ MeV}, \quad (10.38)$$

where these running $\overline{\text{MS}}$ masses are evaluated at the scale $\mu = 2$ GeV.

10.4.4 The strong coupling constant

The strong coupling constant is one of the key parameters of the SM, setting the strength of QCD interactions. While not contributing to the EW precision observables at the leading order, it enters in the EW precision fit via radiative corrections, most notably to hadronic observables at the one-loop order or to the W mass and the weak mixing angle starting at two loops. From the point of view of EW precision observables, in particular measurements of the Z-lineshape, the relevant scale is $Q^2 \sim M_Z^2$, and the SM EW precision fit provides a determination of $\alpha_s(M_Z^2)$. It is important to complement the information from the EW fit on this input with additional measurements at lower and higher energy scales. Alternative determinations, both from low- and high-energy observables are available, and reduce the dependence of the extraction of $\alpha_s(M_Z^2)$ on potential new physics effects. These determinations differ in statistical precision, experimental systematic uncertainties, and uncertainties from theoretical considerations. Considering the total uncertainty, some of these determinations are more precise than the one from the EW fit, e.g., from lattice QCD, PDF fits. LHC data, or from τ decays. However, the EW fit provides a determination of $\alpha_s(M_Z^2)$ with the smallest uncertainty from missing higher orders or nonperturbative effects compared to other measurements, making it an important element in the combination with other determinations. We refer to Section 9 on Quantum Chromodynamics in this Review for more details on the different methods to obtain α_s and probe its energy dependence.

While measurements of the Z-lineshape have the power to determine $\alpha_s(M_Z^2)$ without further experimental input, the most precise test of the EW sector of the SM is obtained by including external information on $\alpha_s(M_Z^2)$. Following the methods reported in the *Review on Quantum Chromodynamics*, we consider the average of $\alpha_s(M_Z^2)$ excluding information from the EW fit, and before combining it with the lattice QCD results,

$$\alpha_s(M_Z^2) = 0.1171 \pm 0.0011$$
 (PDG 2025 average without EW fit), (10.39)

and perform an unweighted average of this value with the FLAG 2024 estimate, combining the best results from lattice QCD, $\alpha_s(M_Z^2) = 0.1183 \pm 0.0007$ [261]. This results in

$$\alpha_s(M_Z^2) = 0.1177 \pm 0.0009 ,$$
 (10.40)

which we use as a constraint in our fits.

10.4.5 The weak mixing angle

The quantities $\sin^2 \theta_W$ and M_W can be calculated from M_Z , $\alpha(M_Z^2)$, and G_F , when values for m_t and M_H are given, or conversely, M_H can be constrained by $\sin^2 \theta_W$ and M_W . The value of $\sin^2 \theta_W$ depends on the renormalization prescription. There are a number of popular schemes [9] leading to values which differ by small factors depending on m_t and M_H . The notation for these schemes is shown in Table 10.2.

(i) As proposed in Ref. [22], the OS scheme promotes the tree-level formula $\sin^2 \theta_W = 1 - M_W^2 / M_Z^2$

Table 10.2: Notations and numerical values of the weak mixing angle $\sin^2 \theta_W$ discussed in the text. The effective weak mixing angle \bar{s}_{ℓ}^2 is obtained using the two-loop results of Ref. [106] with the direct experimental measurements of $\alpha_s(M_Z^2)$, $\Delta \alpha_{\rm had}^{(5)}(M_Z^2)$, M_Z , m_t , and M_H as input parameters, given in Table 10.5 below. The on-shell and $\overline{\rm MS}$ quantities are derived from \bar{s}_{ℓ}^2 . The uncertainties induced by the imperfectly known input parameters and unknown higher orders [106] are also given.

Scheme	Notation	Value	Uncertainty
On-shell	s_W^2	0.22342	± 0.00009
Effective angle	$ar{s}_\ell^2$	0.23154	± 0.00006
$\overline{ m MS}$	\widehat{s}_Z^2	0.23122	± 0.00006
$\overline{\mathrm{MS}}$ (ND)	$\widehat{s}_{ ext{ND}}^{2}$	0.23140	± 0.00006

to a definition of the renormalized $\sin^2 \theta_W$ to all orders in perturbation theory, i.e.,

$$\sin^2 \theta_W \to s_W^2 \equiv 1 - \frac{M_W^2}{M_Z^2} \,,$$
 (10.41a)

$$M_W = \frac{A_0}{s_W (1 - \Delta r)^{1/2}} , \qquad M_Z = \frac{M_W}{c_W} , \qquad (10.41b)$$

where $c_W \equiv \cos \theta_W$, $A_0 = (\pi \alpha(0)/\sqrt{2}G_F)^{1/2} = 37.28038(1)$ GeV, and Δr includes the radiative corrections relating $\alpha(0)$, $\alpha(M_Z^2)$, G_F , M_W , and M_Z (see Sect. 10.2.5).

Other definitions are motivated by the tree-level coupling constant definition $\theta_W = \tan^{-1}(g'/g)$:

(ii) In particular, the $\overline{\rm MS}$ scheme introduces the quantity.

$$\sin^2 \hat{\theta}_W(\mu^2) \equiv \frac{\hat{g}'(\mu^2)^2}{\hat{g}(\mu^2)^2 + \hat{g}'(\mu^2)^2} , \qquad (10.42)$$

where the couplings \widehat{g} and \widehat{g}' are defined by modified minimal subtraction and the scale μ is conveniently chosen to be M_Z for many EW processes. The value of $\widehat{s}_Z^2 \equiv \sin^2 \widehat{\theta}_W(M_Z^2)$ is less sensitive than s_W^2 to m_t (by a factor of $\tan^2 \theta_W$), and is less sensitive to most types of new physics. It is also useful for comparisons with the predictions of grand unification. There are several definitions of $\sin^2 \widehat{\theta}_W(M_Z^2)$, which differ in whether and how finite $\alpha \ln(m_t/M_Z)$ terms are decoupled (i.e. subtracted from the couplings). One cannot entirely decouple these terms from all EW quantities because $m_t \gg m_b$ breaks SU(2) symmetry. The scheme adopted in the EW fits presented in the previous editions of this *Review* decouples the $\alpha \ln(m_t/M_Z)$ terms from the γ -Z mixing [26, 262], essentially eliminating any $\ln(m_t/M_Z)$ dependence in the formulae for asymmetries at the Z pole when written in terms of \widehat{s}_Z^2 . (A similar definition is used for $\widehat{\alpha}$.) The OS and $\overline{\rm MS}$ definitions are related by

$$\hat{s}_Z^2 = c(m_t, M_H) s_W^2 = (1.0349 \pm 0.0003) s_W^2 . \tag{10.43}$$

The quadratic m_t dependence is given by $c \sim 1 + \Delta \rho_t / \tan^2 \theta_W$. The expressions for M_W and M_Z in the $\overline{\rm MS}$ scheme are

$$M_W = \frac{A_0}{\hat{s}_Z (1 - \Delta \hat{r}_W)^{1/2}} , \qquad M_Z = \frac{M_W}{\hat{\rho}^{1/2} \hat{c}_Z} , \qquad (10.44)$$

and one predicts $\Delta \hat{r}_W = 0.06937 \pm 0.00006$. $\Delta \hat{r}_W$ has no quadratic m_t dependence, because shifts in M_W are absorbed into the observed G_F , so that the error in $\Delta \hat{r}_W$ is almost entirely

due to $\Delta r_0 = 1 - \alpha(0)/\hat{\alpha}(M_Z^2)$. The quadratic m_t dependence has been shifted into $\hat{\rho} \sim 1 + \Delta \rho_t$, where including bosonic loops, $\hat{\rho} = 1.01016 \pm 0.00009$.

(iii) A variant $\overline{\rm MS}$ quantity $\widehat{s}_{\rm ND}^2$ (used in the 1992 edition of this Review) does not decouple the $\alpha \ln(m_t/M_Z)$ terms [263]. It is related to \widehat{s}_Z^2 by

$$\widehat{s}_{\mathrm{ND}}^{2} = \widehat{s}_{Z}^{2} \left(1 + \frac{\widehat{\alpha}}{\pi} d \right), \qquad d = \frac{1}{3} \left(\frac{1}{\widehat{s}^{2}} - \frac{8}{3} \right) \left[\left(1 + \frac{\alpha_{s}}{\pi} \right) \ln \frac{m_{t}}{M_{Z}} - \frac{15\alpha_{s}}{8\pi} \right]. \tag{10.45}$$

Thus, $\hat{s}_Z^2 - \hat{s}_{ND}^2 = -0.00018$.

- (iv) Another very useful definition of the mixing angle, known as the effective weak mixing angle [264, 265] $\bar{s}_f^2 \equiv \sin^2 \theta_{\text{eff}}^f$, is based on effective couplings of a fermion f to the Z boson on the Z pole, as discussed in detail in Sec. 10.4.6 below.
- (v) In previous versions of this Review, special attention was dedicated to EW precision observables obtained at low momentum transfers [266], i.e., $|Q^2| \ll M_Z^2$, in particular those measured in neutrino and electron scattering experiments, namely ν -hadron, ν -e, as well as parity violating e-hadron and e-e neutral-current processes. Within the SM, these are sensitive to the weak mixing angle at almost vanishing momentum transfer $\hat{s}_0^2 \equiv \sin^2 \hat{\theta}_W(0)$ [162, 267–269]. Similarly, new physics effects contributing to the EW neutral-currents interactions or new particle exchanges in the form of additional four-fermion interactions could be tested in these types of processes.

A precise determination of the OS quantity s_W^2 , which depends only very weakly on m_t and M_H , is obtained from deep inelastic scattering (DIS) of neutrinos [270, 271] from (approximately) isoscalar targets. The ratio $R_{\nu} \equiv \sigma_{\nu N}^{NC}/\sigma_{\nu N}^{CC}$ of neutral-to-charged-current cross sections has been measured to 1% accuracy by CDHS [272] and CHARM [273] at CERN. CCFR [274] at Fermilab has obtained an even more precise result. The NuTeV collaboration found $s_W^2 = 0.2277 \pm 0.0016$, which was $\sim 3\sigma$ higher than the SM prediction [275]. However, since then several groups have raised concerns about the interpretation of the NuTeV result, which could affect the extracted value of s_W^2 . A detailed discussion and a list of references can be found in the 2016 edition of this Review. Similarly, experiments of parity violation electron scattering can probe the weak mixing angle by measuring the parity violating left-right (LR) asymmetry $A_{\rm LR} \equiv \frac{\sigma_{\rm L} - \sigma_{\rm R}}{\sigma_{\rm L} + \sigma_{\rm R}}$. This was determined by the SLAC polarized electron-deuteron DIS (eDIS) experiment [276] and improved by the Jefferson Lab Hall A collaboration [277, 278], measuring the weak mixing angle to 2% precision, $\hat{s}_Z^2 = 0.2299 \pm 0.0043$. $A_{\rm LR}$ can also be measured in fixed target polarized Møller scattering, and has been determined at low $Q^2 = 0.026 \text{ GeV}^2$ in the SLAC E158 experiment [279], yielding $\hat{s}^2(161 \text{ MeV}) = 0.2403 \pm 0.0013$, and, as shown in Fig. 10.1, established the scale dependence of the weak mixing angle at the level of 6σ . Finally, measurement of the nuclear weak charge, $Q_W(Z,N)$, in experiments of atomic parity violation, in particular for Cesium, when interpreted in terms of the SM lead to value of the weak mixing angle $\hat{s}^2(2.4 \text{ MeV}) = 0.2349 \pm 0.0018 \text{ [280-287]}$. We refer to the review article by M. A. and C. Bouchiat [288] and to previous editions of this Review for a much more in-depth description of these types of low-energy probes of the weak mixing angle.

The scale dependence of the weak mixing angle defined in the $\overline{\rm MS}$ scheme [162,268] is shown in Fig. 10.1.

10.4.6 Z-pole physics

If the CM energy \sqrt{s} is large compared to the fermion mass m_f , the unpolarized Born cross section for $e^+e^- \to f\bar{f}$, including γ exchange, Z-boson exchange, and γ -Z interference can be

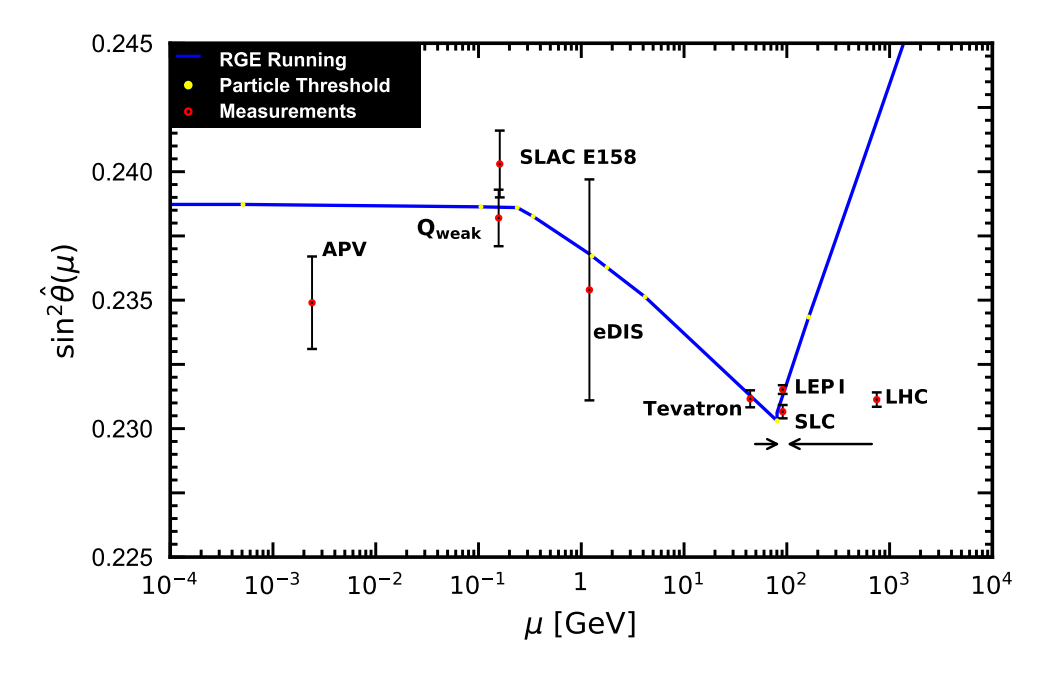


Figure 10.1: Scale dependence of the weak mixing angle defined in the $\overline{\rm MS}$ scheme [162,268] (for the scale dependence in a mass-dependent renormalization scheme, see Ref. [267]). The minimum of the curve corresponds to $\mu=M_W$, below which we switch to an effective theory with the W^\pm bosons integrated out, and where the β -function for $\hat{s}^2(\mu^2)$ changes sign. At M_W and each fermion mass there are also discontinuities arising from scheme dependent matching terms, which are necessary to ensure that the various effective field theories within a given loop order describe the same physics. However, in the $\overline{\rm MS}$ scheme these are very small numerically and barely visible in the figure provided one decouples quarks at $\mu=\hat{m}_q(\hat{m}_q^2)$. The width of the curve exceeds the theory uncertainty from strong interaction effects which at low energies is at the level of $\pm 2 \times 10^{-5}$ [162]. The Tevatron and LHC measurements are strongly dominated by invariant masses of the final-state di-lepton pair of $\mathcal{O}(M_Z)$ and can thus be considered as additional Z pole data points. For clarity we displayed the Tevatron and LHC points horizontally to the left and right, respectively. Figure taken from the previous edition of this Review, which we refer to for more details [289].

written as [290]

$$\frac{d\sigma}{d\cos\theta} = \frac{\pi\alpha^2(s)}{2s} \left[F_1(1+\cos^2\theta) + 2F_2\cos\theta \right] + B , \qquad (10.46a)$$

$$F_1 = Q_e^2 Q_f^2 - 2\chi Q_e Q_f \bar{g}_V^e \bar{g}_V^f \cos \delta_R + \chi^2 (\bar{g}_V^{e2} + \bar{g}_A^{e2}) (\bar{g}_V^{f2} + \bar{g}_A^{f2}) , \qquad (10.46b)$$

$$F_2 = -2\chi Q_e Q_f \bar{g}_A^e \bar{g}_A^f \cos \delta_R + 4\chi^2 \bar{g}_V^e \bar{g}_A^e \bar{g}_V^f \bar{g}_A^f , \qquad (10.46c)$$

where

$$\tan \delta_R = \frac{\overline{M}_Z \overline{\Gamma}_Z}{\overline{M}_Z^2 - s} , \qquad \chi = \frac{G_F}{2\sqrt{2}\pi\alpha(s)} \frac{s\overline{M}_Z^2}{\left[(\overline{M}_Z^2 - s)^2 + \overline{M}_Z^2 \overline{\Gamma}_Z^2\right]^{1/2}} . \qquad (10.47)$$

Here, B accounts for box graphs involving virtual Z and W bosons, and the $\bar{g}_{V,A}^f$ are defined in Eq. (10.48) below. \overline{M}_Z and $\overline{\Gamma}_Z$ correspond to mass and width definitions based on a Breit–Wigner shape with an energy-independent width (see Sec. 10.2.4 and Section 55 on the "Z Boson" in this Review). The differential cross section receives important corrections from QED effects in the initial and final states, and interference between the two [291]. For $q\bar{q}$ production, there are additional final-state QCD corrections, which are relatively large. Note also that the equations above are written in the CM frame of the incident e^+e^- system, which may be boosted due to the initial-state QED radiation.

Some of the leading virtual EW corrections are captured by the running QED coupling $\alpha(s)$ and the Fermi constant G_F . The remaining corrections to the $Zf\bar{f}$ interactions are absorbed by replacing the tree-level couplings in Eq. (10.7) with the s-dependent effective couplings [138],

$$\bar{g}_V^f = \sqrt{\rho_f} \left(t_{3L}^f - 2Q_f \kappa_f \sin^2 \theta_W \right) , \qquad (10.48a)$$

$$\bar{g}_A^f = \sqrt{\rho_f} t_{3L}^f . \tag{10.48b}$$

In these equations, the effective couplings are to be taken at the scale \sqrt{s} , but for notational simplicity we do not show this explicitly. At tree level, $\rho_f = \kappa_f = 1$, but inclusion of EW radiative corrections leads to $\rho_f \neq 1$ and $\kappa_f \neq 1$, which depend on the fermion f and on the renormalization scheme. In the OS scheme, the quadratic m_t dependence is given by,

$$\rho_f \sim 1 + \Delta \rho_t , \qquad \kappa_f \sim 1 + \frac{\Delta \rho_t}{\tan^2 \theta_W} , \qquad (10.49)$$

while in $\overline{\text{MS}}$, $\widehat{\rho}_f \sim \widehat{\kappa}_f \sim 1$, for $f \neq b$, and

$$\widehat{\rho}_b \sim 1 - \frac{4}{3} \Delta \rho_t \;, \qquad \widehat{\kappa}_b \sim 1 + \frac{2}{3} \Delta \rho_t \;, \qquad (10.50)$$

which account for the non-flavor-universal effects arising from diagrams where a virtual top quark couples to a W boson inducing a correction to the $Zb\bar{b}$ vertex. In the $\overline{\rm MS}$ scheme the normalization is changed according to $G_FM_Z^2/2\sqrt{2}\pi \to \hat{\alpha}/4\hat{s}_Z^2\hat{c}_Z^2$ in the second Eq. (10.47).

As reviewed in Sec. 10.2.5, for the high precision Z pole observables discussed below, many additional bosonic and fermionic loop effects, vertex corrections, and higher order contributions, etc., must be included. For example, in the $\overline{\rm MS}$ scheme one then has $\hat{\rho}_{\ell}=0.9977$, $\hat{\kappa}_{\ell}=1.0014$, $\hat{\rho}_{b}=0.9867$, and $\hat{\kappa}_{b}=1.0068$.

To connect to measured quantities, it is convenient to define the effective angle

$$\bar{s}_f^2 \equiv \sin^2 \bar{\theta}_{Wf} \equiv \hat{\kappa}_f \hat{s}_Z^2 = \kappa_f s_W^2 \,, \tag{10.51}$$

in terms of which \bar{g}_V^f and \bar{g}_A^f are given by $\sqrt{\rho_f}$ times their tree-level formulae. One finds that the $\hat{\kappa}_f$ $(f \neq b)$ are almost independent of m_t and M_H , and thus one can write,

$$\bar{s}_{\ell}^2 = \hat{s}_Z^2 + 0.00032 , \qquad (10.52)$$

while the κ_f for the OS scheme are m_t dependent.

High-precision measurements of various Z pole ($\sqrt{s} \approx M_Z$) observables [9, 301, 302] have been performed at LEP 1 and SLC [138, 298, 299, 303, 304], as summarized in Table 10.3. These include the Z mass and total width, Γ_Z , and partial widths $\Gamma_{f\bar{f}}$ for $Z \to f\bar{f}$, where $f = e, \mu, \tau$, light

Table 10.3: Principal Z-pole observables and their SM predictions. The first M_Z is from LEP 1 [138] and the second from CDF [211]. The first \bar{s}_ℓ^2 is the effective weak mixing angle extracted from the hadronic charge asymmetry at LEP 1 [138], the second is the combined value from the Tevatron [292], and the third is from the LHC [293–297]. The values of A_e are (i) from A_{LR} for hadronic final states [298]; (ii) from A_{LR} for leptonic final states and from polarized Bhabha scattering [299]; and (iii) from the angular distribution of the τ polarization at LEP 1 [138]. The A_τ values are from SLD [299], the total τ polarization from LEP [138] and from CMS [300], respectively. The SM predictions are obtained using the values of the first five parameters listed in the second column of Table 10.5. Note that the SM errors in Γ_Z , the R_ℓ , and $\sigma_{\rm had}$ are largely dominated by the uncertainty in α_s .

Quantity	Value	Standard Model
$\overline{M_Z \; [{ m GeV}]}$	91.1876 ± 0.0021	
	91.192 ± 0.007	
Γ_Z [GeV]	2.4955 ± 0.0023	2.4942 ± 0.0005
$\sigma_{\rm had} \; [{\rm nb}]$	41.4802 ± 0.0325	41.492 ± 0.008
R_e	20.804 ± 0.050	20.747 ± 0.006
R_{μ}	20.784 ± 0.034	20.747 ± 0.006
$R_{ au}$	20.764 ± 0.045	20.794 ± 0.006
R_b	0.21629 ± 0.00066	0.21588 ± 0.00003
R_c	0.1721 ± 0.0030	0.17220 ± 0.00003
$A_{ m FB}^e$	0.0145 ± 0.0025	0.01618 ± 0.00006
$A_{ m FB}^{\mu}$	0.0169 ± 0.0013	
$A_{ m FB}^ au$	0.0188 ± 0.0017	
$A_{ m FB}^{b}$	0.0996 ± 0.0016	0.1030 ± 0.0003
A_{FB}^{c}	0.0707 ± 0.0035	0.0736 ± 0.0002
$A_{ m FB}^s$	0.0976 ± 0.0114	0.1027 ± 0.0002
$ar{s}_\ell^2$	0.2324 ± 0.0012	0.23154 ± 0.00006
	0.23148 ± 0.00033	
	0.23145 ± 0.00028	
A_e	0.15138 ± 0.00216	0.1469 ± 0.0004
	0.1544 ± 0.0060	
	0.1498 ± 0.0049	
A_{μ}	0.142 ± 0.015	
$A_{ au}$	0.136 ± 0.015	
	0.1439 ± 0.0043	
	0.144 ± 0.015	
A_b	0.923 ± 0.020	0.93474 ± 0.00003
A_c	0.670 ± 0.027	0.6678 ± 0.0002
A_s	0.895 ± 0.091	0.9357 ± 0.00004

hadrons, b, and c. It is convenient to use the variables, also called "pseudo-observables" because these need to be determined from cross-section measurements,

$$M_Z, \qquad \Gamma_Z, \qquad \sigma_{\text{had}} \equiv \frac{12\pi\Gamma_{e^+e^-}\Gamma_{\text{had}}}{M_Z^2\Gamma_Z^2}, \qquad R_\ell \equiv \frac{\Gamma_{\text{had}}}{\Gamma_{\ell^+\ell^-}}, \qquad R_q \equiv \frac{\Gamma_{q\bar{q}}}{\Gamma_{\text{had}}}, \qquad (10.53)$$

for $\ell = e, \mu$, or τ , and q = b or c, where $\Gamma_{\rm had}$ is the partial decay width into hadrons. ¹⁴ Most of these are weakly correlated experimentally. These quantities have been obtained by the LEP collaborations from fits to the measured cross sections around the Z pole in e^+e^- collisions. Initial-state radiation reduces the peak cross section by more than 25%, where $\mathcal{O}(\alpha^3)$ QED effects and the dependence on Γ_Z induce an anti-correlation of about -30% between Γ_Z and $\sigma_{\rm had}$, and correlations of about 10% between $\sigma_{\rm had}$ and R_e , R_μ , and R_τ . Newer calculations of beam-beam effects on the luminosity measurement at LEP [305] and an improved Bhabha cross section [214], which was underestimated by 0.048% when the measurements were done, result in updated values

$$\Gamma_Z = 2.4955 \pm 0.0023 \text{ GeV}$$
 and $\sigma_{\text{had}} = 41.480 \pm 0.033 \text{ nb.}$ (10.54)

The anti-correlation between R_b and R_c amounts to -18% [138]. The R_ℓ are insensitive to m_t except for the $Z \to b\bar{b}$ vertex, final-state corrections, and the implicit dependence through $\sin^2 \theta_W$. Thus, they are especially useful for constraining $\alpha_s(M_Z^2)$.

Very important constraints follow from measurements of various Z-pole asymmetries. These include the FB asymmetry $A_{\rm FB}$, and the polarization or LR asymmetry $A_{\rm LR}$, defined by

$$A_{\rm FB}^f = \frac{\sigma_{\rm F}^f - \sigma_{\rm B}^f}{\sigma_{\rm F}^f + \sigma_{\rm B}^f} , \qquad A_{\rm LR} = \frac{\sigma_{\rm L}^f - \sigma_{\rm R}^f}{\sigma_{\rm L}^f + \sigma_{\rm R}^f} . \qquad (10.55)$$

Here, $\sigma_{F(B)}^f$ are the cross sections to produce a fermion in the forward (backward) hemisphere, defined with respect to the direction of the electron beam, and $\sigma_{L(R)}^f$ are the total cross sections for left-handed (right-handed) incoming electrons. The LR asymmetry was measured precisely by the SLD collaboration at the SLC [298] using a polarized electron beam, and has the advantages of being very sensitive to \bar{s}_ℓ^2 and that systematic uncertainties largely cancel. After removing initial-state QED corrections and contributions from photon exchange, γ –Z interference, as well as the EW boxes in Eq. (10.46a), one can use the effective tree-level expressions,

$$A_{\rm LR} = A_e P_e ,$$
 $A_{\rm FB}^f = \frac{3}{4} A_f \frac{A_e + P_e}{1 + P_e A_e} ,$ (10.56)

where,

$$A_f \equiv \frac{2\bar{g}_V^f \bar{g}_A^f}{\bar{g}_V^{f2} + \bar{g}_A^{f2}} = \frac{1 - 4|Q_f|\bar{s}_f^2}{1 - 4|Q_f|\bar{s}_f^2 + 8Q_f^2\bar{s}_f^4} \ . \tag{10.57}$$

 P_e is the initial e^- polarization. The Z-pole FB asymmetries at LEP 1 ($P_e=0$) are given by $A_{\rm FB}^f=\frac{3}{4}A_eA_f$ for $f=e,~\mu,~\tau,~b,~c,~s$ [138], and q, and where $A_{\rm FB}^q$ refers to the hadronic charge asymmetry. Corrections for t-channel exchange and s/t-channel interference cause $A_{\rm FB}^e$ to be strongly anti-correlated with R_e with a coefficient of -37%. The m_b -dependence [306] of the $\mathcal{O}(\alpha_s^2)$ QCD correction [307], affecting the reference axis of the b-quark asymmetry [308], increased the extracted $A_{\rm FB}^b$ by about 0.2σ . The correlation between $A_{\rm FB}^b$ and $A_{\rm FB}^c$ amounts to 15%.

¹⁴In this review, we only consider Z-pole observables corrected for radiative effects, photon exchange, γ –Z interference, and EW boxes. These are denoted with a superscript '0' in the original LEP literature, e.g. $\sigma_{\rm had}^0$, but here we drop the '0' from the superscript.

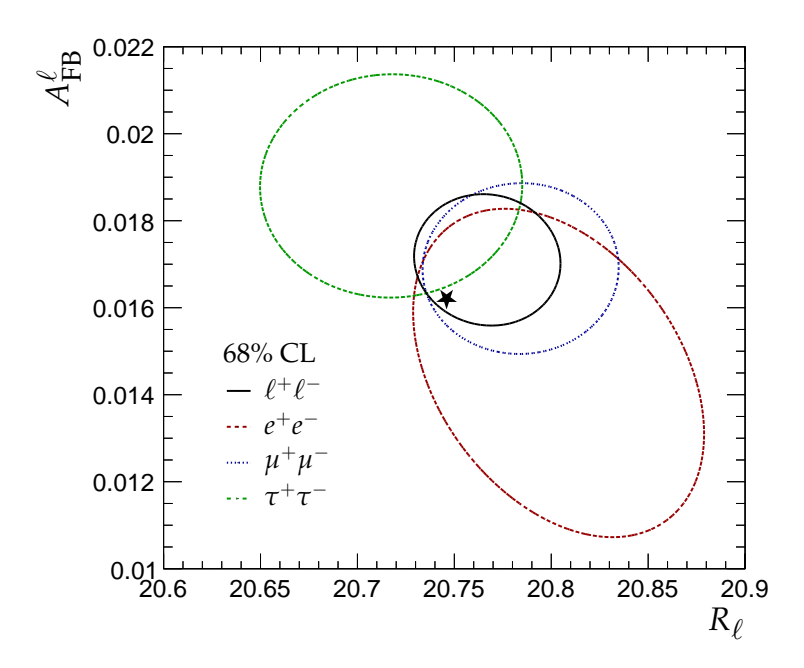


Figure 10.2: Contour lines at 68% confidence level for the LEP 1 measurements of R_{ℓ} and $A_{\rm FB}^{\ell}$ for e^+e^- , $\mu^+\mu^-$, $\tau^+\tau^-$ final states, and all leptons combined. The value of R_{τ} has been corrected for mass effects, shifting the measurement by -0.047. The SM prediction for massless leptons is shown as a black star.

The six measured values of R_{ℓ} and $A_{\rm FB}^{\ell}$ are consistent with lepton universality¹⁵ within their 68% confidence level contours, as shown in Fig. 10.2. The value of R_{τ} has been corrected for mass effects [110] to be comparable to R_e and R_{μ} . In our global SM fit, we use the combined values

$$R_{\ell} = 20.767 \pm 0.025$$
, $A_{\rm FB}^{\ell} = 0.0171 \pm 0.0010$, (10.58)

obtained for massless leptons with an anti-correlation of -5.6% [138].

The SLD collaboration extracted the final-state couplings A_b , A_c [138], A_s [303], A_{τ} , and A_{μ} [299], from left–right forward–backward asymmetries, using

$$A_{LR}^{FB}(f) = \frac{\sigma_{LF}^f - \sigma_{LB}^f - \sigma_{RF}^f + \sigma_{RB}^f}{\sigma_{LF}^f + \sigma_{LB}^f + \sigma_{RF}^f + \sigma_{RB}^f} = \frac{3}{4} A_f , \qquad (10.59)$$

where, for example, σ_{LF}^f is the cross section for a left-handed incident electron to produce a fermion f traveling in the forward hemisphere. We note that A_{LR}^{FB} is equal to A_{FB}^f in Eq. (10.56) for $P_e = 1$. Similarly, A_{τ} and A_e were measured at LEP 1 [138] (A_{τ} also very recently by CMS [300]) through the τ polarization, \mathcal{P}_{τ} , as a function of the scattering angle θ , which can be written as,

$$\mathcal{P}_{\tau} = -\frac{A_{\tau}(1 + \cos^2 \theta) + 2A_e \cos \theta}{(1 + \cos^2 \theta) + 2A_{\tau}A_e \cos \theta} \ . \tag{10.60}$$

The average polarization, $\langle \mathcal{P}_{\tau} \rangle$, obtained by integrating over $\cos \theta$ in the numerator and denominator of Eq. (10.60), yields $\langle \mathcal{P}_{\tau} \rangle = -A_{\tau}$, and A_e can be extracted from the \mathcal{P}_{τ} angular distribution. The

Tests of lepton universality of the neutral current are also available from hadron collider data. The ratio of branching fractions for Z bosons decaying into e^+e^- relative to $\mu^+\mu^-$ final states has also been measured by ATLAS [309], obtaining $R_{e/\mu}=1.0026\pm0.0050$, in perfect agreement with lepton universality. Similar tests have also been performed with $Z\to\tau^+\tau^-$ decays by the LHCb collaboration, finding also good agreement with lepton universality at the percent level: $R_{\tau/e}=1.02\pm0.06$, $R_{\tau/\mu}=1.01\pm0.05$ [310].

initial-state coupling, A_e , was also determined through the LR charge asymmetry [304] and in polarized Bhabha scattering [299] at the SLC. Because \bar{g}_V^{ℓ} is very small, not only $A_{\text{LR}} = A_e$, A_{FB}^{ℓ} , and \mathcal{P}_{τ} , but also A_{FB}^q for q = b, c, and s, as well as the hadronic asymmetries are mainly sensitive to \bar{s}_{ℓ}^2 . The leptonic results are compatible with lepton universality and can be combined into [138]

$$A_{\ell}(\text{SLD}) = 0.1513 \pm 0.0021$$
, $A_{\ell}(\text{LEP}) = 0.1465 \pm 0.0033$, (10.61)

where the first value is obtained from SLD data and the second one from LEP. The two values are statistically compatible within 1.2 standard deviations and are compatible with the CMS determination [300]

$$A_{\tau}(CMS) = 0.144 \pm 0.015$$
 (10.62)

The combination of all LEP and SLC asymmetries (but excluding other observables such as R_{ℓ}) yields [138]

$$\bar{s}_{\ell}^2 = 0.23151 \pm 0.00016 \text{ (LEP + SLC)}$$
. (10.63)

As for hadron colliders, the FB asymmetry, $A_{\rm FB}$, for e^+e^- and $\mu^+\mu^-$ final states (with invariant masses restricted to or dominated by values around M_Z) in $p\bar{p}$ collisions has been measured by the CDF [311] and DØ [312] collaborations, and the values $\bar{s}_\ell^2 = 0.23221 \pm 0.00046$ and $\bar{s}_\ell^2 = 0.23095 \pm 0.00040$ were extracted, respectively. The combination of these measurements (which differ by more than 2 σ) yields [292],

$$\bar{s}_{\ell}^2 = 0.23148 \pm 0.00033 \text{ (Tevatron)}$$
. (10.64)

By varying the invariant mass and the scattering angle (and assuming the electron couplings), information on the effective Z couplings to light quarks, $\bar{g}_{V,A}^{u,d}$, could also be obtained [313,314], but with large uncertainties, mutual correlations, and not independently of \bar{s}_{ℓ}^2 above. Similar analyses have also been reported by the H1 [315] and ZEUS [316] collaborations at HERA and by the LEP collaborations [138]. This kind of measurement is harder in the pp environment due to the difficulty to assign the initial quark and antiquark in the underlying Drell–Yan process to the protons, thus requiring excellent control of uncertainties from parton distribution functions. ATLAS obtained $\bar{s}_{\ell}^2 = 0.2308 \pm 0.0012$ using 7 TeV data [293] and a preliminary result $\bar{s}_{\ell}^2 = 0.23140 \pm 0.00036$ at 8 TeV [294], while CMS measured $\bar{s}_{\ell}^2 = 0.23101 \pm 0.00053$ at 8 TeV [295]. The LHCb collaboration measured $\bar{s}_{\ell}^2 = 0.23142 \pm 0.00106$ using 7 and 8 TeV data, analyzing $\mu^+\mu^-$ final states [297]. The PDG combination of LEP, Tevatron, and LHC results is still mostly dominated by the lepton collider measurement and gives

$$\bar{s}_{\ell}^2 = 0.23148 \pm 0.00013$$
 (collider average) . (10.65)

Since this average includes \bar{s}_{ℓ}^2 determinations from asymmetry measurements at LEP and SLC, it cannot be used in a global EW fit that already includes these measurements. Instead, we use a combination of hadron collider measurements, obtained from the above Tevatron average, Eq. (10.64), the ATLAS, CMS, and LHCb results, and recent results from 13 TeV data by CMS, $\bar{s}_{\ell}^2 = 0.23152 \pm 0.00031$ [317], and LHCb, $\bar{s}_{\ell}^2 = 0.23147 \pm 0.00050$ [318]. Assuming that the PDF uncertainties are fully correlated between the ATLAS and CMS measurements and 50% correlated between all other measurements, results in a hadron collider (HC) value of

$$\bar{s}_{\ell}^2 = 0.23152 \pm 0.00023 \text{ (HC)} .$$
 (10.66)

Variations of the PDF correlations lead to small shifts in the central value that have been included in the total uncertainty.

10.4.7 W and Z decays

The partial widths of weak gauge boson decays into massless fermion pairs $f_1\bar{f}_2$ (the numerical values include the small EW radiative corrections and final-state mass effects) are given by,

$$\Gamma(W^+ \to e^+ \nu_e) = \frac{M_W^3 G_F}{6\sqrt{2}\pi} = 226.29 \pm 0.04 \,\text{MeV} ,$$
 (10.67a)

$$\Gamma(W^+ \to u_i \bar{d}_j) = \frac{M_W^3 G_F}{6\sqrt{2}\pi} |V_{ij}|^2 \mathcal{R}_V^q = (705.3 \pm 0.4 \,\text{MeV}) |V_{ij}|^2 ,$$
 (10.67b)

$$\Gamma(Z \to f\bar{f}) = \frac{M_W^3 G_F}{6\sqrt{2}\pi} \left[\mathcal{R}_V^f \bar{g}_V^{f2} + \mathcal{R}_A^f \bar{g}_A^{f2} \right] , \qquad (10.67c)$$

where the result for the latter are shown in Table 10.4. Final-state QED and QCD corrections [319] to the vector and axial-vector form factors are given by,

$$\mathcal{R}_{V,A}^{f} = N_C \left[1 + \frac{3}{4} \left(Q_f^2 \frac{\alpha(s)}{\pi} + \frac{N_C^2 - 1}{2N_C} \frac{\alpha_s(s)}{\pi} \right) + \cdots \right] , \qquad (10.68)$$

where $N_C = 3$ (1) is the color factor for quarks (leptons) and the dots indicate finite fermion mass effects proportional to m_f^2/s which are different for \mathcal{R}_V^f and \mathcal{R}_A^f , as well as higher-order QCD corrections [320], which are known to $\mathcal{O}(\alpha_s^4)$ [321]. For the Z boson, these include singlet contributions starting from two-loop order in QCD that are large, strongly top-quark mass dependent, family universal, and flavor non-universal [322–326]. The $\mathcal{O}(\alpha^2)$ self-energy corrections from Ref. [327] are also taken into account.

For the W decay into quarks, Eq. (10.67b), only the universal massless part (non-singlet and $m_q=0$) of the final-state QCD radiator function in \mathcal{R}_V from Eq. (10.68) is used, and the QED corrections are modified. Expressing the widths in terms of $G_F M_{W,Z}^3$ incorporates the largest radiative corrections from the running QED coupling. EW corrections to the Z widths are then taken into account through the effective couplings $\bar{g}_{V,A}^{i2}$. Hence, in the OS scheme the Z widths are proportional to $\rho_i \sim 1 + \Delta \rho_t$. There is additional (negative) quadratic m_t dependence in the $Z \to b\bar{b}$ vertex corrections [328,329] which causes $\Gamma_{b\bar{b}}$ to decrease with m_t . The dominant effect is to multiply $\Gamma_{b\bar{b}}$ by the vertex correction $1 + \delta \rho_{b\bar{b}}$, where $\delta \rho_{b\bar{b}} \sim 10^{-2} (-\frac{1}{2} m_t^2/M_Z^2 + \frac{1}{5})$. In practice, the corrections are included in $\hat{\rho}_b$ and $\hat{\kappa}_b$, as discussed in Sec. 10.4.

Starting at $\mathcal{O}(\alpha \alpha_s)$, the factorized form indicated in Eq. (10.67) is violated and corrections need to be included [330–332]. They add coherently, resulting in a sizable effect, and shift $\alpha_s(M_Z^2)$ when extracted from Z lineshape observables by about +0.0007. Similar non-factorizable corrections are also known for mixed QED-EW corrections [106, 108, 109].

For three fermion families, the total widths of the Z [53,333–336] and W [25,135] bosons are predicted to be

$$\Gamma_Z = 2.4944 \pm 0.0006 \,\text{GeV}$$
, $\Gamma_W = 2.090 \pm 0.001 \,\text{GeV}$. (10.69)

The uncertainties in these predictions are almost entirely induced by the parametric error from the strong coupling constant, $\alpha_s(M_Z^2) = 0.1177 \pm 0.0009$, from the average in Eq. (10.40). These predictions can be compared with the experimental results, $\Gamma_Z = 2.4955 \pm 0.0023$ GeV [138,214] and the average from LEP, Tevatron and ATLAS, $\Gamma_W = 2.14 \pm 0.05$ GeV presented in the Gauge & Higgs Bosons Particle Listings in this *Review*. The different leptonic branching fractions of the W boson, $\mathcal{B}(W \to \ell \nu_{\ell})$ have been measured at high precision by the LEP 2 experiments [215]. The measurements of the total and partial widths are generally in good agreement with the SM.

Table 10.4: SM predictions for the partial and total Z decay widths [in MeV]. The results are derived from Table 10.3 and the corresponding covariance matrices [138,214]. In the (second) third column lepton universality is (not) assumed.

Quantity	Value	Value (universal)	Standard Model
$\overline{\Gamma_{e^+e^-}}$	83.87 ± 0.12	83.942 ± 0.085	83.983 ± 0.018
$\Gamma_{\mu^+\mu^-}$	83.95 ± 0.18	83.941 ± 0.085	83.982 ± 0.018
$\Gamma_{ au^+ au^-}$	84.03 ± 0.21	83.759 ± 0.085	83.793 ± 0.018
$\Gamma_{ m inv}$	$498.9 \hspace{0.2cm} \pm 2.5$	500.5 ± 1.5	501.605 ± 0.048
$\Gamma_{uar{u}}$	_		299.88 ± 0.16
$\Gamma_{car{c}}$	300.3 ± 5.3	300.0 ± 5.2	299.80 ± 0.16
$\Gamma_{dar{d}}, \Gamma_{sar{s}}$	_		382.82 ± 0.12
$arGamma_{bar{b}}$	377.4 ± 1.3	377.0 ± 1.2	375.90 ± 0.20
$\Gamma_{ m had}$	1744.8 ± 2.6	1743.2 ± 1.9	1741.21 ± 0.65
Γ_Z	2495.5 ± 2.3	2495.5 ± 2.3	2494.56 ± 0.73

The exceptions are Γ_W , which is 1.3σ larger than the SM prediction, and the branching fraction $W \to \tau + \nu_{\tau}$ from LEP 2, which is 2.6σ larger than the electron–muon average [215]. However, a measurement from ATLAS more precise than LEP 2 on the ratio of branching fractions $W \to \tau + \nu_{\tau}$ to $W \to \mu + \nu_{\mu}$, using top quark decays, shows good agreement with the SM prediction and lepton universality [337]. Additional measurements from ATLAS, CMS, and LHCb, on ratios of branching fractions for W decays into different lepton flavors are also in agreement with lepton universality [309, 337–340].

The invisible decay width, $\Gamma_{\rm inv} = \Gamma_Z - \Gamma_{e^+e^-} - \Gamma_{\mu^+\mu^-} - \Gamma_{\tau^+\tau^-} - \Gamma_{\rm had}$, can be used to determine the number of neutrino flavors, N_{ν} , much lighter than $M_Z/2$. The hadronic peak cross section, and therefore the extracted $\Gamma_{\rm had}$, relies on the precise knowledge of the LEP luminosity measured by each experiment using small-angle Bhabha scattering. However, the earlier prediction for the Bhabha cross section was found to be overestimated, and consequently the luminosity underestimated [214]. An updated analysis led to a significant reduction in $\sigma_{\rm had}$ and a small increase in Γ_Z , as given in Eq. (10.54). The resulting value, $N_{\nu} = 2.9963 \pm 0.0074$ [214], is in agreement with the observed number of three fermion generations $N_{\nu} = 3$.

10.5 Global fit results

In this section, we present the results of global fits, subject to the experimental data and theoretical predictions discussed in Sections 10.2–10.4. For earlier analyses and other recent global fits, see Refs. [80,126,130,131,138,341–344] and previous editions of this Review. We recall that the latter have been obtained with the GAPP package [132], which consistently employs $\overline{\rm MS}$ -renormalized quantities. For the results given here, we use the observables summarized in Table 10.5. This includes non-Z-pole observables such as the values of m_t (see Sec. 10.4.3), M_H [345,346], M_W [219, 221], Γ_W [215,221,222], and $\mathcal{BR}(W \to \ell \nu)$ [215,338]. We also use the values of $\alpha_s(M_Z^2)$, $\Delta \alpha_{\rm had}^{(5)}(M_Z^2)$, and the heavy-quark masses as inputs, as explained in the previous sections. The heavy-quark masses, other than m_t , have a negligible impact on the fit and are omitted in Table 10.5. The principal Z-pole observables from the LEP 1 averages of the ALEPH, DELPHI, L3, and OPAL results include the corresponding correlations [138,214]. We assume lepton universality throughout this section, as confirmed by the measurements discussed above. In the SM fit, we use as inputs the combinations of leptonic observables obtained under this assumption. The recent τ -polarization

Table 10.5: Electroweak precision observables included in the SM fit. The first column gives the experimental input, the second the result of the full fit, the third shows the value of the parameter in this line if the respective parameter is not included in the fit, and the last column gives the pull of the parameter. The pull is defined as the difference between the experimental value and the value of the indirect determination, divided by the total uncertainty, given by the quadratic sum of experimental uncertainty and uncertainty in the prediction. The first set of five parameters consists of the SM input parameters in the LEP input scheme, where G_F and $\alpha(0)$ are fixed. These five input parameters are constrained by the observables included in the fit, also encompassing their direct experimental measurements. The other three sets of parameters are measurements related to the W boson, leptonic Z-pole observables together with Γ_Z , σ_{had} and the hadron collider average of \bar{s}_{ℓ}^2 from Eq. (10.66), and asymmetries of heavy quarks.

Parameter	Experimental value	SM fit	Indirect determination	Pull
$\alpha_s(M_Z^2)$	0.1177 ± 0.0009	0.1179 ± 0.0009	0.1201 ± 0.0028	-0.8
$\Delta \alpha_{\rm had}^{(5)}(M_Z^2)^{(\triangle)}$	0.02758 ± 0.00010	0.02757 ± 0.00009	0.02734 ± 0.00037	+0.6
M_Z [GeV]	91.1880 ± 0.0020	91.1883 ± 0.0020	91.1979 ± 0.0093	-1.0
$m_t \; [\text{GeV}]^{(\bigtriangledown)}$	172.56 ± 0.61	172.70 ± 0.58	$174.36^{+2.08}_{-2.09}$	-0.8
M_H [GeV]	125.1 ± 0.1	$125.1_{-0.1}^{+0.1}$	$174.36^{+2.08}_{-2.09} \\ 104.5^{+23.5}_{-19.9}$	+1.0
$\overline{M_W \text{ [GeV]}}$	80.369 ± 0.013	80.359 ± 0.006	80.356 ± 0.006	+0.9
Γ_W [GeV]	2.140 ± 0.050	2.090 ± 0.001	2.090 ± 0.001	+1.0
$\mathcal{BR}(W \to \ell \bar{\nu}_{\ell})$	0.1088 ± 0.0006	0.10838 ± 0.00002	0.10838 ± 0.00002	+0.7
$\bar{s}_{\ell}^2 = \sin^2 \theta_{\text{eff}}^{\ell}(\text{HC})$	0.23152 ± 0.00023	0.23152 ± 0.00006	0.23152 ± 0.00006	0.0
$\bar{s}_{\ell}^2 = \sin^2 \theta_{\mathrm{eff}}^{\ell}(Q_{\mathrm{FB}})$	0.2324 ± 0.0012	0.23152 ± 0.00006	0.23152 ± 0.00006	+0.7
$A_{\ell}(\mathrm{LEP})$	0.1465 ± 0.0033	0.1470 ± 0.0004	0.1470 ± 0.0004	-0.2
$A_{\ell}(\mathrm{SLD})$	0.1513 ± 0.0021	0.1470 ± 0.0004	0.1468 ± 0.0004	+2.1
Γ_Z [GeV]	2.4955 ± 0.0023	2.4945 ± 0.0005	2.4944 ± 0.0006	+0.5
$\sigma_{ m had} [m nb]$	41.480 ± 0.033	41.490 ± 0.008	41.491 ± 0.008	-0.3
R_{ℓ}	20.767 ± 0.025	20.749 ± 0.006	20.748 ± 0.006	+0.8
$A_{ m FB}^\ell$	0.0171 ± 0.0010	0.01621 ± 0.0001	0.01620 ± 0.0001	+0.9
R_b	0.21629 ± 0.00066	0.21587 ± 0.00003	0.21587 ± 0.00003	+0.6
R_c	0.1721 ± 0.0030	0.17220 ± 0.00003	0.17220 ± 0.00003	0.0
$A_{ m FB}^b$	0.0996 ± 0.0016	0.1031 ± 0.0003	0.1032 ± 0.0003	-2.2
$A_{ m FB}^c$	0.0707 ± 0.0035	0.0736 ± 0.0002	0.0736 ± 0.0002	-0.8
A_b	0.923 ± 0.020	0.93475 ± 0.00003	0.93475 ± 0.00003	-0.6
A_c	0.670 ± 0.027	0.6679 ± 0.00019	0.6679 ± 0.00019	+0.1
A_s	0.895 ± 0.091	0.9357 ± 0.00004	0.9357 ± 0.00004	-0.5

 $^{(\}triangle)$ Rescaled due to α_s dependency. (∇) Combination of experimental (0.31 GeV) and theory uncertainty (0.52 GeV).

measurement from CMS [300] (10.62) is not included in the fit, because of its negligible impact due to its large uncertainty compared to the LEP and SLD measurements. The heavy-flavor results [138, 306] of LEP 1 and SLD are based on common inputs, and are thus correlated as well. For the effective weak mixing angle, we use the value extracted from the hadronic charge asymmetry at LEP 1 [138] and the hadron-collider (HC) average from Eq. (10.66).

Next to the experimental values in Table 10.5, we report the SM predictions from the EW fit. In the column labelled "SM fit", the result is shown from a fit with all experimental inputs included. The next column, labelled "indirect determination", shows the result of the fit where the observable in the given line is excluded from the fit. This column can be understood as the unbiased prediction for a given observable, obtained from the current best theoretical knowledge for the given observable, combined with the best experimental and theoretical knowledge of all observables relevant for the corresponding prediction. The fits presented in this Review have been performed using the HEPfit [127] and Gfitter [123] codes. The HEPfit results are derived following a Bayesian statistical analysis of the data and hypotheses, whereas Gfitter follows a frequentist approach with a global least-squares (χ^2) fit. Experimental uncertainties of all input observables are treated as one standard deviation of a Gaussian function. For simplicity, theoretical uncertainties estimating the size of missing higher-order contributions are also treated as Gaussian. However, we note that, this assumption that is not strictly fulfilled. This choice is justified by the fact that current theory uncertainties are smaller by more than a factor of two than the experimental uncertainties, so that the fit result is driven by the experimental uncertainties. The main uncertainties associated with missing higher-order corrections are given by [110]

$$\delta_{\rm th} M_W = 4\,{\rm MeV}\,, \quad \delta_{\rm th} \sin^2\theta_{\rm eff}^f = 4.7\cdot 10^{-5}\,, \quad \delta_{\rm th} \Gamma_Z = 0.4\,{\rm MeV}\,, \quad \delta_{\rm th} \sigma_{\rm had} = 6\,{\rm pb}\,, \quad (10.70)\,, \\ \delta_{\rm th} R_\ell = 0.006\,, \quad \delta_{\rm th} R_c = 0.00005\,, \quad \delta_{\rm th} R_b = 0.0001\,.$$

The reported uncertainty for each parameter is defined from the 68.3% probability range, upon profiling or marginalizing (depending on the approach) over the other parameters. These uncerainties are, in general, well approximated by the 1σ errors obtained from the values satisfying $\Delta\chi^2 = \chi^2 - \chi^2_{\rm min} = 1$. For the two-dimensional figures presented here, we show contours corresponding to the 68.3% and 95.5% confidence levels.

All results presented here have been obtained with both fit programs, HEPfit and Gfitter. We cross-checked these against each other and found excellent agreement between the numerical results from the two programs, with differences typically smaller than 10% of the quoted uncertainties in the predictions. In the Bayesian approach of HEPfit, the shapes of most of the posterior distributions follow Gaussian functions to a good approximation, such that the uncertainties from the two fit programs agree very well.

The agreement between the measurements and the predictions is generally very good. Despite the few discrepancies addressed in the following, the global EW fit describes the data very well, with a $\chi^2/\text{d.o.f.} = 14.4/16$, corresponding to a p-value of 57%. The largest tensions are only at the 2σ level, which correspond to $A_{\ell}(\text{SLD})$, A_{FB}^b from LEP 1, and $\Gamma_W(\text{ATLAS})$. Also, there is currently no understanding as to why the M_W value reported by the CDF collaboration [211] is significantly larger than the measurements by other experiments. We also emphasize that there are a number of discrepancies among individual measurements of certain quantities, as discussed in previous sections, but these are not reflected in the overall χ^2 of the fit as only the corresponding combinations are used as constraints.

There is still a long-standing tension in the EW fit with the combined measurement of the bottom-quark asymmetry $A_{\rm FB}^b$ that is below the SM prediction by 2.2σ , despite a slight improvement in recent years thanks to developments in related theory calculations [306]. The value of A_b can be extracted from $A_{\rm FB}^b$ when $A_e=0.1501\pm0.0016$ is taken from a fit to leptonic asymmetries. The result, $A_b=0.885\pm0.017$, is 2.9σ below the SM prediction¹⁶ and also 1.4σ below $A_b=0.923\pm0.020$ obtained from $A_{\rm LR}^{\rm FB}(b)$ at SLD. Thus, it seems that at least some of the tension in A_b is due to a statistical fluctuation. We note that the uncertainties in $A_{\rm FB}^b$ from LEP 1 and $A_{\rm LR}$

Alternatively, one can use $A_{\ell} = 0.1481 \pm 0.0027$, which is from LEP 1 alone and in excellent agreement with the SM, and obtain $A_b = 0.897 \pm 0.022$, which is 1.7σ low.

Table 10.6: Contributions to the parametric uncertainties in the SM predictions of different EW precision observables. The contribution from the uncertainty in M_H is negligible and is omitted here. The last column shows the present experimental precision in the respective observable for comparison.

Contribution to parametric uncertainty					Total	Total
	$\alpha_s(M_Z^2)$	$\Delta lpha_{ m had}^{(5)}(M_Z^2)$	M_Z	m_t	param. unc.	exp. unc.
$\overline{M_W \; [\mathrm{GeV}]}$	0.0006	0.0018	0.0025	0.0036	0.0048	0.013
Γ_W [GeV]	0.00036	0.00014	0.00020	0.00028	0.00052	0.050
$\mathcal{BR}(W o \ellar u_\ell)$	$2.1\cdot10^{-5}$	_	$2.0 \cdot 10^{-7}$	$2.2\cdot 10^{-7}$	$2.1 \cdot 10^{-5}$	$6 \cdot 10^{-4}$
$\bar{s}_{\ell}^2 = \sin^2 \theta_{ ext{eff}}^{\ell}$	$3.0 \cdot 10^{-6}$	$3.5 \cdot 10^{-5}$	$1.4 \cdot 10^{-5}$	$1.8 \cdot 10^{-5}$	$4.2 \cdot 10^{-5}$	$2.3 \cdot 10^{-4}$
Γ_Z [GeV]	0.00044	$9.5 \cdot 10^{-5}$	0.00020	0.00014	0.00052	0.0023
$\sigma_{\mathrm{had}} \; [\mathrm{nb}]$	± 0.0044	0.00018	0.0019	0.00041	0.0048	0.033
R_ℓ	0.0055	0.00061	0.00026	0.00026	0.0056	0.025
$A_{ m FB}^\ell$	$5.1\cdot10^{-6}$	$6.1 \cdot 10^{-5}$	$2.5\cdot 10^{-5}$	$3.1\cdot10^{-5}$	$7.3 \cdot 10^{-5}$	0.0010
A_{ℓ}	$2.3 \cdot 10^{-5}$	0.00027	0.00011	0.00014	0.00033	0.0021
R_b	$9.9 \cdot 10^{-6}$	$1.1 \cdot 10^{-6}$	$5.5\cdot10^{-7}$	$2.0 \cdot 10^{-5}$	$2.3 \cdot 10^{-5}$	$6.6 \cdot 10^{-4}$
R_c	$1.7 \cdot 10^{-5}$	$2.0 \cdot 10^{-6}$	$7.1\cdot10^{-7}$	$6.9 \cdot 10^{-6}$	$1.9 \cdot 10^{-5}$	0.0030
$A_{ m FB}^b$	$1.6 \cdot 10^{-5}$	0.00019	$8.0 \cdot 10^{-5}$	$9.6 \cdot 10^{-5}$	0.00023	0.0016
$A_{ m FB}^c$	$1.3\cdot 10^{-5}$	0.00015	$6.2\cdot10^{-5}$	$7.8\cdot10^{-5}$	0.00018	0.0035
A_b	$1.6 \cdot 10^{-6}$	$2.2\cdot 10^{-5}$	$9.1 \cdot 10^{-6}$	$4.0\cdot10^{-6}$	$2.5\cdot 10^{-5}$	0.020
A_c	$1.1\cdot 10^{-5}$	0.00012	$4.9\cdot 10^{-5}$	$6.6\cdot10^{-5}$	0.00015	0.027
A_s	$1.8\cdot 10^{-6}$	$2.2\cdot 10^{-5}$	$9.0 \cdot 10^{-6}$	$1.2\cdot 10^{-5}$	$2.7\cdot 10^{-5}$	0.091

from SLD are dominated by the statistical component. The combined value, $A_b = 0.901 \pm 0.013$ deviates by 2.6σ from the SM prediction.

The left-right asymmetry $A_{\rm LR}^0=0.15138\pm0.00216$ [298], obtained by counting hadronically decaying Z bosons for each electron-beam polarization at SLD, differs by 2σ from the SM fit value of 0.1470 ± 0.0004 . The combined value of $A_\ell=0.1513\pm0.0021$ from SLD is also 2.1σ above the SM prediction; but there is experimental agreement between this SLD value and the LEP 1 value, $A_\ell=0.1481\pm0.0027$, obtained from a fit to $A_{\rm FB}^\ell$, $A_e(\mathcal{P}_\tau)$, and $A_\tau(\mathcal{P}_\tau)$.

The third and fourth columns in Table 10.5 reveal that the results from the full fit, including the Higgs-boson mass [345,346], do not deviate from the indirect determinations by more than 1σ . Except for the input parameters, each parameter can be predicted with a precision better than the experimental precision. The indirect determinations of the input parameters M_H and m_t have uncertainties of about $^{+24}_{-20}$ GeV and ± 2.1 GeV, compared to experimental precisions of 0.1 GeV and 0.31 GeV, respectively. The logarithmic dependence of the SM predictions on M_H results in an uncertainty much larger than the experimental precision from the kinematic reconstruction of the Higgs boson. The precision of the indirect determination of m_t is strongly influenced by the uncertainty in the M_W measurement. In the full fit in column three, no input parameter is pulled from its measured value by more than 1σ , with small correlations among the input parameters. Moreover, because the SM parameters entering the predictions of the EW observables are measured with high precision, the parametric uncertainties in the predictions are currently smaller than the corresponding experimental uncertainties. This is shown in Table 10.6, indicating the contribution from the experimental measurements in each of the input parameters to the total uncertainty in a given observable.

$\overline{M_Z \; [{ m GeV}]}$	91.209 ± 0.040	1.00				
m_t [GeV]	$179.8^{+9.1}_{-10.5}$	-0.64	1.00			
M_H [GeV]	52^{+420}_{-33}	0.24	0.46	1.00		
$\alpha_s(M_Z^2)$	0.1194 ± 0.0043	-0.74	0.57	-0.12	1.00	
$\Delta \alpha_{\rm had}^{(5)}(M_Z^2)$	0.02729 ± 0.00093	0.02	-0.36	-0.67	0	1.00

Table 10.7: Values of the SM input parameters from a simultaneous indirect determination from the SM fit to all other EW precision measurements. We also show the correlations from the fit.

Despite the high precision of the direct measurements of the chosen set of SM input parameters, M_Z , M_H , m_t , $\Delta \alpha_{\rm had}^{(5)}(M_Z^2)$, and $\alpha_s(M_Z^2)$, it is interesting to note that the data allow for a simultaneous determination of these parameters from the global EW fit without constraints from direct measurements. Excluding the direct measurement of the SM input parameters from the fit, the resulting values for each of these inputs and their correlations are shown in Table 10.7. Whereas M_Z and $\alpha_{\rm em}(M_Z^2)$ enter the predictions of most observables at the tree level, the dependence on M_H , m_t , and $\alpha_s(M_Z^2)$ is solely through radiative corrections. We note the consistency between the values in Table 10.7 and the actual measurements in Table 10.5.

From the EW precision observables, the strong coupling constant $\alpha_s(M_Z^2)$ is determined mainly through R_ℓ , Γ_Z , $\sigma_{\rm had}$, but Γ_W and the W branching fractions also have an impact. When including only the most sensitive observables in the fit, together with the experimental constraints on the input parameters but leaving $\alpha_s(M_Z^2)$ unconstrained, we obtain the following values:

$$R_{\ell}: \alpha_s(M_Z^2) = 0.1211 \pm 0.0042,$$
 (10.71)

$$\Gamma_Z : \alpha_s(M_Z^2) = 0.1214 \pm 0.0049,$$
(10.72)

$$\sigma_{\text{had}}: \alpha_s(M_Z^2) = 0.1199 \pm 0.0068,$$
(10.73)

all three:
$$\alpha_s(M_Z^2) = 0.1210 \pm 0.029$$
. (10.74)

The values of $\alpha_s(M_Z^2)$ are compatible with each other within the uncertainties. The corrections from beam-beam effects on the luminosity measurement at LEP [305] and the improved Bhabha cross section [214] result in an upwards shift in $\alpha_s(M_Z^2)$ from $\sigma_{\rm had}$ and as a consequence the fit with all three observables gives a very small $\chi^2/{\rm d.o.f.} = 0.03/2$. The full EW fit gives

$$\alpha_s(M_Z^2) = 0.1201 \pm 0.0028 \,, \tag{10.75}$$

with a central value very close to the one from the reduced fit to R_{ℓ} , Γ_Z , and $\sigma_{\rm had}$, and only a slightly smaller uncertainty. This value is compatible at about 1σ with the averages obtained from τ decays ($\alpha_s(M_Z^2) = 0.1171^{+0.0018}_{-0.0017}$), heavy quarkonia spectroscopy (0.1181±0.0037), DIS and global PDF fits (0.1161±0.0022), hadronic final states of e^+e^- annihilations (0.1189±0.0037), hadron colliders (0.1168±0.0027), as well as lattice QCD simulations (0.1184±0.0008). For more details, other determinations, and references, see Section 9 on "Quantum Chromodynamics" in this *Review*.

The loop-level sensitivity of the EW fit to M_H and m_t comes mainly from M_W and \bar{s}_ℓ^2 . The dependence of M_W on m_t is illustrated in Fig. 10.3. The EW fit result, including all observables except M_W and m_t , approaches the precision of the direct measurements. Without M_W included in the fit, the uncertainty in the predicted value of m_t is ± 4.1 GeV. Without an experimental constraint on M_H , the allowed range for m_t is significantly larger, increasing to $^{+9.8}_{-8.1}$ GeV. The measurements of A_ℓ , \bar{s}_ℓ^2 , and $A_{\rm FB}^b$ result in a determination of m_t with an uncertainty of about ± 7 ,

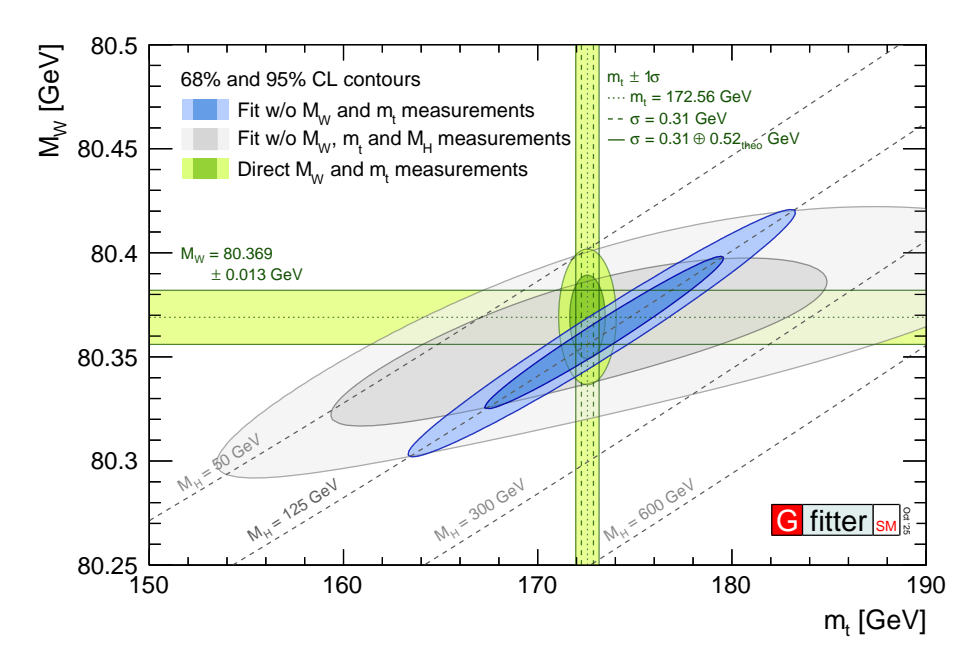


Figure 10.3: Determination of the W-boson and top-quark masses from the EW fit, compared to the experimental values. Shown are the 68% and 95% confidence level contours, together with the SM prediction of M_W as a function of m_t , where the other input parameters are given in Table 10.5. The grey contours show the EW fit without using the measured M_H as input.

 ± 7.5 , and ± 8 GeV, respectively. The strongest constraint on m_t comes from the measurement of M_W , resulting in $m_t = 174.7 \pm 2.4$ GeV. The slight preference for a larger value of m_t compared to the experimental measurement is correlated with the equally slightly larger observed value of M_W compared to the prediction, see Table 10.5 and Fig. 10.3. The result is, in any case, compatible with the direct constraint at less than 1σ , illustrating again the good agreement of the SM with data.

In Fig. 10.4, we compare the predictions of M_W and \bar{s}_ℓ^2 with the experimental measurements. The largest uncertainties in the prediction of M_W are the parametric uncertainties in m_t and $\alpha_s(M_Z^2)$ and the theoretical uncertainties ± 4 MeV from missing higher orders and $\Delta m_{\rm MC}$ from Eq. (10.36). In the prediction of \bar{s}_ℓ^2 , the largest uncertainties are the parametric uncertainties in $\Delta \alpha_{\rm had}^{(5)}(M_Z^2)$, m_t , and M_Z , which are of similar size as the uncertainty from missing higher orders, $4.7 \cdot 10^{-5}$. The experimental uncertainty in M_W comes from a combination of results from the LEP, Tevatron, and LHC experiments. The experimental uncertainty in \bar{s}_ℓ^2 is still dominated by the precise asymmetry measurements from LEP 1, but hadron-collider measurements start to become relevant. In hadron-collider measurements, the uncertainty in \bar{s}_ℓ^2 is currently dominated by PDF uncertainties, but with a prospect of reduced future uncertainties because PDFs can be simultaneously constrained with \bar{s}_ℓ^2 using large data sets. When the experimental value of M_H is not included in the fit, but Z-pole observables are included instead, the uncertainty in the prediction increases by a factor of about 2.5, matching the experimental precision in M_W , but the fit result for \bar{s}_ℓ^2 is still more precise than its direct hadron-collider value. Without M_H and no Z-pole observables, the prediction becomes undetermined in the $\bar{s}_\ell^2 - M_W$ plane.

The sensitivity of the EW fit to M_H is substantially increased when including the measurements of the other SM input parameters, as illustrated in Fig. 10.5. Despite the very precise determinations of these observables, the sensitivity to the actual value of M_H is diminished by the fact that the

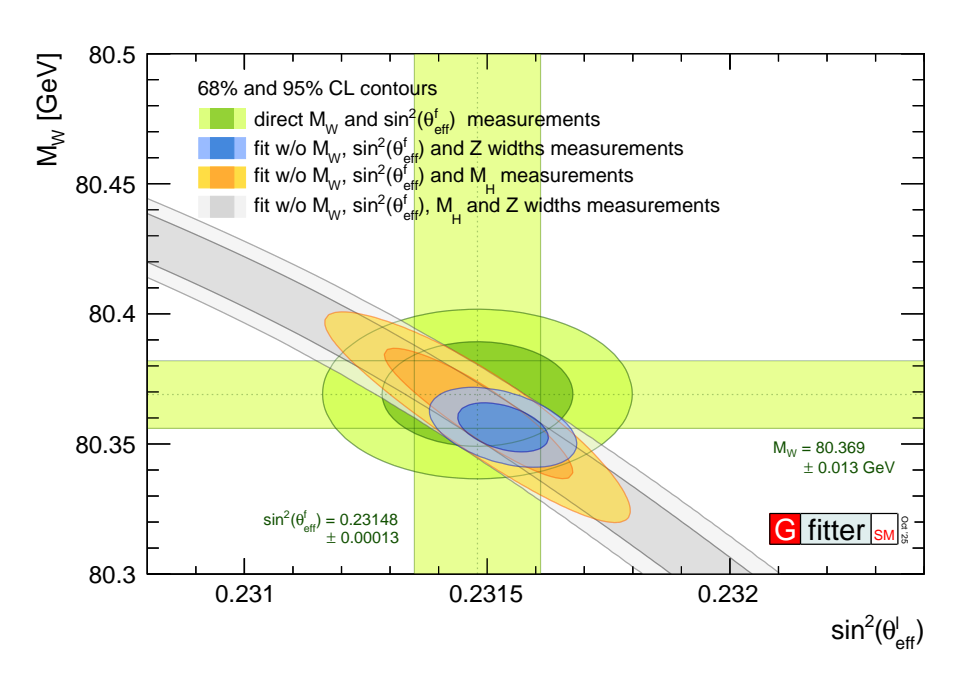


Figure 10.4: Prediction of the W-boson mass and \bar{s}_{ℓ}^2 in the EW fit (blue contours), obtained with the input values from Table 10.5, compared to the world average of M_W and the collider average of \bar{s}_{ℓ}^2 (10.65) (green contours). Shown are the 68% and 95% confidence level contours. The orange contours show a fit result without M_H , but including Z-pole data, while the grey contours show the fit result without M_H and without Z-pole data.

leading contributions to the predictions of EW observables is logarithmic. Removing the direct LHC measurements of M_H from the EW fit results in a loop-level determination of M_H from precision data, given in the fourth column in Table 10.5. At 68% confidence level,

$$85 \text{ GeV} < M_H < 128 \text{ GeV},$$
 (10.76)

which encloses the observed value in Eq. (10.33). The measurements of \bar{s}_{ℓ}^2 , M_W , A_{ℓ} , and $A_{\rm FB}^b$ show the highest sensitivity to M_H . Including only one of these observables at a time, the value of M_H is determined to be

$$\bar{s}_{\ell}^2: M_H = 123_{-49}^{+78} \text{ GeV},$$
 (10.77)

$$M_W: M_H = 100^{+29}_{-24} \text{ GeV},$$
 (10.78)

$$A_{\ell}(SLD): M_H = 36.6^{+31.4}_{-18.8} \text{ GeV},$$
 (10.79)

$$A_{\ell}(\text{LEP}): M_H = 140^{+190}_{-84} \text{ GeV},$$
 (10.80)

$$A_{\rm FB}^b: M_H = 487_{-212}^{+398} \text{ GeV}.$$
 (10.81)

The obtained values agree well within the uncertainties, except for the values from $A_{\rm FB}^b$ and $A_{\ell}({\rm SLD})$, which are apart by about 2.2σ . The predicted value from the full EW fit,

$$M_H = 104.5^{+23.5}_{-19.9} \text{ GeV},$$
 (10.82)

agrees with the individual values and the direct measurement, evidencing the excellent internal consistency of the SM and its capability of predicting observables to very high precision.

In summary, the remarkable agreement between SM predictions and experimental EW precision data, which is reached only after including radiative (meaning quantum) corrections, impressively confirms the model as a quantum field theory, while tree-level predictions (without quantum corrections) are away from data by many standard deviations.

10.6 Constraints on new physics

The precise measurements of EW observables available at different energies and their overall agreement with the SM predictions can be used to set strong limits on new physics modifying, in particular, the properties of the EW gauge bosons. Since the LEP era, the limits from EW precision measurements have typically been interpreted in terms of the so-called oblique new physics, which assumes only modifications in the gauge-boson self-energies coming from new particles (e.g., heavy particles with masses $\Lambda \gg M_W$), and have been traditionally parametrized in terms of the Peskin-Takeuchi S, T, and U parameters [347].¹⁷ Denoting the contributions of new physics to the various self-energies by Π_{ij}^{new} , we have

$$\alpha(M_Z^2)T \equiv \frac{\Pi_{WW}^{\text{new}}(0)}{M_W^2} - \frac{\Pi_{ZZ}^{\text{new}}(0)}{M_Z^2} , \qquad (10.83a)$$

$$\frac{\alpha(M_Z^2)}{4s_W^2 c_W^2} S \equiv \frac{\Pi_{ZZ}^{\text{new}}(M_Z^2) - \Pi_{ZZ}^{\text{new}}(0)}{M_Z^2} - \frac{c_W^2 - s_W^2}{c_W s_W} \frac{\Pi_{Z\gamma}^{\text{new}}(M_Z^2)}{M_Z^2} - \frac{\Pi_{\gamma\gamma}^{\text{new}}(M_Z^2)}{M_Z^2} , \qquad (10.83b)$$

$$\frac{\alpha(M_Z^2)}{4 s_W^2} (S+U) \equiv \frac{\Pi_{WW}^{\text{new}}(M_W^2) - \Pi_{WW}^{\text{new}}(0)}{M_W^2} - \frac{c_W}{s_W} \frac{\Pi_{Z\gamma}^{\text{new}}(M_Z^2)}{M_Z^2} - \frac{\Pi_{\gamma\gamma}^{\text{new}}(M_Z^2)}{M_Z^2} \ . \tag{10.83c}$$

The S, T, and U parameters are defined with a coupling factor proportional to α , so that they are expected to be of order unity in the presence of new physics. The S parameter measures the momentum dependence of custodial-symmetric new-physics effects modifying the neutral-current interactions. On the other hand, the parameter T only receives contributions from custodial SU(2) breaking new physics, measuring the difference between contributions to neutral and charged-current processes at low energies. Finally, the momentum dependence of such contributions is probed by the U parameter. Note that the full SM contributions to S, T, and U are gauge dependent, which is the reason that the gauge-boson self-energies are restricted to their non-standard contributions $\Pi_{VV'}^{\text{new}}(q^2)$, with SM parts subtracted for a given input scenario.

The STU formalism was also the approach taken in previous versions of this Review, and its results can be translated into bounds of a large class of new-physics models, as long as the leading-order effects are oblique in the previous sense, and therefore also flavor universal. The available EW precision data does, however, allow to test a larger type of new-physics effects beyond the one of oblique nature. For instance, new physics that couples directly to ordinary fermions cannot be fully parametrized in the STU framework. Such examples include heavy Z' bosons [352], mixing with exotic fermions [9,353,354], leptoquark exchange [215,355,356], supersymmetric models, strong EW dynamics [357], Little Higgs models [358,359], and TeV-scale extra spatial dimensions [360–363] (for more details and references, see Section 84 on "Extra Dimensions" in this Review). These types of new-physics scenarios, and more, can be described within the more general framework of $Effective\ Field\ Theories\ (EFTs)$.

Under the assumptions that new physics is heavy compared to the scale of energies explored so far, and that at those energies the symmetries and field content are those of the SM, with the Higgs field being part of an SU(2) doublet ϕ like in the SM, ¹⁸ the so-called *Standard Model*

¹⁷We note that other parametrizations exist, see for example Refs. [348–351].

 $^{^{18}}$ A more general type of EFT, known as *Higgs Effective Field Theory (HEFT)* [364–366], relaxes this assumption by allowing the physical Higgs field to be a gauge singlet and including the Goldstone fields as SU(2) triplet in some non-linear field representation.

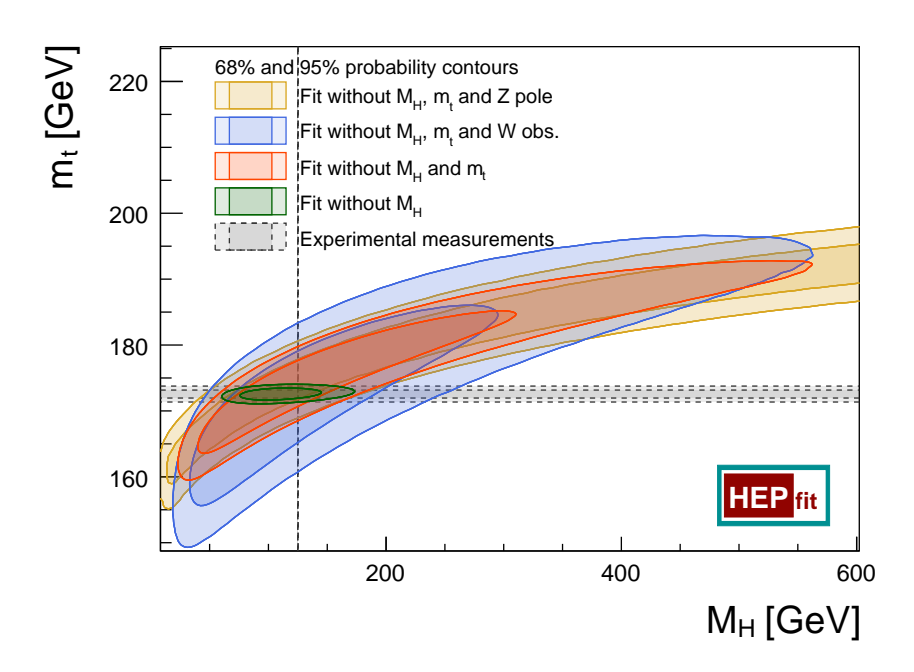


Figure 10.5: Bayesian probability contours at 68% and 95% for the Higgs-boson and top-quark masses from EW fits excluding different sets of input measurements. The grey bands indicate the experimental precision of the direct measurements of the two parameters. The width of the vertical band, corresponding to the precision in M_H , is not visible on the scale of the plot.

Effective Field Theory (SMEFT) [367, 368] provides a rather general description of new-physics effects, parametrized in terms of an expansion in higher-dimensional operators, suppressed by the cut-off of the EFT, $\Lambda \gg v$, where new physics is expected to complete the SM:

$$\mathcal{L} = \mathcal{L}_{SM} + \sum_{d>4} \sum_{i} \frac{C_i}{\Lambda^{d-4}} \mathcal{O}_i . \tag{10.84}$$

In this $1/\Lambda$ expansion, the observable effects of each higher-dimensional operator are suppressed by increasing powers of E/Λ , with $E \ll \Lambda$ the typical energy of a physical process. For a given level of experimental precision δ , one can then truncate the EFT expansion as long as $(E/\Lambda)^{d-4} \ll \delta$ and work with a finite number of operators. In this regard, although the EFT is technically non-renormalizable in the strict sense, at each order in the EFT expansion only a finite number of counterterms is needed, and the theory remains predictive at the desired level of experimental precision. In Eq. (10.84) the specific information about the new physics is encoded in the values of the Wilson coefficients C_i . These can be computed in terms of the masses and couplings of the new particles in a given model by, e.g., matching the EFT and model results for a representative set of amplitudes.

Assuming lepton and baryon number conservation and a SMEFT-type new physics scenario, the leading-order new-physics effects in the $1/\Lambda$ expansion are given by dimension-six operators, and we restrict the discussion to this level of approximation in the following.¹⁹ The full set of all possible new-physics effects can be parametrized in a widely model-independent way specifying a basis for the SMEFT at each order in the $1/\Lambda$ expansion and, to dimension six, several bases have been

¹⁹From the point of view of observables measuring the W and Z boson properties, with experimental precision in some cases at the per-mil level, this truncation is justified if new physics is not present well below the TeV scale, in which case effects of dimension-eight operators are suppressed by $M_W^4/(1\,\text{TeV})^4 \sim \mathcal{O}(10^{-4})$.

proposed [366–369]. In particular, the so-called Warsaw basis [368] presented the first complete set of physically independent dimension-six interactions which, assuming individual conservation of baryon and lepton number, contains a total of 59 operator structures, and 2499 interactions for three generations of fermions. Despite this large number of operators, at the (leading) order of $1/\Lambda$ only a relatively small number of operators modify the SM predictions for the EW precision observables measuring the properties of the W and Z bosons. For instance, assuming fermion-universal new-physics effects, in the Warsaw basis only 10 operators modify the SM predictions at order $1/\Lambda^2$ and tree level. These are:²⁰

$$\mathcal{O}_{\phi D} = (\phi^{\dagger} D_{\mu} \phi)^* (\phi^{\dagger} D^{\mu} \phi), \qquad \mathcal{O}_{\phi W B} = (\phi^{\dagger} \sigma_a \phi) (B^{\mu \nu} W^a_{\mu \nu}), \qquad (10.85)$$

$$(\mathcal{O}_{\phi F}^{(1)})_{ij} = i(\phi^{\dagger} \overset{\leftrightarrow}{D}_{\mu} \phi) \, (\overline{F_L^i} \gamma^{\mu} F_L^j), \qquad (\mathcal{O}_{\phi F}^{(3)})_{ij} = i(\phi^{\dagger} \overset{\leftrightarrow}{D}_{\mu}^a \phi) \, (\overline{F_L^i} \gamma^{\mu} F_L^j),$$

$$(\mathcal{O}_{\phi f})_{ij} = i(\phi^{\dagger} \stackrel{\leftrightarrow}{D}_{\mu} \phi) (\overline{f_R^i} \gamma^{\mu} f_R^j), \qquad F = l, q, \quad f = e, u, d, \qquad (10.86)$$

$$(\mathcal{O}_{ll})_{1221} = (\overline{l_L^1} \gamma_\mu l_L^2) (\overline{l_L^2} \gamma^\mu l_L^1). \tag{10.87}$$

The effects of the operators $\mathcal{O}_{\phi WB}$ and $\mathcal{O}_{\phi D}$ can be described in terms of the oblique S and T parameters introduced above, respectively. To be more precise, the S and T parameters can be directly associated to linear combinations of these two dimension-six bosonic operators and fermion-universal contributions from the interactions $\mathcal{O}_{\phi F}^{(1),(3)}$ and $\mathcal{O}_{\phi f}$ in Eq. (10.86) [370]. These operators also describe cases where new physics couples to the different SM fermion generations in a non-universal manner. These induce modifications to the EW couplings to the Z and W bosons parameterized by:

$$(\Delta g_L^f)_{ij} = -\frac{1}{2} \left(C_{\phi F}^{(1)} \pm C_{\phi F}^{(3)} \right)_{ij} \frac{v^2}{\Lambda^2}, \qquad (\Delta g_R^f)_{ij} = -\frac{1}{2} (C_{\phi f})_{ij} \frac{v^2}{\Lambda^2}, \tag{10.88}$$

$$(\Delta U_L^f)_{ij} = (C_{\phi F}^{(3)})_{ij} \frac{v^2}{\Lambda^2}.$$
 (10.89)

In Eq. (10.88), Δg_L^f and Δg_R^f , give the corrections to the left-handed and right-handed neutral currents, respectively, and the plus (minus) sign corresponds to fermions of weak isospin -1/2 (+1/2). On the other hand, Eq. (10.89) denote the modifications of the (left-handed) charged currents. For simplicity, for the quark interactions we have ignored the CKM effects that would be introduced when rotating to the physical basis. Finally, the operator $(\mathcal{O}_{ll})_{1221}$ in Eq. (10.87) contributes to the muon decay and, therefore, the determination of the Fermi constant. In recent years, NLO calculations including the complete dimension-six effects in EW precision observables have become available [371, 372], including also calculations in different input schemes [373]. More details can be found in the original references.

The EFT formalism also gives additional context to the description of EW precision observables via oblique parameters and the connection to new physics generating these effects. For instance, while the S and T parameters arise from contributions of dimension-six operators, the U parameter is a dimension-eight effect, and it is therefore expected to be parametrically suppressed with respect to S and T by a factor M_Z^2/Λ^2 . Furthermore, additional oblique effects coming from the q^4 terms of the expansions of the gauge-boson self-energies also contribute to EW observables at the level of dimension-six EFT operators. Their inclusion leads to the so-called W and Y parameters [351], which, however, also generate universal four-fermion interactions whose effects are expected to be better constrained at high-energy $2 \rightarrow 2$ fermion processes.

The hermitian covariant derivatives $\overset{\leftrightarrow}{D}$ and $\overset{\leftrightarrow}{D}^a$ appearing below are defined as $\overset{\leftrightarrow}{D}_{\mu} = D_{\mu} - \overset{\leftarrow}{D}_{\mu}, \overset{\leftrightarrow}{D}_{\mu}^a = \sigma_a D_{\mu} - \overset{\leftarrow}{D}_{\mu} \sigma_a$, with σ_a the Pauli matrices.

	Result	Correlation		Result	Correlation		1
\overline{S}	0.026 ± 0.075	1.00		0.021 ± 0.096	1.00		
T	0.047 ± 0.066	0.90	1.00	0.04 ± 0.12	0.91	1.00	
U	0	_	_	0.008 ± 0.092	-0.62	-0.83	1.00

Table 10.8: Results of the global fit of the oblique parameters to all EW precision observables. The left half of the table presents the results assuming U=0, whereas this parameter is an independent degree of freedom in the fit in the right half of the table.

As in previous editions of this Review, in this section we update the results coming from the interpretation of the EW precision measurements in terms of the STU formalism, and the implications for several types of new-physics models. These results are then extended beyond the case of fermion-universal theories with the interpretation within the SMEFT formalism, where we discuss the bounds from EW precision observables on the leading interactions in the dimension-six effective Lagrangian, keeping the discussion at a more model-independent level.

The results of the EW fit extending the SM with the S, T, and U parameters are presented in Table 10.8. We present the cases where U=0, as a proxy for the case of heavy decoupling new physics where $|U| \ll |S|, |T|$, and a scenario where all three parameters are freely floating. Regardless of whether U is assumed to be zero or not, the results from the EW fit to the oblique parameters is fully consistent with the SM hypothesis.²¹ The impact of the different EW observables in the S-T plane, assuming U=0, is shown in Figure 10.6. The shape of these regions can be understood from the fact that, in the LEP scheme used in this figure, Γ_Z only depends on the combination

$$-10(3 - 8s_W^2)S + (63 - 126s_W^2 - 40s_W^4)T,$$

the U parameter only contributes to the W mass and width via

$$S - 2c_W^2 T - \frac{c_W^2 - s_W^2}{2s_W^2} U,$$

and the corrections to all other EW precision observables can be written in terms of

$$S - 4c_W^2 s_W^2 T.$$

From the results in Table 10.8 one can also derive individual limits on each parameter (i.e. assuming all the other oblique parameters are zero). We obtain the following 95% probability individual bounds,

$$T, U = 0: -0.088 \le S \le 0.045; \quad S > -0.082 \quad (S \le 0); \quad S < 0.054 \quad (S \ge 0); \quad (10.90a)$$

$$S, U = 0: -0.032 \le T \le 0.084; \quad T > -0.043 \quad (T \le 0); \quad T < 0.078 \quad (T \ge 0); \quad (10.90b)$$

$$T,U=0: \quad -0.088 \leq S \leq 0.045; \quad S>-0.082 \quad (S\leq 0); \quad S<0.054 \quad (S\geq 0); \quad (10.90a)$$

$$S,U=0: \quad -0.032 \leq T \leq 0.084; \quad T>-0.043 \quad (T\leq 0); \quad T<0.078 \quad (T\geq 0); \quad (10.90b)$$

$$S,T=0: \quad -0.047 \leq U \leq 0.120; \quad U>-0.062 \quad (U\leq 0); \quad U<0.110 \quad (U\geq 0); \quad (10.90c)$$

where the numbers in each row are obtained assuming the corresponding parameter can have any sign, or is restricted to be negative or positive, respectively.

As mentioned above, the STU results can be used to set constraints on a relatively large class of new physics models inducing universal corrections to the SM predictions. For instance, the T parameter modifies the ρ parameter according to

$$\Delta \rho = \alpha(M_Z^2)T \ . \tag{10.91}$$

²¹For a discussion of the impact of the M_W CDF measurement [211] on the EW fit, we refer the reader to, e.g., Refs. [131, 374–377] and to the previous edition of this Review.

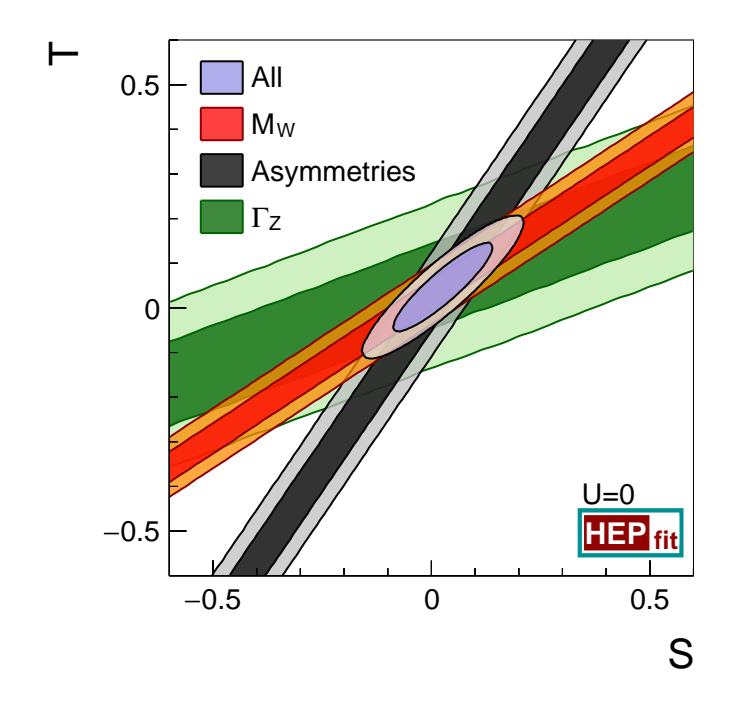


Figure 10.6: EW precision constraints on the S and T plane (assuming U=0). The boundaries of the dark and light regions correspond to the 68% and 95% probability contours, respectively. We also show the constraints imposed by different sets of EW precision measurements. See text for details.

In this way, T can be connected to new physics violations of custodial symmetry. These can be generated by additional sources of SU(2) breaking not induced by Higgs doublets, via

$$\rho = \frac{\sum_{i} [T_i(T_i + 1) - T_{3i}^2] |v_i|^2}{2\sum_{i} T_{3i}^2 |v_i|^2} , \qquad (10.92)$$

where v_i is the expectation value of the neutral component of a Higgs multiplet with weak isospin T_i and third component T_{3i} . Thus, the limits on T can be translated into constraints on higher-dimensional Higgs representations, such that their vacuum expectation values can only be less than a few percent of those of the doublets.

Similarly, the bounds on T can be used to set constraints on non-degenerate multiplets of heavy fermions or scalars, since these break the vector part of weak SU(2) and lead to a decrease in the value of M_Z/M_W . Each non-degenerate SU(2) doublet $\binom{f_1}{f_2}$ yields a positive contribution to ρ (and therefore T) [37,378,379] of

$$\frac{N_C G_F}{8\sqrt{2}\pi^2} \Delta m^2 , \qquad (10.93)$$

where

$$\Delta m^2 \equiv m_1^2 + m_2^2 - \frac{4m_1^2 m_2^2}{m_1^2 - m_2^2} \ln \frac{m_1}{m_2} \ge (m_1 - m_2)^2 , \qquad (10.94)$$

and $N_C = 1$ (3) for color singlets (triplets). The limit on the T parameter (assuming $T \ge 0$) taken together with Eq. (10.91) and Eq. (10.93) implies the following constraint on the mass splitting at

the 95% probability,

$$\sum_{i} \frac{N_C^i}{3} \Delta m_i^2 < (44 \text{ GeV})^2 , \qquad (10.95)$$

where the sum runs over all new-physics doublets, for example fourth-family quarks or leptons, $\binom{t'}{b'}$ or $\binom{\nu'}{\ell'-}$, vector-like fermion doublets (which contribute to the sum in Eq. (10.95) with an extra factor of 2), and scalar doublets such as $\binom{\tilde{t}}{\tilde{b}}$ in supersymmetry (in the absence of L-R mixing).

Non-degenerate multiplets usually imply $\Delta \rho > 0$ (T > 0). Similarly, heavy Z' bosons decrease the prediction for M_Z due to mixing and generally lead to $\Delta \rho > 0$ (T > 0) [352]. On the other hand, extra Higgs doublets participating in spontaneous symmetry breaking [380–382] or heavy lepton doublets involving Majorana neutrinos [383], both of which have more complicated expressions, and the v_i of higher-dimensional Higgs representations can contribute to ρ with either sign.

The effects of non-standard Higgs representations cannot be separated from heavy non-degenerate multiplets unless the new physics has other consequences, such as vertex corrections. Most of the original papers defined T to include the effects of loops only. However, the way T has been defined here includes all new sources of SU(2) breaking, including non-standard Higgs bosons.

A multiplet of heavy degenerate chiral fermions yields

$$S = \frac{N_C}{3\pi} \sum_{i} \left(T_{3i}^L - T_{3i}^R \right)^2 , \qquad (10.96)$$

where $T_{3i}^{L,R}$ is the third component of weak isospin of the left-(right-)handed component of fermion i. For example, a heavy degenerate ordinary or mirror family would contribute $2/(3\pi)$ to S. Therefore, the S parameter can also be used to constrain the number of fermion families, under the assumption that there are no other contributions to T or U, and therefore that any new families are degenerate. Then an extra generation of SM fermions is excluded with more than 7σ confidence, corresponding to $N_F = 2.90 \pm 0.16$. Allowing T to vary as well, the constraint on a fourth family is weaker [384]. However, a heavy fourth family would increase the Higgs production cross section through gluon fusion by a factor of about nine [385, 386], which has been excluded by ATLAS and CMS at the LHC [387]. Combining the limits from EW precision data with the measured Higgs production rate and limits from direct searches for heavy quarks [388], a fourth family of chiral fermions is now excluded by more than five standard deviations [389,390]. Similar remarks apply to a heavy mirror family [391] involving right-handed SU(2) doublets and left-handed singlets. In contrast, new doublets that receive most of their mass from a different source than the Higgs vacuum expectation value, such as vector-like fermion doublets or scalar doublets in supersymmetry, give small or no contribution to S, T, U, and the Higgs production cross section and are therefore still not excluded. Partial or complete vector-like fermion families are predicted in many Grand Unified Theories [392] (see Section 92 on "Grand Unified Theories" in this Review), and many other models including supersymmetric and superstring inspired ones [393–396].

In models with warped extra dimensions [397], sizeable corrections to the S parameter are generated through mixing between the SM gauge bosons and their Kaluza-Klein (KK) excitations, and one finds $S \approx 30 \, v^2 M_{KK}^{-2}$ [398], where M_{KK} is the mass scale of the KK gauge bosons. Large positive values of S can also be generated in models with dynamical EW symmetry breaking, where the Higgs boson is composite. In simple composite Higgs models, the dominant contribution stems from heavy spin-1 resonances of the strong dynamics leading to $S \approx 4\pi v^2 (M_V^{-2} + M_A^{-2})$, where $M_{V,A}$ are the masses of the lightest vector and axial-vector resonances, respectively [399]. From the results in Table 10.8 one obtains $S \leq 0.18$ at 95% probability, which puts the constraint $M_{KK} \gtrsim 3.2$ TeV on

the masses of KK gauge bosons in warped extra dimensions. In minimal composite Higgs models, the bound on S requires $M_V \gtrsim 3.8$ TeV, which is obtained from the one-sided 95% probability bound on S > 0 for T = 0 and using Weinberg sum rules [400]. However, this constraint can be relaxed, e.g., if the fermionic sector is also allowed to be partially composite [357, 401] and in soft-wall models [402].

Negative values of S are possible, for example, in composite Higgs models with larger gauge group representations [403, 404], or from loops involving scalars or Majorana particles [405–407]. The simplest origin of S < 0 would probably be an additional heavy Z' boson [352]. Supersymmetric extensions of the SM [408, 409] generally give very small effects. For more details and references, see Refs. [410–419] and Sections 87,88 on "Supersymmetry" in this *Review*. Most simple types of new physics yield U = 0, although there are counter-examples, such as the effects of anomalous triple gauge vertices [420].

We conclude this section by moving beyond fermion-universal extensions of the SM and presenting the results of a SMEFT fit to electroweak precision observables. In this case, we adopt the G_F -scheme (with G_F , M_Z , M_W as input), which has become the standard in SMEFT combinations of different observables with LHC measurements [421].²² We assume all the operators in Eqs. (10.85)–(10.87) can be generated by new physics. On the lepton side we allow new-physics corrections to be non-universal. Because of this, and contrary to what was done for the SM fits, for the fits in the SMEFT formalism we use as experimental inputs for leptonic observables, such as the ratios $R_{e,\mu,\tau}$ and asymmetries $A_{e,\mu,\tau}$, the values reported in [138,214,215,338] without assuming lepton flavor universality. For quarks, we impose a U(2) flavor symmetry on the first two families to avoid large contributions to flavor-changing neutral currents. The third family is defined in flavor space along the direction of the top-quark. The operators in Eqs. (10.85)-(10.87) are the interactions that enter in EW precision observables at leading EFT order and tree level. Although many other operators contribute at NLO, we restrict the fit to this setup, as a full global analysis taking into account the constraints on all interactions would require combining with numerous additional data sets, which is beyond the scope of this Review. Finally, in the calculation of new-physics effects, we work consistently with the truncation of the SMEFT Lagrangian to dimension six, i.e. up to $O(1/\Lambda^2)$, and keep only corrections of this order in the observables.

It is well known that in the Warsaw basis the EW fit has two blind directions [422, 423]. In Table 10.9 we present the central values and 1σ uncertainties from this EW SMEFT fit, in terms of the following combinations of Wilson coefficients at the EW scale [422]:

$$\hat{C}_{\phi f}^{(1)} = \frac{C_{\phi f}^{(1)}}{\Lambda^2} - \frac{Y_f}{4} \frac{C_{\phi D}}{\Lambda^2}, \quad f = l, q, e, u, d,
\hat{C}_{\phi f}^{(3)} = \frac{C_{\phi f}^{(3)}}{\Lambda^2} + \frac{c_W^2}{4s_W^2} \frac{C_{\phi D}}{\Lambda^2} + \frac{c_W}{s_W} \frac{C_{\phi WB}}{\Lambda^2}, \quad f = l, q,
\hat{C}_{ll} = \frac{1}{2} \frac{(C_{ll})_{1221} + (C_{ll})_{2112}}{\Lambda^2} = \frac{(C_{ll})_{1221}}{\Lambda^2}.$$
(10.97)

For the case of left-handed quarks, we further consider the combination $(\hat{C}_{\phi q}^{(+)})_{33} = ((\hat{C}_{\phi q}^{(1)})_{33} + (\hat{C}_{\phi q}^{(3)})_{33})/2$, which modifies the $Z \to b_L \bar{b}_L$ vertex, whereas the orthogonal combination modified the corresponding top-quark coupling and does not enter in the fit at the tree level. (In the previous expressions, s_W , c_W are the tree-level values of the sine and cosine of the weak mixing angle and Y_f denotes the fermion hypercharge.) In order to resolve the blind directions of this SMEFT EW

 $^{^{22}}$ One of the main reasons is practical, since including the EW gauge-boson masses reduces the SMEFT dependences in propagators, but any choice for the EW input scheme will lead to equivalent fit results within theoretical uncertainties.

$(\hat{C}_{\phi l}^{(1)})_{11}$	$(\hat{C}_{\phi l}^{(1)})_{22}$	$(\hat{C}_{\phi l}^{(1)})_{33}$	$(\hat{C}_{\phi l}^{(3)})_{11}$	$(\hat{C}_{\phi l}^{(3)})_{22}$	$(\hat{C}_{\phi l}^{(3)})_{33}$	$(\hat{C}_{\phi e})_{11}$	$(\hat{C}_{\phi e})_{22}$	$(\hat{C}_{\phi e})_{33}$
0.29 ± 0.21	0.26 ± 0.21	0.25 ± 0.21	-0.91 ± 0.71	-0.90 ± 0.71	-0.88 ± 0.71	0.52 ± 0.41	0.51 ± 0.41	0.49 ± 0.41
$(\hat{C}_{\phi q}^{(1)})_{aa}$	$(\hat{C}_{\phi q}^{(3)})_{aa}$	$(\hat{C}_{\phi q}^{(+)})_{33}$	$(\hat{C}_{\phi d})_{aa}$	$(\hat{C}_{\phi d})_{33}$	$(\hat{C}_{\phi u})_{aa}$			$(\hat{C}_{ll})_{1221}$
-0.09 ± 0.15	-0.95 ± 0.72	-0.54 ± 0.39	-0.35 ± 0.81	-0.54 ± 0.30	-0.24 ± 0.32			0.47 ± 0.41

Table 10.9: Results from the global SMEFT fit discussed in the text, in terms of the combinations of Wilson coefficients in Eq. (10.97). All the operators in those combinations as well as the SM input parameters are taken as free parameters in the fit. The coefficients $(\hat{C}_{\phi l,\phi e}^{(1),(3)})_{11,22,33}$ denote interactions with each of the three lepton generations. For quarks, interactions with the light two families are assumed to be flavour universal, denoted by $(\hat{C}_{\phi q,\phi u,\phi d}^{(1),(3)})_{aa}$, but independent of the ones with the third family. Results in units of TeV⁻².

$\delta g_L^{ u_e}$	$\delta g_L^{ u_\mu}$	$\delta g_L^{ u_ au}$	δg_L^e	δg_L^μ	$\delta g_L^ au$	δg_R^e	δg^{μ}_R	$\delta g_R^{ au}$
-0.33 ± 0.46	-0.07 ± 0.42	0.02 ± 0.63	0.066 ± 0.096	-0.09 ± 0.39	0.00 ± 0.20	-0.20 ± 0.12	-0.01 ± 0.59	0.25 ± 0.27
$\delta g_L^{u=c}$	$\delta g_L^{d=s}$	δg_L^b	$\delta g_R^{u=c}$	$\delta g_R^{d=s}$	δg_R^b			
-0.54 ± 0.92	-0.5 ± 1.2	-0.77 ± 0.37	2.2 ± 3.5	22 ± 35	31 ± 12			

Table 10.10: Projection of the results in Table 10.9 in terms of relative modifications of the neutral-current effective EW couplings of the different SM fermions $\delta g_{\rm eff} = \Delta g_{\rm eff}/g_{\rm SM}$. The numbers are given in percent.

fit, one would need to add additional observables, e.g. Higgs observables or measurements from diboson processes [422]. These, however, introduce further dependences on operators not entering in the EW fit and, in general, extra flat directions that need to be resolved including additional data. Eventually, this leads to the study of global SMEFT analyses that are becoming more popular in the literature, both from the theory and experimental sides, and that combine many types of observables from the EW, Higgs, top, and flavor sectors, to constrain as many directions in the SMEFT parameter space as possible. Some examples of these studies, with different levels of completeness in terms of both the scope of experimental observables included and the number of new-physics interactions considered, are presented in Refs. [424–434].

The presence of flat directions in the SMEFT fit is, however, not an impediment to derive interesting conclusions about the physics in the EW sector. For instance, the results in Table 10.9 can be translated into the space allowed for the modifications of the *effective* EW couplings of the fermions to the neutral currents in the SMEFT formalism, $\Delta g_{\rm eff}$, defined such that the tree-level relations between the EW pseudo-observables and couplings are preserved in the presence of new-physics effects. The corresponding values are shown in Table 10.10.

In general, the results of the fit show again good agreement with the SM, with the data suggesting that new-physics modifications of the leptonic couplings must be below a few per-mil, whereas the bounds are significantly weaker for quarks. There is one notable exception to this good agreement with the SM predictions. As discussed in Sec. 10.5, there is a $3.6 \pm 1.4\%$ deviation in the asymmetry parameter A_b . This becomes manifest in the results in Table 10.10 in terms of a preference for a non-SM value of the $Z \to b_R \bar{b}_R$ vertex with right-handed b quarks (equivalently, in a non-zero value for the coefficient $(\hat{C}_{\phi d})_{33}$ in Table 10.9). Similarly, the $Z \to b_L \bar{b}_L$ vertex with left-handed b quarks also shows a tension with the SM prediction, and both corrections are highly correlated. This is due to the fact that R_b is in good agreement with the SM, and is also much better determined than A_b . Given the size of the correction to the $Zb\bar{b}$ interactions required to

account for the deviation in A_b , it is difficult to attribute this solely to new physics entering through radiative corrections. Thus, if new physics is responsible, it is most likely of tree-level origin and affects preferentially the third generation. Examples include the decay of a scalar neutrino resonance [435], mixing of the b quark with heavy exotic particles [436], and a heavy Z' with family non-universal couplings [437,438]. It is difficult, however, to simultaneously account for R_b without tuning, which has been measured on the Z peak and off-peak [439] at LEP 1. Measurements at future e^+e^- colliders will help to test different scenarios modifying the $Zb\bar{b}$ interaction [440].

References

- [1] S. Glashow, Nucl. Phys. **22**, 579 (1961).
- [2] S. Weinberg, Phys. Rev. Lett. 19, 1264 (1967).
- [3] A. Salam, Conf. Proc. C **680519**, 367 (1968).
- [4] S. Glashow, J. Iliopoulos and L. Maiani, Phys. Rev. D 2, 1285 (1970).
- [5] N. Cabibbo, Phys. Rev. Lett. **10**, 531 (1963).
- [6] M. Kobayashi and T. Maskawa, Prog. Theor. Phys. 49, 652 (1973).
- [7] S. Descotes-Genon and P. Koppenburg, Ann. Rev. Nucl. Part. Sci. **67**, 97 (2017), [arXiv:1702.08834].
- [8] E. Commins and P. Bucksbaum, Weak Interactions of Leptons and Quarks, Cambridge Univ. Pr., Cambridge, USA (1983), ISBN 978-0-521-27370-1.
- [9] P. Langacker, editor, Precision tests of the standard electroweak model, volume 14, WSP, Singapore (1996).
- [10] P. Langacker, The standard model and beyond, CRC Pr., Boca Raton, USA (2010), ISBN 978-1-4200-7906-7.
- [11] T. Kinoshita, editor, Quantum electrodynamics, volume 7, WSP, Singapore (1990).
- [12] S. G. Karshenboim, Phys. Rept. **422**, 1 (2005), [hep-ph/0509010].
- [13] J. Erler and S. Su, Prog. Part. Nucl. Phys. **71**, 119 (2013), [arXiv:1303.5522].
- [14] T. Kinoshita, J. Math. Phys. 3, 650 (1962).
- [15] T. D. Lee and M. Nauenberg, Phys. Rev. 133, B1549 (1964).
- [16] F. Jegerlehner, Eur. Phys. J. C 18, 673 (2001), [hep-th/0005255].
- [17] W. B. Kilgore, Phys. Rev. D 83, 114005 (2011), [arXiv:1102.5353].
- [18] H. Bélusca-Maïto et al., Symmetry 15, 3, 622 (2023), [arXiv:2303.09120].
- [19] L. Chen, JHEP **2023**, 11, 30 (2023), [arXiv:2304.13814].
- [20] P. L. Ebert et al., JHEP **01**, 114 (2025), [arXiv:2411.02543].
- [21] D. A. Ross and J. C. Taylor, Nucl. Phys. B51, 125 (1973), [Erratum: Nucl. Phys. B58 (1973) 643].
- [22] A. Sirlin, Phys. Rev. D **22**, 971 (1980).
- [23] K.-i. Aoki et al., Prog. Theor. Phys. 65, 1001 (1981).
- [24] M. Böhm, H. Spiesberger and W. Hollik, Fortsch. Phys. 34, 687 (1986).
- [25] A. Denner, Fortsch. Phys. 41, 307 (1993), [arXiv:0709.1075].
- [26] S. Fanchiotti, B. A. Kniehl and A. Sirlin, Phys. Rev. D 48, 307 (1993), [hep-ph/9212285].
- [27] A. Denner and S. Dittmaier, Phys. Rept. 864, 1 (2020), [arXiv:1912.06823].
- [28] S. Actis et al., Nucl. Phys. B777, 1 (2007), [hep-ph/0612122].

- [29] S. Actis and G. Passarino, Nucl. Phys. B777, 35 (2007), [hep-ph/0612123].
- [30] S. Actis and G. Passarino, Nucl. Phys. B777, 100 (2007), [hep-ph/0612124].
- [31] A. Sirlin and R. Zucchini, Nucl. Phys. B **266**, 389 (1986).
- [32] J. Fleischer and F. Jegerlehner, Phys. Rev. **D23**, 2001 (1981).
- [33] S. Dittmaier and H. Rzehak, JHEP **05**, 125 (2022), [arXiv:2203.07236].
- [34] G. Altarelli, R. Kleiss and C. Verzegnassi, editors, Z physics at LEP 1. Vol. 1: Standard Physics, CERN, Geneva (1989), CERN-89-08, URL http://www.slac.stanford.edu/spires/find/books/www?cl=QCD161:L39:1989.
- [35] D. Bardin, W. Hollik, G. Passarino, editor, *Electroweak working group report* (1995), CERN-95-03, [hep-ph/9709229], URL http://doc.cern.ch/cernrep/1995/95-03/95-03.html.
- [36] D. A. Ross and M. J. G. Veltman, Nucl. Phys. B **95**, 135 (1975).
- [37] M. Veltman, Nucl. Phys. B **123**, 89 (1977).
- [38] M. Chiesa, F. Piccinini and A. Vicini, Phys. Rev. D **100**, 7, 071302 (2019), [arXiv:1906.11569].
- [39] D. Y. Bardin et al., Phys. Lett. B 206, 539 (1988).
- [40] P. Gambino and P. A. Grassi, Phys. Rev. D 62, 076002 (2000), [hep-ph/9907254].
- [41] P. A. Grassi, B. A. Kniehl and A. Sirlin, Phys. Rev. D 65, 085001 (2002), [hep-ph/0109228].
- [42] A. Freitas et al., Nucl. Phys. B 632, 189 (2002), [Erratum: Nucl. Phys. B 666, 305 (2003)], [hep-ph/0202131].
- [43] A. Denner et al., Nucl. Phys. B724, 247 (2005), [Erratum: Nucl. Phys. B 854 (2012) 504], [hep-ph/0505042].
- [44] R. Frederix et al., JHEP 07, 185 (2018), [Erratum: JHEP 11, 085 (2021)], [arXiv:1804.10017].
- [45] A. Sirlin, Phys. Rev. Lett. **67**, 2127 (1991).
- [46] W. Beenakker et al., Nucl. Phys. B 500, 255 (1997), [hep-ph/9612260].
- [47] F. Jegerlehner, M. Y. Kalmykov and O. Veretin, Nucl. Phys. B 641, 285 (2002), [hep-ph/0105304].
- [48] F. Jegerlehner, M. Y. Kalmykov and O. Veretin, Nucl. Phys. B 658, 49 (2003), [hep-ph/0212319].
- [49] S. P. Martin, Phys. Rev. D 91, 11, 114003 (2015), [arXiv:1503.03782].
- [50] S. P. Martin, Phys. Rev. D **92**, 1, 014026 (2015), [arXiv:1505.04833].
- [51] R. G. Stuart, Phys. Lett. **B262**, 113 (1991).
- [52] A. Aeppli, G. J. van Oldenborgh and D. Wyler, Nucl. Phys. B428, 126 (1994), [hep-ph/9312212].
- [53] D. Bardin *et al.*, Z. Phys. C **44**, 493 (1989).
- [54] D. Yu. Bardin, M. Grünewald and G. Passarino, "Precision calculation project report," (1999), [hep-ph/9902452].
- [55] D. Y. Bardin and G. Passarino, The standard model in the making: Precision study of the electroweak interactions (1999).
- [56] S. Dittmaier and M. Huber, JHEP **01**, 060 (2010), [arXiv:0911.2329].
- [57] G. Passarino, C. Sturm and S. Uccirati, Nucl. Phys. B 834, 77 (2010), [arXiv:1001.3360].
- [58] L. Chen and A. Freitas, SciPost Phys. Codeb. **2023**, 18 (2023), [arXiv:2211.16272].
- [59] S. Jadach et al., Phys. Lett. B 417, 326 (1998), [hep-ph/9705429].

- [60] W. Beenakker, F. A. Berends and A. P. Chapovsky, Nucl. Phys. B548, 3 (1999), [hep-ph/9811481].
- [61] A. Denner et al., Nucl. Phys. B **587**, 67 (2000), [hep-ph/0006307].
- [62] M. W. Grünewald et al., in S. Jadach, G. Passarino, R. Pittau, editor, "Reports of the Working Groups on Precision Calculations for LEP2 Physics," 1–135, CERN (2000), CERN-2000-009, [hep-ph/0005309].
- [63] S. Dittmaier, G. Knippen and C. Schwan, JHEP **02**, 003 (2020), [arXiv:1912.04117].
- [64] G. Aad et al. (ATLAS), Phys. Rept. 1116, 4 (2025), [arXiv:2404.05498].
- [65] G. Aad et al. (ATLAS), Phys. Rept. 1116, 57 (2025), [arXiv:2404.06829].
- [66] G. Aad et al. (ATLAS), Phys. Rept. 1116, 127 (2025), [arXiv:2404.10674].
- [67] A. Hayrapetyan et al. (CMS), Phys. Rept. 1115, 3 (2025), [arXiv:2405.18661].
- [68] S. Amoroso *et al.*, in "11th Les Houches Workshop on Physics at TeV Colliders: PhysTeV Les Houches," (2020), [arXiv:2003.01700].
- [69] F. Maltoni et al. (2022), [arXiv:2210.02591].
- [70] A. Huss et al. (2025), [arXiv:2504.06689].
- [71] G. Heinrich, Phys. Rept. **922**, 1 (2021), [arXiv:2009.00516].
- [72] J. Alwall et al., JHEP **06**, 128 (2011), [arXiv:1106.0522].
- [73] V. Hirschi et al., JHEP **1105**, 044 (2011), [arXiv:1103.0621].
- [74] M. H. Seymour, Z. Phys. C56, 161 (1992).
- [75] K. Hamilton and P. Richardson, JHEP **07**, 010 (2006), [hep-ph/0603034].
- [76] T. Sjöstrand et al., Comput. Phys. Commun. 191, 159 (2015), [arXiv:1410.3012].
- [77] T. Gleisberg et al., JHEP **02**, 007 (2009), [arXiv:0811.4622].
- [78] M. Schönherr and F. Krauss, JHEP 12, 018 (2008), [arXiv:0810.5071].
- [79] S. Höche, S. Schumann and F. Siegert, Phys. Rev. **D81**, 034026 (2010), [arXiv:0912.3501].
- [80] J. Erler and M. Schott, Prog. Part. Nucl. Phys. **106**, 68 (2019), [arXiv:1902.05142].
- [81] W. Hollik, Fortsch. Phys. **38**, 165 (1990).
- [82] A. Djouadi and C. Verzegnassi, Phys. Lett. B 195, 265 (1987).
- [83] A. Djouadi, Nuovo Cim. A **100**, 357 (1988).
- [84] K. Chetyrkin, J. H. Kuhn and M. Steinhauser, Phys. Lett. B 351, 331 (1995), [hep-ph/9502291].
- [85] L. Avdeev et al., Phys. Lett. B 336, 560 (1994), [Erratum: Phys. Lett. B 349, 597 (1995)], [hep-ph/9406363].
- [86] Y. Schroder and M. Steinhauser, Phys. Lett. B **622**, 124 (2005), [hep-ph/0504055].
- [87] K. Chetyrkin et al., Phys. Rev. Lett. 97, 102003 (2006), [hep-ph/0605201].
- [88] R. Boughezal and M. Czakon, Nucl. Phys. B **755**, 221 (2006), [hep-ph/0606232].
- [89] B. A. Kniehl, J. H. Kuhn and R. Stuart, Phys. Lett. B 214, 621 (1988).
- [90] B. A. Kniehl, Nucl. Phys. B **347**, 86 (1990).
- [91] F. Halzen and B. A. Kniehl, Nucl. Phys. B **353**, 567 (1991).
- [92] A. Djouadi and P. Gambino, Phys. Rev. D 49, 3499 (1994), [Erratum: Phys. Rev. D 53, 4111 (1996)], [hep-ph/9309298].

- [93] S. Dittmaier, T. Schmidt and J. Schwarz, JHEP 12, 201 (2020), [arXiv:2009.02229].
- [94] A. Anselm, N. Dombey and E. Leader, Phys. Lett. B **312**, 232 (1993).
- [95] K. Chetyrkin, J. H. Kuhn and M. Steinhauser, Phys. Rev. Lett. 75, 3394 (1995), [hep-ph/9504413].
- [96] J. van der Bij et al., Phys. Lett. B 498, 156 (2001), [hep-ph/0011373].
- [97] M. Faisst et al., Nucl. Phys. B 665, 649 (2003), [hep-ph/0302275].
- [98] L. Chen and A. Freitas, JHEP **07**, 210 (2020), [arXiv:2002.05845].
- [99] L. Chen and A. Freitas, JHEP **03**, 215 (2021), [arXiv:2012.08605].
- [100] M. Awramik et al., Phys. Rev. Lett. 93, 201805 (2004), [hep-ph/0407317].
- [101] W. Hollik, U. Meier and S. Uccirati, Nucl. Phys. B **731**, 213 (2005), [hep-ph/0507158].
- [102] M. Awramik, M. Czakon and A. Freitas, Phys. Lett. B **642**, 563 (2006), [hep-ph/0605339].
- [103] W. Hollik, U. Meier and S. Uccirati, Nucl. Phys. B **765**, 154 (2007), [hep-ph/0610312].
- [104] M. Awramik et al., Nucl. Phys. B 813, 174 (2009), [arXiv:0811.1364].
- [105] I. Dubovyk et al., Phys. Lett. B **762**, 184 (2016), [arXiv:1607.08375].
- [106] M. Awramik, M. Czakon and A. Freitas, JHEP 11, 048 (2006), [hep-ph/0608099].
- [107] A. Freitas, Phys. Lett. B **730**, 50 (2014), [arXiv:1310.2256].
- [108] A. Freitas, JHEP **04**, 070 (2014), [arXiv:1401.2447].
- [109] I. Dubovyk et al., Phys. Lett. B 783, 86 (2018), [arXiv:1804.10236].
- [110] I. Dubovyk et al., JHEP **08**, 113 (2019), [arXiv:1906.08815].
- [111] R. Barbieri et al., Nucl. Phys. B 409, 105 (1993).
- [112] J. Fleischer, O. Tarasov and F. Jegerlehner, Phys. Lett. B 319, 249 (1993).
- [113] G. Degrassi, P. Gambino and A. Vicini, Phys. Lett. B 383, 219 (1996), [hep-ph/9603374].
- [114] G. Degrassi, P. Gambino and A. Sirlin, Phys. Lett. B **394**, 188 (1997), [hep-ph/9611363].
- [115] A. Freitas et al., Phys. Lett. B 495, 338 (2000), [Erratum: Phys. Lett. B 570, 265 (2003)], [hep-ph/0007091].
- [116] M. Awramik and M. Czakon, Phys. Lett. B **568**, 48 (2003), [hep-ph/0305248].
- [117] M. Awramik and M. Czakon, Phys. Rev. Lett. 89, 241801 (2002), [hep-ph/0208113].
- [118] A. Onishchenko and O. Veretin, Phys. Lett. B **551**, 111 (2003), [hep-ph/0209010].
- [119] M. Awramik et al., Phys. Rev. D 69, 053006 (2004), [hep-ph/0311148].
- [120] G. Degrassi, P. Gambino and P. P. Giardino, JHEP **05**, 154 (2015), [arXiv:1411.7040].
- [121] S. P. Martin and D. G. Robertson, Phys. Rev. D **100**, 7, 073004 (2019), [arXiv:1907.02500].
- [122] S. P. Martin (2025), [arXiv:2507.15946].
- [123] H. Flacher *et al.*, Eur. Phys. J. C **60**, 543 (2009), [Erratum: Eur. Phys. J.C 71, 1718 (2011)], [arXiv:0811.0009].
- [124] M. Baak et al., Eur. Phys. J. C 72, 2205 (2012), [arXiv:1209.2716].
- [125] M. Baak et al. (Gfitter Group), Eur. Phys. J. C 74, 3046 (2014), [arXiv:1407.3792].
- [126] J. Haller et al., Eur. Phys. J. C 78, 8, 675 (2018), [arXiv:1803.01853].
- [127] J. de Blas et al., Eur. Phys. J. C 80, 5, 456 (2020), [arXiv:1910.14012].
- [128] M. Ciuchini et al., JHEP 08, 106 (2013), [arXiv:1306.4644].
- [129] J. de Blas et al., JHEP 12, 135 (2016), [arXiv:1608.01509].

- [130] J. de Blas et al., Phys. Rev. D 106, 3, 033003 (2022), [arXiv:2112.07274].
- [131] J. de Blas et al., Phys. Rev. Lett. 129, 27, 271801 (2022), [arXiv:2204.04204].
- [132] J. Erler (1999), [hep-ph/0005084].
- [133] D. Y. Bardin, P. K. Khristova and O. M. Fedorenko, Nucl. Phys. B 197, 1 (1982).
- [134] D. Y. Bardin, S. Riemann and T. Riemann, Z. Phys. C 32, 121 (1986).
- [135] A. Denner and T. Sack, Z. Phys. C 46, 653 (1990).
- [136] A. Arbuzov et al., Comput. Phys. Commun. 174, 728 (2006), [hep-ph/0507146].
- [137] A. Akhundov et al., Phys. Part. Nucl. 45, 3, 529 (2014), [arXiv:1302.1395].
- [138] S. Schael et al. (ALEPH, DELPHI, L3, OPAL, SLD, LEP Electroweak Working Group, SLD Electroweak Group, SLD Heavy Flavour Group), Phys. Rept. 427, 257 (2006), [hep-ex/0509008].
- [139] S. Schael et al. (ALEPH, DELPHI, L3, OPAL, LEP Electroweak), Phys. Rept. 532, 119 (2013), [arXiv:1302.3415].
- [140] W. E. Thirring, Phil. Mag. Ser. 7 41, 1193 (1950).
- [141] S. Dittmaier, Phys. Lett. B **409**, 509 (1997), [hep-ph/9704368].
- [142] X. Fan et al., Phys. Rev. Lett. 130, 7, 071801 (2023), [arXiv:2209.13084].
- [143] T. Aoyama et al., Phys. Rev. Lett. 109, 111808 (2012), [arXiv:1205.5370].
- [144] T. Aoyama, T. Kinoshita and M. Nio, Atoms 7, 1, 28 (2019).
- [145] S. Volkov (2024), [arXiv:2404.00649].
- [146] R. Aliberti et al., Phys. Rept. 1143, 1 (2025), [arXiv:2505.21476].
- [147] L. Morel et al., Nature **588**, 7836, 61 (2020).
- [148] R. H. Parker et al., Science **360**, 191 (2018), [arXiv:1812.04130].
- [149] P. Achard *et al.* (L3), Phys. Lett. B **623**, 26 (2005), [hep-ex/0507078].
- [150] G. Abbiendi et al. (OPAL), Eur. Phys. J. C 45, 1 (2006), [hep-ex/0505072].
- [151] K. Chetyrkin, J. H. Kuhn and M. Steinhauser, Nucl. Phys. B 482, 213 (1996), [hep-ph/9606230].
- [152] A. V. Nesterenko, Strong interactions in spacelike and timelike domains: dispersive approach, Elsevier (2016), ISBN 978-0-12-803448-4.
- [153] M. Steinhauser, Phys. Lett. B **429**, 158 (1998), [hep-ph/9803313].
- [154] C. Sturm, Nucl. Phys. B 874, 698 (2013), [arXiv:1305.0581].
- [155] M. Cè et al., JHEP 08, 220 (2022), [arXiv:2203.08676].
- [156] S. Groote et al., Phys. Lett. B 440, 375 (1998), [hep-ph/9802374].
- [157] N. Krasnikov and R. Rodenberg, Nuovo Cim. A 111, 217 (1998), [hep-ph/9711367].
- [158] J. H. Kuhn and M. Steinhauser, Phys. Lett. B 437, 425 (1998), [hep-ph/9802241].
- [159] A. D. Martin, J. Outhwaite and M. Ryskin, Phys. Lett. B 492, 69 (2000), [hep-ph/0008078].
- [160] J. de Troconiz and F. Yndurain, Phys. Rev. D 65, 093002 (2002), [hep-ph/0107318].
- [161] H. Burkhardt and B. Pietrzyk, Phys. Rev. D 84, 037502 (2011), [arXiv:1106.2991].
- [162] J. Erler and R. Ferro-Hernández, JHEP **03**, 196 (2018), [arXiv:1712.09146].
- [163] A. Blondel et al., editors, Theory for the FCC-ee: Report on the 11th FCC-ee Workshop Theory and Experiments, volume 3/2020 of CERN Yellow Reports: Monographs, CERN, Geneva (2019), [arXiv:1905.05078].

- [164] M. Davier et al., Eur. Phys. J. C 80, 3, 241 (2020), [arXiv:1908.00921].
- [165] A. Keshavarzi, D. Nomura and T. Teubner, Phys. Rev. D 101, 1, 014029 (2020), [arXiv:1911.00367].
- [166] M. Davier et al., Eur. Phys. J. C 71, 1515 (2011), [Erratum: Eur. Phys. J. C 72, 1874 (2012)], [arXiv:1010.4180].
- [167] S. Schael et al. (ALEPH), Phys. Rept. 421, 191 (2005), [hep-ex/0506072].
- [168] M. Fujikawa et al. (Belle), Phys. Rev. D 78, 072006 (2008), [arXiv:0805.3773].
- [169] S. Anderson et al. (CLEO), Phys. Rev. D 61, 112002 (2000), [hep-ex/9910046].
- [170] K. Ackerstaff et al. (OPAL), Eur. Phys. J. C 7, 571 (1999), [hep-ex/9808019].
- [171] F. V. Ignatov et al. (CMD-3), Phys. Rev. D 109, 11, 112002 (2024), [arXiv:2302.08834].
- [172] D. Webber et al. (MuLan), Phys. Rev. Lett. 106, 041803 (2011), [arXiv:1010.0991].
- [173] V. Tishchenko et al. (MuLan), Phys. Rev. D 87, 5, 052003 (2013), [arXiv:1211.0960].
- [174] T. Kinoshita and A. Sirlin, Phys. Rev. 113, 1652 (1959).
- [175] T. van Ritbergen and R. G. Stuart, Nucl. Phys. B **564**, 343 (2000), [hep-ph/9904240].
- [176] M. Steinhauser and T. Seidensticker, Phys. Lett. B 467, 271 (1999), [hep-ph/9909436].
- [177] Y. Nir, Phys. Lett. B **221**, 184 (1989).
- [178] A. Pak and A. Czarnecki, Phys. Rev. Lett. 100, 241807 (2008), [arXiv:0803.0960].
- [179] A. Ferroglia, G. Ossola and A. Sirlin, Nucl. Phys. B 560, 23 (1999), [hep-ph/9905442].
- [180] M. Fael, K. Schönwald and M. Steinhauser, Phys. Rev. D 104, 1, 016003 (2021), [arXiv:2011.13654].
- [181] M. Czakon, A. Czarnecki and M. Dowling, Phys. Rev. D **103**, L111301 (2021), [arXiv:2104.05804].
- [182] D. P. Aguillard *et al.* (Muon g-2) (2025), [arXiv:2506.03069].
- [183] B. Abi et al. (Muon g-2), Phys. Rev. Lett. 126, 14, 141801 (2021), [arXiv:2104.03281].
- [184] D. P. Aguillard et al. (Muon g-2), Phys. Rev. Lett. 131, 16, 161802 (2023), [arXiv:2308.06230].
- [185] G. Bennett et al. (Muon g-2), Phys. Rev. Lett. 92, 161802 (2004), [hep-ex/0401008].
- [186] T. Aoyama et al., Phys. Rept. 887, 1 (2020), [arXiv:2006.04822].
- [187] T. Aoyama et al., PTEP **2012**, 01A107 (2012).
- [188] P. Baikov, A. Maier and P. Marquard, Nucl. Phys. B 877, 647 (2013), [arXiv:1307.6105].
- [189] S. Laporta, Phys. Lett. B 772, 232 (2017), [arXiv:1704.06996].
- [190] G. Li, R. Mendel and M. A. Samuel, Phys. Rev. D 47, 1723 (1993).
- [191] S. Laporta and E. Remiddi, Phys. Lett. B 301, 440 (1993).
- [192] S. Laporta and E. Remiddi, Phys. Lett. B 379, 283 (1996), [hep-ph/9602417].
- [193] A. Czarnecki and M. Skrzypek, Phys. Lett. B 449, 354 (1999), [hep-ph/9812394].
- [194] J. Erler and M. Luo, Phys. Rev. Lett. 87, 071804 (2001), [hep-ph/0101010].
- [195] S. J. Brodsky and J. D. Sullivan, Phys. Rev. **156**, 1644 (1967).
- [196] T. Burnett and M. Levine, Phys. Lett. B 24, 467 (1967).
- [197] R. Jackiw and S. Weinberg, Phys. Rev. D 5, 2396 (1972).
- [198] I. Bars and M. Yoshimura, Phys. Rev. D 6, 374 (1972).
- [199] K. Fujikawa, B. Lee and A. Sanda, Phys. Rev. D 6, 2923 (1972).

- [200] W. A. Bardeen, R. Gastmans and B. Lautrup, Nucl. Phys. B 46, 319 (1972).
- [201] T. Kukhto et al., Nucl. Phys. B **371**, 567 (1992).
- [202] S. Peris, M. Perrottet and E. de Rafael, Phys. Lett. B 355, 523 (1995), [hep-ph/9505405].
- [203] A. Czarnecki, B. Krause and W. J. Marciano, Phys. Rev. D 52, 2619 (1995), [hep-ph/9506256].
- [204] A. Czarnecki, B. Krause and W. J. Marciano, Phys. Rev. Lett. 76, 3267 (1996), [hep-ph/9512369].
- [205] C. Gnendiger, D. Stöckinger and H. Stöckinger-Kim, Phys. Rev. D 88, 053005 (2013), [arXiv:1306.5546].
- [206] G. Degrassi and G. Giudice, Phys. Rev. D 58, 053007 (1998), [hep-ph/9803384].
- [207] A. Czarnecki, W. J. Marciano and A. Vainshtein, Phys. Rev. D 67, 073006 (2003), [Erratum: Phys. Rev. D 73, 119901 (2006)], [hep-ph/0212229].
- [208] F. V. Ignatov et al. (CMD-3), Phys. Rev. Lett. 132, 23, 231903 (2024), [arXiv:2309.12910].
- [209] J. L. Lopez, D. V. Nanopoulos and X. Wang, Phys. Rev. D 49, 366 (1994), [hep-ph/9308336].
- [210] H. Davoudiasl, H.-S. Lee and W. J. Marciano, Phys. Rev. D **86**, 095009 (2012), [arXiv:1208.2973].
- [211] T. Aaltonen et al. (CDF), Science **376**, 6589, 170 (2022).
- [212] V. Chekhovsky et al. (CMS) (2024), [arXiv:2412.13872].
- [213] R. Aaij et al. (LHCb), Phys. Rev. Lett. 135, 16, 161802 (2025), [arXiv:2505.15582].
- [214] P. Janot and S. Jadach, Phys. Lett. B 803, 135319 (2020), [arXiv:1912.02067].
- [215] S. Schael *et al.* (ALEPH, DELPHI, L3, OPAL, LEP Electroweak), Phys. Rept. **532**, 119 (2013), [arXiv:1302.3415].
- [216] T. A. Aaltonen et al. (CDF, DØ), Phys. Rev. D 88, 5, 052018 (2013), [arXiv:1307.7627].
- [217] M. Aaboud *et al.* (ATLAS), Eur. Phys. J. C **78**, 2, 110 (2018), [Erratum: Eur. Phys. J. C **78**, 898 (2018)], [arXiv:1701.07240].
- [218] R. Aaij et al. (LHCb), JHEP **01**, 036 (2022), [arXiv:2109.01113].
- [219] S. Amoroso *et al.* (LHC-TeV MW Working Group), Eur. Phys. J. C **84**, 5, 451 (2024), [arXiv:2308.09417].
- [220] T.-J. Hou et al. (2019), [arXiv:1908.11394].
- [221] G. Aad et al. (ATLAS), Eur. Phys. J. C 84, 12, 1309 (2024), [arXiv:2403.15085].
- [222] Technical Report TEVEWWG/WZ 2010/01, FERMILAB, Batavia (2010), [arXiv:1003.2826], URL https://www-d0.fnal.gov/Run2Physics/WWW/results/prelim/EW/E34.
- [223] G. Aad et al. (ATLAS), Phys. Lett. B **716**, 1 (2012), [arXiv:1207.7214].
- [224] S. Chatrchyan et al. (CMS), Phys. Lett. B 716, 30 (2012), [arXiv:1207.7235].
- [225] G. Aad et al. (ATLAS), Phys. Rev. Lett. 131, 25, 251802 (2023), [arXiv:2308.04775].
- [226] A. Hayrapetyan et al. (CMS), Phys. Rev. D 111, 9, 092014 (2025), [arXiv:2409.13663].
- [227] G. Aad et al. (ATLAS), Rept. Prog. Phys. 88, 5, 057803 (2025), [arXiv:2412.01548].
- [228] D. de Florian et al. (LHC Higgs Cross Section Working Group) (2016), [arXiv:1610.07922].
- [229] T. Aaltonen et al. (CDF, DØ, Tevatron Electroweak Working Group) (2016), [arXiv:1608.01881].
- [230] A. Hayrapetyan et al. (ATLAS, CMS) (2023), [arXiv:2402.08713].

- [231] A. Tumasyan et al. (CMS), Eur. Phys. J. C 83, 10, 963 (2023), [arXiv:2302.01967].
- [232] A. Tumasyan et al. (CMS), Eur. Phys. J. C 83, 7, 560 (2023), [arXiv:2211.01456].
- [233] A. M. Sirunyan et al. (CMS), Eur. Phys. J. C 79, 5, 368 (2019), [arXiv:1812.10505].
- [234] A. M. Sirunyan et al. (CMS), Eur. Phys. J. C 79, 4, 313 (2019), [arXiv:1812.10534].
- [235] A. Tumasyan et al. (CMS), JHEP 12, 161 (2021), [arXiv:2108.10407].
- [236] A. Hayrapetyan et al. (CMS), Phys. Rept. 1115, 116 (2025), [arXiv:2403.01313].
- [237] G. Aad et al. (ATLAS), JHEP **06**, 019 (2023), [arXiv:2209.00583].
- [238] G. Aad et al. (ATLAS), Phys. Lett. B 867, 139608 (2025), [arXiv:2502.18216].
- [239] Technical Report ATLAS-CONF-2023-058, CERN, Geneva (2022), URL http://cds.cern.ch/record/2826701.
- [240] A. H. Hoang, Ann. Rev. Nucl. Part. Sci. 70, 225 (2020), [arXiv:2004.12915].
- [241] G. Aad *et al.* (ATLAS), Eur. Phys. J. C **74**, 10, 3109 (2014), [Addendum: Eur. Phys. J. C **76**, 642 (2016)], [arXiv:1406.5375].
- [242] M. Aaboud et al. (ATLAS), Eur. Phys. J. C 77, 11, 804 (2017), [arXiv:1709.09407].
- [243] G. Aad et al. (ATLAS) (2025), [arXiv:2509.15066].
- [244] S. Chatrchyan *et al.* (CMS), Phys. Lett. B **728**, 496 (2014), [Erratum: Phys. Lett. B 738, 526 (2014)], [arXiv:1307.1907].
- [245] V. Khachatryan et al. (CMS), JHEP 08, 029 (2016), [arXiv:1603.02303].
- [246] A. M. Sirunyan et al. (CMS), JHEP 09, 051 (2017), [arXiv:1701.06228].
- [247] A. M. Sirunyan et al. (CMS), Eur. Phys. J. C 79, 5, 368 (2019), [arXiv:1812.10505].
- [248] A. H. Hoang, S. Plätzer and D. Samitz, JHEP 10, 200 (2018), [arXiv:1807.06617].
- [249] J. Kieseler, K. Lipka and S.-O. Moch, Phys. Rev. Lett. **116**, 16, 162001 (2016), [arXiv:1511.00841].
- [250] B. Dehnadi et al., JHEP 12, 065 (2023), [arXiv:2309.00547].
- [251] M. Beneke et al., Phys. Lett. B 775, 63 (2017), [arXiv:1605.03609].
- [252] P. Marquard et al., Phys. Rev. Lett. 114, 14, 142002 (2015), [arXiv:1502.01030].
- [253] M. Beneke, Phys. Rept. **317**, 1 (1999), [hep-ph/9807443].
- [254] S. Catani et al., JHEP 07, 100 (2019), [arXiv:1906.06535].
- [255] S. Catani et al., Eur. Phys. J. C 81, 6, 491 (2021), [arXiv:2102.03256].
- [256] A. M. Sirunyan et al. (CMS), Eur. Phys. J. C 80, 7, 658 (2020), [arXiv:1904.05237].
- [257] G. Aad et al. (ATLAS), JHEP 11, 150 (2019), [arXiv:1905.02302].
- [258] A. Tumasyan et al. (CMS), JHEP **07**, 077 (2023), [arXiv:2207.02270].
- [259] G. Aad et al. (ATLAS, CMS), JHEP 07, 213 (2023), [arXiv:2205.13830].
- [260] J. Erler, P. Masjuan and H. Spiesberger, Eur. Phys. J. C **82**, 11, 1023 (2022), [arXiv:2203.02348].
- [261] Y. Aoki et al. (Flavour Lattice Averaging Group (FLAG)) (2024), [arXiv:2411.04268].
- [262] W. J. Marciano and J. L. Rosner, Phys. Rev. Lett. 65, 2963 (1990), [Erratum: Phys. Rev. Lett. 68, 898 (1992)].
- [263] G. Degrassi, S. Fanchiotti and A. Sirlin, Nucl. Phys. B **351**, 49 (1991).
- [264] G. Degrassi and A. Sirlin, Nucl. Phys. B **352**, 342 (1991).

- [265] P. Gambino and A. Sirlin, Phys. Rev. D 49, 1160 (1994), [hep-ph/9309326].
- [266] J. Erler and M. J. Ramsey-Musolf, Prog. Part. Nucl. Phys. 54, 351 (2005), [hep-ph/0404291].
- [267] A. Czarnecki and W. J. Marciano, Int. J. Mod. Phys. A 15, 2365 (2000), [hep-ph/0003049].
- [268] J. Erler and M. J. Ramsey-Musolf, Phys. Rev. D 72, 073003 (2005), [hep-ph/0409169].
- [269] K. Kumar et al., Ann. Rev. Nucl. Part. Sci. 63, 237 (2013), [arXiv:1302.6263].
- [270] J. M. Conrad, M. H. Shaevitz and T. Bolton, Rev. Mod. Phys. 70, 1341 (1998), [hep-ex/9707015].
- [271] J. Formaggio and G. Zeller, Rev. Mod. Phys. 84, 1307 (2012), [arXiv:1305.7513].
- [272] A. Blondel et al., Z. Phys. C 45, 361 (1990).
- [273] J. Allaby et al. (CHARM), Z. Phys. C 36, 611 (1987).
- [274] K. S. McFarland et al. (CCFR, E744, E770), Eur. Phys. J. C 1, 509 (1998), [hep-ex/9701010].
- [275] G. Zeller *et al.* (NuTeV), Phys. Rev. Lett. **88**, 091802 (2002), [Erratum: Phys. Rev. Lett. 90, 239902 (2003)], [hep-ex/0110059].
- [276] C. Prescott et al., Phys. Lett. B 84, 524 (1979).
- [277] D. Wang et al. (PVDIS), Nature **506**, 7486, 67 (2014).
- [278] D. Wang et al., Phys. Rev. C 91, 4, 045506 (2015), [arXiv:1411.3200].
- [279] P. Anthony et al. (SLAC E158), Phys. Rev. Lett. 95, 081601 (2005), [hep-ex/0504049].
- [280] C. Wood et al., Science **275**, 1759 (1997).
- [281] J. Guena, M. Lintz and M. Bouchiat, Phys. Rev. A **71**, 042108 (2005), [arXiv:physics/0412017].
- [282] A. Derevianko, Phys. Rev. Lett. 85, 1618 (2000), [hep-ph/0005274].
- [283] W. Johnson, I. Bednyakov and G. Soff, Phys. Rev. Lett. 87, 233001 (2001), [Erratum: Phys. Rev. Lett. 88, 079903 (2002)], [hep-ph/0110262].
- [284] M. Kuchiev and V. Flambaum, Phys. Rev. Lett. 89, 283002 (2002), [hep-ph/0206124].
- [285] A. Milstein, O. Sushkov and I. Terekhov, Phys. Rev. Lett. 89, 283003 (2002), [hep-ph/0208227].
- [286] S. Porsev, K. Beloy and A. Derevianko, Phys. Rev. Lett. **102**, 181601 (2009), [arXiv:0902.0335].
- [287] V. Dzuba et al., Phys. Rev. Lett. 109, 203003 (2012), [arXiv:1207.5864].
- [288] M.-A. Bouchiat and C. Bouchiat, Rep. Prog. Phys. **60**, 11, 1351 (1997).
- [289] S. Navas et al. (Particle Data Group), Phys. Rev. D 110, 3, 030001 (2024).
- [290] G. Passarino and M. Veltman, Nucl. Phys. B **160**, 151 (1979).
- [291] W. Hollik and G. Duckeck, Springer Tracts Mod. Phys. 162, 1 (2000).
- [292] T. A. Aaltonen et al. (CDF, DØ), Phys. Rev. D 97, 11, 112007 (2018), [arXiv:1801.06283].
- [293] G. Aad et al. (ATLAS), JHEP **09**, 049 (2015), [arXiv:1503.03709].
- [294] Technical Report ATLAS-CONF-2018-037, CERN, Geneva (2018), URL https://cds.cern.ch/record/2630340.
- [295] A. M. Sirunyan et al. (CMS), Eur. Phys. J. C 78, 9, 701 (2018), [arXiv:1806.00863].
- [296] Technical Report CMS-PAS-SMP-22-010, CERN, Geneva (2024), URL http://cds.cern. ch/record/2893842.
- [297] R. Aaij et al. (LHCb), JHEP 11, 190 (2015), [arXiv:1509.07645].

- [298] K. Abe et al. (SLD), Phys. Rev. Lett. 84, 5945 (2000), [hep-ex/0004026].
- [299] K. Abe et al. (SLD), Phys. Rev. Lett. 86, 1162 (2001), [hep-ex/0010015].
- [300] A. Hayrapetyan et al. (CMS), JHEP **01**, 101 (2024), [arXiv:2309.12408].
- [301] D. Kennedy et al., Nucl. Phys. B **321**, 83 (1989).
- [302] S. Riemann, Rept. Prog. Phys. **73**, 126201 (2010).
- [303] K. Abe et al. (SLD), Phys. Rev. Lett. 85, 5059 (2000), [hep-ex/0006019].
- [304] K. Abe et al. (SLD), Phys. Rev. Lett. 78, 17 (1997), [hep-ex/9609019].
- [305] G. Voutsinas et al., Phys. Lett. B 800, 135068 (2020), [arXiv:1908.01704].
- [306] W. Bernreuther et al., JHEP **01**, 053 (2017), [arXiv:1611.07942].
- [307] S. Catani and M. H. Seymour, JHEP **07**, 023 (1999), [hep-ph/9905424].
- [308] A. Djouadi, J. H. Kuhn and P. Zerwas, Z. Phys. C 46, 411 (1990).
- [309] M. Aaboud et al. (ATLAS), Eur. Phys. J. C 77, 6, 367 (2017), [arXiv:1612.03016].
- [310] R. Aaij et al. (LHCb), JHEP **09**, 159 (2018), [arXiv:1806.05008].
- [311] T. A. Aaltonen *et al.* (CDF), Phys. Rev. D **93**, 11, 112016 (2016), [Addendum: Phys.Rev.D **95**, 119901 (2017)], [arXiv:1605.02719].
- [312] V. M. Abazov et al. (DØ), Phys. Rev. Lett. **120**, 24, 241802 (2018), [arXiv:1710.03951].
- [313] V. Abazov et al. (DØ), Phys. Rev. D 84, 012007 (2011), [arXiv:1104.4590].
- [314] D. Acosta et al. (CDF), Phys. Rev. D 71, 052002 (2005), [hep-ex/0411059].
- [315] V. Andreev et al. (H1), Eur. Phys. J. C 78, 9, 777 (2018), [arXiv:1806.01176].
- [316] H. Abramowicz et al. (ZEUS), Phys. Rev. D 93, 9, 092002 (2016), [arXiv:1603.09628].
- [317] A. Hayrapetyan et al. (CMS), Phys. Lett. B 866, 139526 (2025), [arXiv:2408.07622].
- [318] R. Aaij et al. (LHCb), JHEP 12, 026 (2024), [arXiv:2410.02502].
- [319] D. Albert et al., Nucl. Phys. B **166**, 460 (1980).
- [320] K. Chetyrkin, J. H. Kuhn and A. Kwiatkowski, Phys. Rept. 277, 189 (1996), [hep-ph/9503396].
- [321] P. Baikov, K. Chetyrkin and J. H. Kuhn, Phys. Rev. Lett. **101**, 012002 (2008), [arXiv:0801.1821].
- [322] B. A. Kniehl and J. H. Kuhn, Nucl. Phys. B **329**, 547 (1990).
- [323] K. Chetyrkin and A. Kwiatkowski, Phys. Lett. B **319**, 307 (1993), [hep-ph/9310229].
- [324] S. Larin, T. van Ritbergen and J. Vermaseren, Phys. Lett. B 320, 159 (1994), [hep-ph/9310378].
- [325] K. Chetyrkin and O. Tarasov, Phys. Lett. B **327**, 114 (1994), [hep-ph/9312323].
- [326] P. Baikov et al., Phys. Rev. Lett. 108, 222003 (2012), [arXiv:1201.5804].
- [327] A. Kataev, Phys. Lett. B **287**, 209 (1992).
- [328] B. W. Lynn and R. G. Stuart, Phys. Lett. B 252, 676 (1990).
- [329] J. Bernabeu, A. Pich and A. Santamaria, Nucl. Phys. B 363, 326 (1991).
- [330] A. Czarnecki and J. H. Kuhn, Phys. Rev. Lett. 77, 3955 (1996), [hep-ph/9608366].
- [331] R. Harlander, T. Seidensticker and M. Steinhauser, Phys. Lett. B 426, 125 (1998), [hep-ph/9712228].
- [332] J. Fleischer et al., Phys. Lett. B 459, 625 (1999), [hep-ph/9904256].

- [333] A. Akhundov, D. Bardin and T. Riemann, Nucl. Phys. B **276**, 1 (1986).
- [334] F. Jegerlehner, Z. Phys. C **32**, 425 (1986), [Erratum: Z. Phys. C 38, 519 (1988)].
- [335] W. Beenakker and W. Hollik, Z. Phys. C 40, 141 (1988).
- [336] A. Borrelli *et al.*, Nucl. Phys. B **333**, 357 (1990).
- [337] G. Aad et al. (ATLAS), Nature Phys. 17, 7, 813 (2021), [arXiv:2007.14040].
- [338] A. Tumasyan et al. (CMS), Phys. Rev. D 105, 7, 072008 (2022), [arXiv:2201.07861].
- [339] G. Aad et al. (ATLAS), Eur. Phys. J. C 84, 10, 993 (2024), [arXiv:2403.02133].
- [340] R. Aaij et al. (LHCb), JHEP 10, 030 (2016), [arXiv:1608.01484].
- [341] U. Amaldi et al., Phys. Rev. D 36, 1385 (1987).
- [342] G. Costa et al., Nucl. Phys. B **297**, 244 (1988).
- [343] P. Langacker and M. Luo, Phys. Rev. D 44, 817 (1991).
- [344] J. Erler and P. Langacker, Phys. Rev. D **52**, 441 (1995), [hep-ph/9411203].
- [345] M. Aaboud et al. (ATLAS), Phys. Lett. B 784, 345 (2018), [arXiv:1806.00242].
- [346] A. M. Sirunyan et al. (CMS), Phys. Lett. B 805, 135425 (2020), [arXiv:2002.06398].
- [347] M. E. Peskin and T. Takeuchi, Phys. Rev. D 46, 381 (1992).
- [348] G. Altarelli, R. Barbieri and S. Jadach, Nucl. Phys. B 369, 3 (1992), [Erratum: Nucl. Phys. B 376, 444 (1992)].
- [349] G. Altarelli, R. Barbieri and F. Caravaglios, Nucl. Phys. B 405, 3 (1993).
- [350] G. Altarelli, R. Barbieri and F. Caravaglios, Int. J. Mod. Phys. A 13, 1031 (1998), [hep-ph/9712368].
- [351] R. Barbieri et al., Nucl. Phys. B **703**, 127 (2004), [hep-ph/0405040].
- [352] P. Langacker and M. Luo, Phys. Rev. D 45, 278 (1992).
- [353] P. Langacker and D. London, Phys. Rev. D 38, 886 (1988).
- [354] F. del Aguila, J. de Blas and M. Perez-Victoria, Phys. Rev. D **78**, 013010 (2008), [arXiv:0803.4008].
- [355] M. Chemtob, Prog. Part. Nucl. Phys. **54**, 71 (2005), [hep-ph/0406029].
- [356] R. Barbier et al., Phys. Rept. 420, 1 (2005), [hep-ph/0406039].
- [357] C. T. Hill and E. H. Simmons, Phys. Rept. **381**, 235 (2003), [Erratum: Phys. Rept. 390, 553 (2004)], [hep-ph/0203079].
- [358] T. Han, H. E. Logan and L.-T. Wang, JHEP **01**, 099 (2006), [hep-ph/0506313].
- [359] M. Perelstein, Prog. Part. Nucl. Phys. 58, 247 (2007), [hep-ph/0512128].
- [360] I. Antoniadis, in "Supergravity, Superstrings and M-Theory," (2001), [hep-th/0102202].
- [361] M. Carena et al., Phys. Rev. D 68, 035010 (2003), [hep-ph/0305188].
- [362] K. Agashe et al., JHEP **08**, 050 (2003), [hep-ph/0308036].
- [363] I. Gogoladze and C. Macesanu, Phys. Rev. D 74, 093012 (2006), [hep-ph/0605207].
- [364] B. Grinstein and M. Trott, Phys. Rev. D 76, 073002 (2007), [arXiv:0704.1505].
- [365] R. Alonso *et al.*, Phys. Lett. B **722**, 330 (2013), [Erratum: Phys. Lett. B **726**, 926 (2013)], [arXiv:1212.3305].
- [366] R. Contino et al., JHEP 07, 035 (2013), [arXiv:1303.3876].
- [367] W. Buchmuller and D. Wyler, Nucl. Phys. B **268**, 621 (1986).

- [368] B. Grzadkowski et al., JHEP 10, 085 (2010), [arXiv:1008.4884].
- [369] S. Weinberg, Phys. Rev. Lett. 43, 1566 (1979).
- [370] J. D. Wells and Z. Zhang, JHEP **01**, 123 (2016), [arXiv:1510.08462].
- [371] S. Dawson and P. P. Giardino, Phys. Rev. D 101, 1, 013001 (2020), [arXiv:1909.02000].
- [372] L. Bellafronte, S. Dawson and P. P. Giardino, JHEP 05, 208 (2023), [arXiv:2304.00029].
- [373] A. Biekötter and B. D. Pecjak, JHEP 07, 134 (2025), [arXiv:2503.07724].
- [374] P. Asadi et al., Phys. Rev. D 108, 5, 055026 (2023), [arXiv:2204.05283].
- [375] E. Bagnaschi et al., JHEP 08, 308 (2022), [arXiv:2204.05260].
- [376] J. Gu et al., Chin. Phys. C 46, 12, 123107 (2022), [arXiv:2204.05296].
- [377] A. Paul and M. Valli, Phys. Rev. D **106**, 1, 013008 (2022), [arXiv:2204.05267].
- [378] M. S. Chanowitz, M. Furman and I. Hinchliffe, Phys. Lett. B 78, 285 (1978).
- [379] J. van der Bij and F. Hoogeveen, Nucl. Phys. B 283, 477 (1987).
- [380] A. Denner, R. Guth and J. H. Kuhn, Phys. Lett. B **240**, 438 (1990).
- [381] W. Grimus et al., J. Phys. G 35, 075001 (2008), [arXiv:0711.4022].
- [382] H. E. Haber and D. O'Neil, Phys. Rev. D 83, 055017 (2011), [arXiv:1011.6188].
- [383] S. Bertolini and A. Sirlin, Phys. Lett. B **257**, 179 (1991).
- [384] J. Erler and P. Langacker, Phys. Rev. Lett. **105**, 031801 (2010), [arXiv:1003.3211].
- [385] J. Gunion, D. W. McKay and H. Pois, Phys. Rev. D 53, 1616 (1996), [hep-ph/9507323].
- [386] A. Denner et al., Eur. Phys. J. C 72, 1992 (2012), [arXiv:1111.6395].
- [387] A. Lenz, Adv. High Energy Phys. **2013**, 910275 (2013).
- [388] S. Chatrchyan et al. (CMS), Phys. Rev. D 86, 112003 (2012), [arXiv:1209.1062].
- [389] A. Djouadi and A. Lenz, Phys. Lett. B 715, 310 (2012), [arXiv:1204.1252].
- [390] O. Eberhardt et al., Phys. Rev. Lett. 109, 241802 (2012), [arXiv:1209.1101].
- [391] J. Maalampi and M. Roos, Phys. Rept. **186**, 53 (1990).
- [392] P. Langacker, Phys. Rept. **72**, 185 (1981).
- [393] J. L. Hewett and T. G. Rizzo, Phys. Rept. 183, 193 (1989).
- [394] J. Kang, P. Langacker and B. D. Nelson, Phys. Rev. D 77, 035003 (2008), [arXiv:0708.2701].
- [395] S. P. Martin, Phys. Rev. D 81, 035004 (2010), [arXiv:0910.2732].
- [396] P. W. Graham et al., Phys. Rev. D 81, 055016 (2010), [arXiv:0910.3020].
- [397] L. Randall and R. Sundrum, Phys. Rev. Lett. 83, 3370 (1999), [hep-ph/9905221].
- [398] M. Carena et al., Nucl. Phys. B **759**, 202 (2006), [hep-ph/0607106].
- [399] R. Contino, in "Theoretical Advanced Study Institute in Elementary Particle Physics: Physics of the Large and the Small," 235–306 (2011), [arXiv:1005.4269].
- [400] A. Pich, I. Rosell and J. Sanz-Cillero, JHEP **01**, 157 (2014), [arXiv:1310.3121].
- [401] G. Panico and A. Wulzer, *The Composite Nambu-Goldstone Higgs*, volume 913, Springer (2016), [arXiv:1506.01961].
- [402] J. A. Cabrer, G. von Gersdorff and M. Quiros, JHEP **05**, 083 (2011), [arXiv:1103.1388].
- [403] D. D. Dietrich, F. Sannino and K. Tuominen, Phys. Rev. D 72, 055001 (2005), [hep-ph/0505059].
- [404] M. T. Frandsen and M. Rosenlyst, JHEP 03, 222 (2023), [arXiv:2207.01465].

- [405] E. Gates and J. Terning, Phys. Rev. Lett. **67**, 1840 (1991).
- [406] H. Georgi, Nucl. Phys. B **363**, 301 (1991).
- [407] M. J. Dugan and L. Randall, Phys. Lett. B **264**, 154 (1991).
- [408] H. E. Haber and G. L. Kane, Phys. Rept. 117, 75 (1985).
- [409] A. Djouadi, Phys. Rept. **459**, 1 (2008), [hep-ph/0503173].
- [410] R. Barbieri et al., Nucl. Phys. B **341**, 309 (1990).
- [411] R. Barbieri, M. Frigeni and F. Caravaglios, Phys. Lett. B **279**, 169 (1992).
- [412] J. Erler and D. M. Pierce, Nucl. Phys. B **526**, 53 (1998), [hep-ph/9801238].
- [413] G.-C. Cho and K. Hagiwara, Nucl. Phys. B **574**, 623 (2000), [hep-ph/9912260].
- [414] G. Altarelli et al., JHEP **06**, 018 (2001), [hep-ph/0106029].
- [415] S. Heinemeyer, W. Hollik and G. Weiglein, Phys. Rept. 425, 265 (2006), [hep-ph/0412214].
- [416] S. P. Martin, K. Tobe and J. D. Wells, Phys. Rev. D 71, 073014 (2005), [hep-ph/0412424].
- [417] M. Ramsey-Musolf and S. Su, Phys. Rept. 456, 1 (2008), [hep-ph/0612057].
- [418] S. Heinemeyer et al., JHEP **04**, 039 (2008), [arXiv:0710.2972].
- [419] O. Buchmueller et al., Eur. Phys. J. C 72, 2020 (2012), [arXiv:1112.3564].
- [420] G. Altarelli and R. Barbieri, Phys. Lett. B **253**, 161 (1991).
- [421] I. Brivio et al. (2021), [arXiv:2111.12515].
- [422] A. Falkowski and F. Riva, JHEP **02**, 039 (2015), [arXiv:1411.0669].
- [423] I. Brivio and M. Trott, JHEP 07, 148 (2017), [Addendum: JHEP 05, 136 (2018)], [arXiv:1701.06424].
- [424] J. Ellis et al., JHEP **04**, 279 (2021), [arXiv:2012.02779].
- [425] J. J. Ethier et al. (SMEFiT), JHEP 11, 089 (2021), [arXiv:2105.00006].
- [426] F. Garosi et al., JHEP 12, 129 (2023), [arXiv:2310.00047].
- [427] L. Allwicher et al., JHEP **03**, 049 (2024), [arXiv:2311.00020].
- [428] R. Bartocci, A. Biekötter and T. Hurth, JHEP 05, 074 (2024), [arXiv:2311.04963].
- [429] E. Celada et al., JHEP **09**, 091 (2024), [arXiv:2404.12809].
- [430] G. Aad et al. (ATLAS), JHEP 11, 097 (2024), [arXiv:2402.05742].
- [431] R. Bartocci, A. Biekötter and T. Hurth, JHEP **05**, 203 (2025), [arXiv:2412.09674].
- [432] V. Chekhovsky et al. (CMS) (2025), [arXiv:2504.02958].
- [433] J. ter Hoeve et al., JHEP 06, 125 (2025), [arXiv:2502.20453].
- [434] J. de Blas et al. (2025), [arXiv:2507.06191].
- [435] J. Erler, J. L. Feng and N. Polonsky, Phys. Rev. Lett. 78, 3063 (1997), [hep-ph/9612397].
- [436] D. Choudhury, T. M. Tait and C. Wagner, Phys. Rev. D 65, 053002 (2002), [hep-ph/0109097].
- [437] J. Erler and P. Langacker, Phys. Rev. Lett. 84, 212 (2000), [hep-ph/9910315].
- [438] P. Langacker and M. Plumacher, Phys. Rev. D 62, 013006 (2000), [hep-ph/0001204].
- [439] P. Abreu et al. (DELPHI), Eur. Phys. J. C 10, 415 (1999).
- [440] S. Gori, J. Gu and L.-T. Wang, JHEP **04**, 062 (2016), [arXiv:1508.07010].